

# Influence of dynamic surface tension on foams: Application in gas well deliquification

MSC THESIS

DELFT UNIVERSITY OF TECHNOLOGY  
FACULTY OF APPLIED SCIENCES  
DEPARTMENT OF MULTI-SCALE PHYSICS

Starting date: 5 September 2011

Defence date: 31 August 2012

*Author:*

Durgesh KAWALE

Student number: 4123344

*Supervisors:*

Ir. A.T. van NIMWEGEN

Dr. Eng. L.M. PORTELA

Dr. M. van DIJK (Shell)

Prof. Dr. Ir. R.A.W.M. Henkes

*Reviewer:*

Dr. ing. G.J.M. KOPER



The experimental work described in this thesis has been carried out during a 10 month visit at the *Shell Technology Center* in Amsterdam. The work is linked to the PhD project by Ir. Dries van Nimwegen on well deliquification using foamers, funded by the *Nederlandse Aardolie Maatschappij* (NAM). Shell and NAM are acknowledged for their support, including their technical input during progress meetings.





Picture courtesy: Chris Lord<sup>©</sup>, Reproduced with permission.  
Website: [www.pixielatedpixels.com](http://www.pixielatedpixels.com)

“There are things known and things unknown and in  
between are the doors of perception.”  
— *Jim Morrison (1943 – 1971)*



# Table of contents

<b>Abstract</b>	<b>xi</b>
<b>1 Introduction</b>	<b>1</b>
1.1 Motivation . . . . .	1
1.2 Foams . . . . .	2
1.2.1 Surface active agents . . . . .	3
1.2.2 Physio-chemical properties of surfactants in water . . . . .	3
1.2.3 Foamability . . . . .	4
1.2.4 Foam formation . . . . .	4
1.3 Rosen's empirical approach . . . . .	5
1.4 Other correlations for <i>foamability</i> . . . . .	6
1.5 Research question . . . . .	8
1.6 Outline . . . . .	8
<b>2 Background theories</b>	<b>9</b>
2.1 Surfactant properties in aqueous solutions . . . . .	9
2.1.1 Equilibrium surface tension . . . . .	9
2.1.2 Dyanamic surface tension . . . . .	13
2.2 Foam structure and density . . . . .	14
2.3 Physiochemical theory of foaming . . . . .	16
2.3.1 Gibbs-Marangoni effect . . . . .	16
2.3.2 Drainage . . . . .	17
2.3.3 Micellar kinetics . . . . .	18
2.4 Methods of foam generation . . . . .	18
2.5 Summary . . . . .	20
<b>3 Experimental setup</b>	<b>21</b>
3.1 Equilibrium surface tension . . . . .	21
3.2 Dynamic surface tension . . . . .	22
3.2.1 Validation and reproducibility . . . . .	23
3.3 Foam column . . . . .	25
3.3.1 Procedure . . . . .	26
3.3.2 Visualization . . . . .	26
3.3.3 Reproducibility . . . . .	28
3.4 Chemicals . . . . .	28

3.5 Summary . . . . .	30
<b>4 Results</b>	<b>31</b>
4.1 Sodium Dodecyl Sulfate (SDS) . . . . .	31
4.1.1 Preparation of the solutions . . . . .	31
4.1.2 Equilibrium surface tension . . . . .	32
4.1.3 Dynamic surface tension (DST) . . . . .	33
4.1.4 Foamability results . . . . .	33
4.2 Cetyltrimethylammonium Bromide (CTAB) . . . . .	40
4.2.1 Equilibrium surface tension . . . . .	40
4.2.2 Dynamic surface tension (DST) . . . . .	41
4.2.3 Foamability results . . . . .	41
4.3 Polyoxyethylene (4) lauryl ether (Brij 30) . . . . .	44
4.3.1 Equilibrium surface tension . . . . .	46
4.3.2 Dynamic surface tension (DST) . . . . .	47
4.3.3 Foamability results . . . . .	47
4.4 Sodium Dodecyl Sulfate (SDS) + Sodium Chloride (NaCl) . . . . .	50
4.4.1 Dynamic surface tension (DST) . . . . .	50
4.4.2 Foamability results . . . . .	53
4.5 Trifoam Block 820 (TB820) . . . . .	53
4.5.1 Dynamic surface tension (DST) . . . . .	53
4.5.2 Foamability results . . . . .	55
4.6 Overall comparisons . . . . .	56
4.6.1 Foam density with Rosen parameter . . . . .	58
4.6.2 Foam density with dynamic surface excess concentration . . . . .	58
4.6.3 Foam density with equilibrium surface pressure . . . . .	58
4.6.4 Maximum unloading with dynamic surface excess concentration . . . . .	58
4.7 Summary . . . . .	61
<b>5 Conclusions and recommendations</b>	<b>63</b>
5.1 Conclusions . . . . .	63
5.1.1 Total produced foam mass . . . . .	64
5.1.2 Foam density . . . . .	64
5.1.3 Limitations and opportunities . . . . .	65
5.2 Recommendations . . . . .	65
<b>Acknowledgements</b>	<b>69</b>
<b>List of symbols</b>	<b>71</b>
<b>Bibliography</b>	<b>75</b>
<b>A Measurement principles</b>	<b>81</b>
A.1 The du Noüy ring method correction factors . . . . .	81
A.1.1 Procedure . . . . .	81
A.2 BPA-1S capillary cleaning procedure . . . . .	82

A.3	Cleaning procedure for the foam column . . . . .	82
<b>B</b>	<b>On the shape of foam bubbles and corresponding foam density</b>	<b>85</b>



## Abstract

In natural gas production, along with gas, a small amount of liquid is produced. Towards the end of a reservoir life, the gas velocity reduces due to a decline in pressure. A low gas velocity in a gas well causes undesirable liquid accumulation (loading) in the production tubing. One of the ways to postpone liquid loading is by injecting surfactants in the well. The agitation by gas/liquid flows causes the surfactants to foam. The actual mechanism of how the surfactant injection which causes deliquification is poorly understood.

There is an impetus from the gas industry to develop a mechanistic foam flow model that can predict the flow in the well for different surfactants. This requires identification of the surfactant properties that influence the flow characteristics. Based on a literature study it was concluded that the dynamic surface tension (DST) and equilibrium surface tension (ST) are few characteristic properties of a surfactant that affects the foaming ability. There is no general agreement about the relation between the foamability and the DST. This thesis is formulated to investigate the influence of the DST and the ST on the foaming ability in a customized setup.

In gas well deliquification, foams serve the purpose of removing liquids. Therefore, in this work foamability is defined as the liquid content of the created foam. The foamability of different surfactants is tested in a modified Bikerman setup, in which foam is generated by sparging  $N_2$  through the surfactant solution. The weight of the produced foam was measured in time. High speed movies were also recorded and analyzed to determine bubble sizes and their velocities in the foam as well as in the bulk liquid. The calculated foam density includes the weight and the foam velocity.

DST is measured by the maximum bubble pressure method in a time range of 1 ms to 100 s and the equilibrium surface tension is measured using the du Noüy ring method. The equilibrium surface tension was compared through the corresponding *surface pressure*, whereas, the DST was compared through the *Rosen parameter* and the *dynamic surface excess concentration*. Dynamic surface excess concentration is defined as the surface excess concentration at the time scale of foaming. In the experiments, Sodium dodecyl sulfate (SDS), cetyltrimethylammonium bromide (CTAB) and polyoxyethylene - 4 lauryl ether (Brij 30) are used as the pure surfactant. In addition a commercial proprietary surfactant successfully applied to deliquify actual gas wells, Trifoam Block 820 (TB820) is also used. The influence of salt is investigated by varying NaCl concentration in a solution with fixed SDS concentration.

In the pre-micellar region the foam density increases with the Rosen parameter. However in the micellar region this trend was not consistent for all the surfactants used. An overall comparison showed a logarithmic dependence of the Rosen parameter on the foam density, whereas a linear dependence of the dynamic surface excess concentration on the foam density was observed. In order to obtain a dense foam,

the Rosen parameter and the dynamic surface excess concentration should be high. More experiments are needed to determine if these trends are general.

This dependence of foam density on DST could assist in choosing the ideal surfactant for a particular gas well deliquification application. A denser foam would potentially be more effective in removing liquids (owing to higher liquid content). The mechanistic foam flow model being developed for real life applications should benefit from this qualitative trend.

---

# 1. Introduction

---

This thesis deals with the characterization of foamers for gas well deliquification. Understanding this topic requires knowledge from different fields, including multi-phase flows and colloid chemistry. While complete understanding is a far fetched objective, this chapter will isolate concepts and gradually motivate the research question of this masters thesis. The last section includes an outline of the whole report.

## 1.1 Motivation

A natural gas reservoir produces small quantities of liquids along with gas. Water is the main component of these liquids. The gas is transported by annular flows from the reservoir to the production facilities. As production continues, the reservoir pressure declines, decreasing the gas velocity. At a certain point, the gas is unable to lift the liquid. Liquids will then accumulate in the well; this is called as liquid loading. Liquid loading poses a major problem for exploiting the maximum potential of a gas reservoir<sup>[2]</sup>.

Several technologies<sup>[2]</sup> are employed to tackle the problem of liquid loading. The most popular and easiest to use is the injection of foamers. Foamers help in producing foam which can remove the liquid at a lower gas velocity. The choice of foamer is made from experience, as the exact mechanism is poorly understood in order to make an educated estimate. There is no single theory which can predict whether the foam will work in a given well. The effect of foam on the flow in a gas well is not modeled. For such a model, it is essential that the foam is characterized. A lot of parameters across over several length scales affect the bulk foaming behaviour in a gas well. Referring to Fig. 1.1, the molecular chemistry ( $\mathcal{O}(\text{\AA})$ ) in a foaming solution affect the behaviour of foam films at  $\mathcal{O}(\text{nm}) - \mathcal{O}(\text{mm})$ , which in turn affects

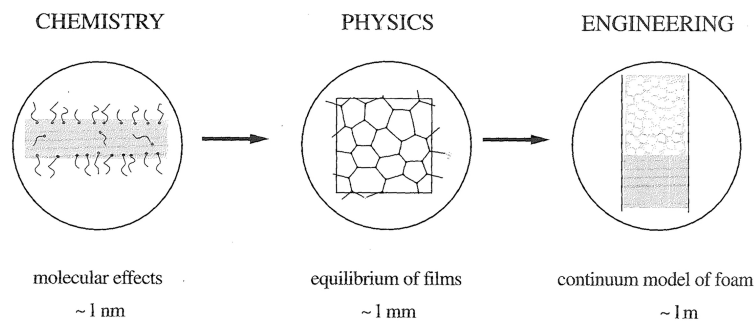


Figure 1.1: Different scales for study of foams<sup>[1]</sup>

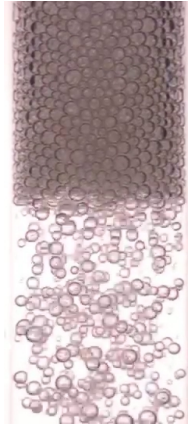
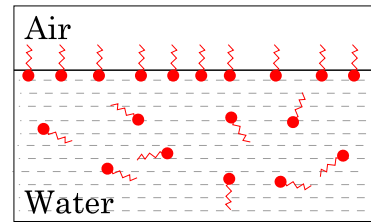
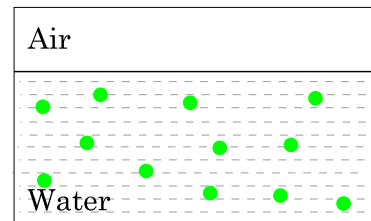


Figure 1.2: Foam produced by bubbling  $N_2$  through needles.



(a) Surface active molecules



(b) Non-surface active molecules

Figure 1.3: Partition of surface active molecules at water-air interface

the (very) large scale in a gas well ( $\mathcal{O}(\text{km})$ ). Understanding the molecular scale effects and their influence on foaming is required to obtain a (mechanistic) model of the foam in the gas well. Considering the complexity, a suitable small scale experiment can serve as characterization. This thesis will focus on the characterization of foamers using a small scale experiment.

The molecular phenomena in aqueous surfactant solutions and their relation with the foam formation, with a focus on physical chemistry, will be the subject of this masters thesis. The large scale flow aspects of the foam are studied in a PhD project by Ir. Dries van Nimwegen at Department of Multi-Scale Physics, Delft University of Technology. Finally it is envisioned that using the learning from this thesis, Ir. Dries van Nimwegen will bridge the gap between the small scale (molecular) and the large scale (flow) phenomena by developing a foam flow model.

## 1.2 Foams

Foam is commonly encountered while using soaps<sup>[3]</sup> or drinking coffee<sup>[4]</sup>. Foam consists of gas dispersed in liquid where the liquid forms a continuous phase. The foam bubbles can be spherical or polyhedral; small or large; monodisperse or polydisperse. The type of foam bubbles obtained changes with the method of foam generation, such as simple shaking, beating, and sparging.

Consider formation of foam due to rising bubbles in a soap solution as shown in Fig. 1.2. As the bubbles reach the solution surface, they retain their form. With more bubbles reaching the surface, a column of bubbles is created. This structure of bubbles stacked together is called a foam. A unit volume of this structure weighs

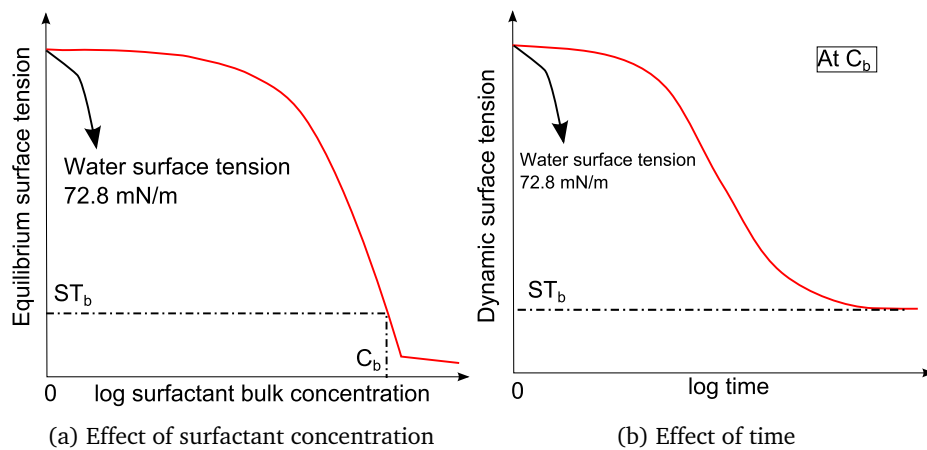


Figure 1.4: Equilibrium and dynamics surface tension of aqueous surfactant solutions

about the same as the amount of water it contains. Thus a foam density,  $\rho_{\text{foam}}$  ( $\text{g}/\text{cm}^3$ ), can be defined to quantify the water content of the foam. Foam with higher  $\rho_{\text{foam}}$  corresponds to larger water content and *vice-versa*.

Several questions arise with such a simplified view such as (i) Why does foam form? (ii) How does the choice of foamers influence the foam density? (iii) Which properties of foamers can serve as a measure of the foam density?

### 1.2.1 Surface active agents

The component in a foamer (soap) responsible for foaming is known as a surfactant. A surfactant is a molecule with two groups; the hydrophilic group forming the ‘head’, and the hydrophobic group forming the ‘tail’.

The head group consists of functional groups which readily dissolve in water. Examples are sulphates ( $\text{OSO}_3^-$ ), amines ( $\text{NH}_2^+$ ), hydroxyl (OH) and ethylene oxide ( $\text{OCH}_2\text{CH}_2$ ). The tail group is made of groups which do not dissolve in water like hydrocarbon (or fluoro hydrocarbon) chains of either aliphatic and aromatic series. For detailed literature on types of surfactant molecules see reference<sup>[3,5]</sup>.

### 1.2.2 Physio-chemical properties of surfactants in water

The presence of a hydrophilic group and a hydrophobic group causes the surfactant to preferentially adsorb at water-gas interface (Fig. 1.3). The surfactant tails have lower surface tension,  $\gamma$  ( $\text{mN}/\text{m}$ ), than water and thus the surface tension of the water-gas interface is lowered. The magnitude of the reduction in  $\gamma$  depends on the type and the number of molecules adsorbed at the interface, which is a function of surfactant bulk concentration. Fig. 1.4a shows how  $\gamma$  of aqueous surfactant solution depends on bulk concentration of surfactants.

Reduction in  $\gamma$  is a dynamic process. When a fresh interface is created ( $t = 0$ ), the

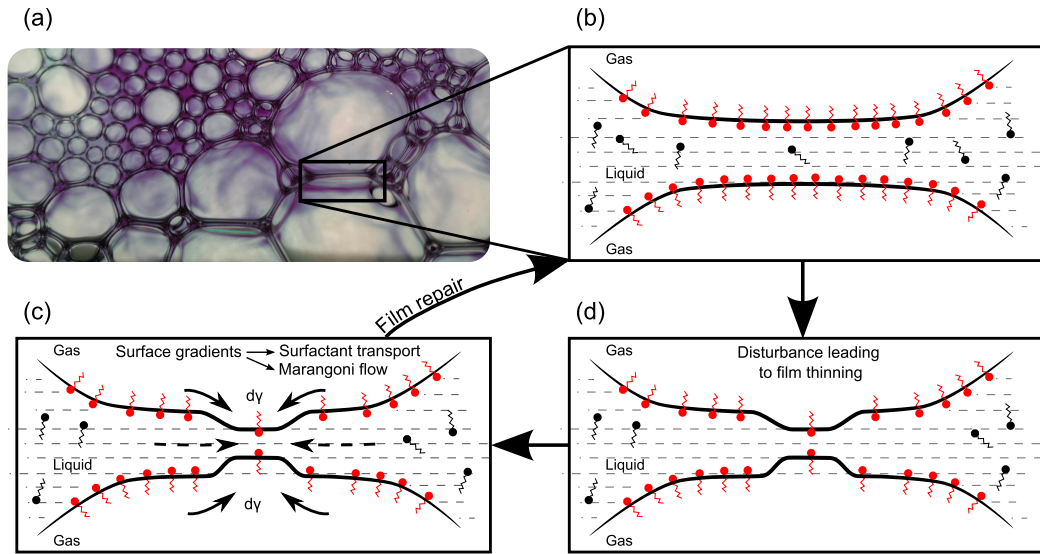


Figure 1.5: Foam structure and internal molecular film repair mechanism by Marangoni flows.

interface consists only of water molecules and  $\gamma = \gamma_{\text{pure solvent}}$  (for water, 72.8 mN/m as shown in Fig. 1.4b). In time surfactant molecules get adsorbed on the surface, reducing  $\gamma$ . The time it takes to reach equilibrium can vary from milliseconds to hours or even days depending on the surfactant. The equilibrium and the dynamic surface tension are discussed in detail in Chapter 2.

### 1.2.3 Foamability

The term ‘foamability’ is ambiguous. To make foamability definite, (i) an experiment must be specified, and (ii) the measured quantity (foam height, foam mass, foam density) must be specified. The measured foam quantities vary substantially for same surfactant solution if the foam is produced in different ways, for instance by shaking or by sparging. The shaking method produces foam by a random and turbulent mixing of the solution and gas. In two independent shaking experiments, the foaming process would vary randomly. On the other hand, the foaming by the sparging method is controllable and reproducible.

In gas well deliquification, foam serves the purpose of removing liquids. Therefore, a foamability is defined as the density of produced foam in a sparging method (see §3.3).

### 1.2.4 Foam formation

Fig. 1.5a shows a typical foam structure. We can see that the bubbles do not coalesce (merge) unlike bubbles in pure water. The bubbles together form a 3D structure (not visible) which possess a certain mechanical strength. "All foams are thermodynamically unstable".

cally unstable, due to their high interfacial free energy"<sup>[6]</sup>. However the presence of surfactants stabilizes the foam films, making them metastable.

The time dependant adsorption of surfactants plays an important role in foaming. Gibbs<sup>[7]</sup> noticed that for an interface with adsorbed surfactant, a change in its surface area causes a change in its surface tension. If an interface is expanded, then the surface tension increases and *vice-versa*. The surface tension changes because the surfactant surface coverage changes. This is known as the Gibbs effect. A perturbed interface will relax over time to its equilibrium surfactant surface coverage. During the relaxation period the surfactant will be transported to or from the perturbed surface.

A foam film (Fig. 1.5b) subjected to disturbance leading to film thinning is seen in Fig. 1.5d. Film thinning leads to an increase in the local surface area. Due to the Gibbs effect, the surface tension at the locally thinned region is higher than at the surrounding regions. These surface tension gradients over the thinned region cause Marangoni flows from the region of low surface tension (healthy film region) to high surface tension (thinned film region). These Marangoni flows transport liquid mass to the thinned film, thus stabilizing it. Thus together, these Gibbs-Marangoni effects assist in repairing the thinned film.

In the case of local thinning within foam films, the Gibbs effect is followed by the relaxation period. The relaxation period includes transport of surfactant due to concentration gradient, and the transport of surfactant via the Marangoni flows. Adsorption of new surfactants from the bulk to the part of the interface with increased surface tension should be sufficiently slow, to allow Marangoni flow to repair the film. Very fast surfactant adsorption does not allow the creation of surface tension gradients. Successful film repair instance requires that sufficient liquid mass is transported to the thinned region before the surface tension gradients disappear.

### 1.3 Rosen's empirical approach

No general theory or model for foamability exists. Few attempts have been made to connect the fundamental properties of the surfactant solution, such as the dynamic surface tension, with the observed foam formation. Different methods to create foam were used in these attempts, making a direct comparison of the results difficult. There is no singular method to produce foams.

Rosen and Hua suggested an empirical approach to link the dynamic surface tension (DST) with foamability. In a series of eight papers they showed a method to analyze DST data using an empirical equation and successfully demonstrated a connection between the DST of surfactants and their foaming behaviour<sup>[8-15]</sup>.

A typical shape of DST curve behaviour such as shown in Fig. 1.4b can be fitted

to the following equation<sup>[8]</sup>,

$$\gamma_t = \gamma_m + \frac{\gamma_0 - \gamma_m}{1 + (t/t^*)^n} \quad (1.1)$$

where  $\gamma_t$  (mN/m) is the surface tension at time  $t$ ,  $\gamma_0$  is surface tension of the solvent (in the current work 72.8 mN/m at 20°C and 1 atm for water). Here  $\gamma_m$ ,  $t^*$  and  $n$  are the fit parameters that are further explained in Chapter 2.

Consider the case of film thinning which increases the surface area initiating the relaxation process. If the relaxation of surfactants is rapid, then the surface tension gradients over the (foam) film surface will disappear halting the Marangoni flows. On the other hand, in the case of slow relaxation, then the (foam) film surface will not see sufficient magnitude of the surface tension gradients for the Marangoni flows. Thus the relaxation in time plays an important role in the total volume transported due to the Marangoni flows. The relaxation behaviour can be studied by the DST curves. A larger gradient of DST indicates rapid relaxation of the surface and *vice-versa*.

Rosen et al.<sup>[11]</sup> showed that  $d\gamma_t/d\log t$  has a maximum at  $t = t^*$ , Differentiating Equation 1.1,

$$\frac{d\gamma_t}{dt} = \frac{(\gamma_0 - \gamma_m)[n(t/t^*)^{n-1}]}{t^*[1 + (t/t^*)^2]^2}$$

At  $t = t^*$

$$\left(\frac{\partial\gamma_t}{\partial t}\right)_{t=t^*} = \frac{n(\gamma_0 - \gamma_m)}{4t^*} \quad (1.2)$$

Parameter  $n(\gamma_0 - \gamma_m)/t^*$  was shown to be strongly correlated with the foamability (See Fig. 1.6). The foaming behaviour was tested by the Ross-Miles test<sup>[16]</sup>, which measures the height of foam created under standard conditions (§2.4).

## 1.4 Other correlations for foamability

The strongest correlation was shown by Rosen et al.<sup>[11]</sup>. Fig. 1.6 and 1.7 show their correlation. This correlation was tested independently by different authors<sup>[17,18]</sup>. An increase in the Rosen parameter was shown to be inversely proportional to the maximum weight of foam produced<sup>[17]</sup> and the initial foam height in the Ross-Miles test<sup>[18]</sup>. This is opposite of the direct proportionality found by Rosen et al.<sup>[11]</sup>. It was suggested that increased surface tension reduction rate decreases foamability because a rapid surfactant transfer to interface does not allow creation of sufficient magnitude and duration of surface tension gradients for healing action by the Marangoni effect<sup>[18,19]</sup>. Contrary to the inverse proportionality dynamic surface activity,  $R_{1/2}$  was shown to be directly proportional to initial foam height in the Bikerman test<sup>[20,21]</sup>.

$$R_{1/2} = \frac{(\gamma_0 - \gamma_m)}{2t^*} \quad (1.3)$$

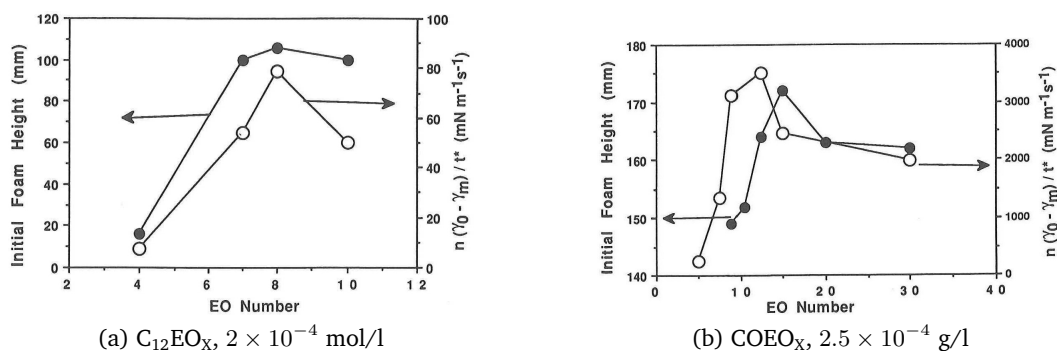


Figure 1.6: Qualitative relation between the foam height and the Rosen parameter vs. oxyethylene group number at  $25^\circ\text{C}$ .  $\text{C}_{12}\text{EO}_X$  is dodecyl (X) polyoxyethylene ether and  $\text{COEO}_X$  is (X) polyoxyethylenated nonylphenols. From Rosen et al. [11].

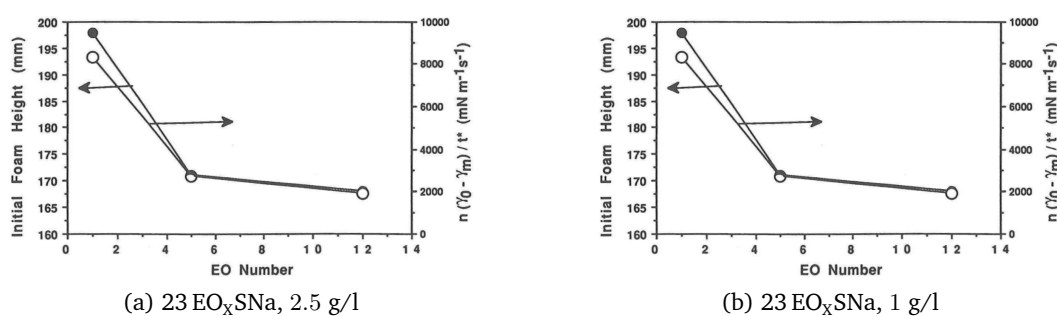


Figure 1.7: Qualitative relation between the foam height and the Rosen parameter at different oxyethylene group numbers at  $25^\circ\text{C}$  in 0.1 M NaCl.  $23\text{EO}_X\text{Na}$  is  $\text{C}_{12-13}\text{H}_{25-27}(\text{OC}_2\text{H}_4)_X\text{SO}_4\text{Na}$ . From Rosen et al. [11].

When air is bubbled rapidly in a very short time using a Bikerman test, if the surfactants cannot adsorb at the air-water interface, then, the foam thus formed will not be stable [20,21].

Prins and van Kalsbeek [22] present a general overview of studies linking foaming behaviour with interfacial dynamics. Several attempts were made to relate dynamic surface tension to foamability [11,17-21,23-25] with varying extent of success. Of these, very few correlations are within the context of gas well deliquification [17,24]. In all these studies a connection between the dynamic surface tension and foamability was found. However, the validity of these results should be carefully evaluated. Nguyen [17] uses the Gibbs isotherm to calculate the surface excess concentration when the bulk concentration is 4 to 20 times the c.m.c. (§2.1.1). It is well known that the Gibbs isotherm is only valid for dilute surfactant solutions [26], such that the activity coefficient equals one. Using the (wrongly) determined surface excess concentration a relation to foamability was shown by Nguyen [17].

Widely contradicting ideas and correlations for foamability are present throughout the literature. Though such contradictions could also be attributed to the method of foaming; it might also indicate that the rate controlling step for foaming varies

with the method of foam generation.

## 1.5 Research question

A model of large scale foam flow is crucial to be able to optimize the use of foamers for the purpose of gas well deliquification. To develop such a large scale model, the foaming behaviour at a small scale should be known, which in turn depends on the dynamics of the surfactants. It is thus important that these dynamics of surfactants and the foaming behaviour are characterized using suitable parameters.

The mass density of foam produced is relevant for the current application as liquid needs to be removed from the gas well. The mass density can be determined using a Bikerman setup (sparging), modified to allow foam overflow into a weighing scale. Surface tension reduction due to surfactants is essential for stabilizing a foam film. As foam is a dynamic structure, the surface tension does not reach the equilibrium value.

The dynamic surface tension has been previously shown to correlate with foaming (Fig. 1.6) and elsewhere<sup>[11,17–21,23–25]</sup> in the literature. However there is no agreement on how exactly, for any experimental setup. It is the intention of the current study to understand the effect of DST on the mass density of foam; which, is crucial for the application in gas well deliquification.

This thesis will answer following the research question,

*How does the dynamic and the equilibrium surface tension relate to the mass density and the total mass of foam generated in a modified Bikerman setup?*

## 1.6 Outline

Chapter 2 presents the theories and concepts which are essential for the reader to comprehend the analysis. The theories of dynamic and equilibrium surface tension relevant to current work are described. In addition, a section on foams will describe the phenomena within foams affecting its foamability/stability. A section on various methods of foam generation and existing correlations for foamability is meant to present the state-of-art.

Chapter 3 describes all the experimental tools employed during the current thesis. Chapter 4 contains important experimental results and their analysis. The research question outlined in the previous section will be answered based on the results from this chapter. Finally, Chapter 5 is dedicated to summarize and conclude the masters thesis. Additional work will be recommended based on the conclusions and experience gained during thesis. These recommendations will indicate the focus areas to continue the current work.

---

## 2. Background theories

---

This chapter will present an overview of the scientific literature relevant for this thesis. Starting with the fundamental properties of aqueous surfactant solutions the discussion will continue to a general physiochemical theory of foams. Additional information on foam drainage and the importance of micellar kinetics in foams is also presented. The typical methods of measuring foamability along with a summary of existing correlations between the dynamic surface tension and the foamability in the literature, are discussed at the end.

### 2.1 Surfactant properties in aqueous solutions

In a surfactant solution, surfactant adsorption at the interface lowers the surface tension. Adsorption is a dynamic process. Therefore properties of aqueous surfactant solutions can be studied at equilibrium and as a function of time.

Bulk concentration and surface tension are directly measurable while adsorption is not. Accordingly, the study of aqueous surfactant solution uses the bulk concentration and the surface tension as a means to determine the adsorption properties.

#### 2.1.1 Equilibrium surface tension

As the bulk concentration,  $c$  (mM/l), increases, the surface tension,  $\gamma$  (mN/m), reduces until the critical micelle concentration (c.m.c.). Beyond the c.m.c.,  $\gamma$  remains almost constant (See Fig. 2.1). At the c.m.c., surfactants in the bulk self-assemble into aggregates known as micelles. Micelles are 3D structures containing at least around hundred monomers<sup>[27]</sup>, arranged such that their hydrophilic heads face the water, shielding the hydrophobic tails from being exposed to water. The c.m.c. is a property of the surfactant in a given solvent and is a measure of the surfactant monomer solubility and its adsorption saturation. The driving force for micellization is related to increasing the total entropy of surfactants and water molecules<sup>[28]</sup>.

Adsorption is quantified using an isotherm which is an equation relating the bulk concentration,  $c$  (mM/l), to the corresponding surface excess concentration,  $\Gamma$  (mol/m<sup>2</sup>). It is derived from fundamental thermodynamic principles. However, in order to obtain  $\Gamma$  from experimentally accessible parameters,  $\gamma$  and  $c$ , a surface equation of state is required in addition to the isotherm.

A surface equation of state can be conceptually compared with an equation of

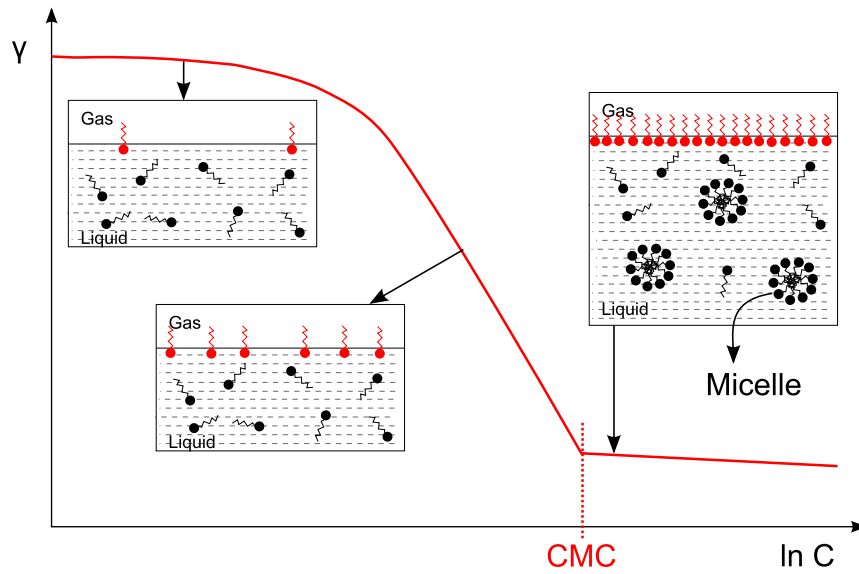


Figure 2.1: Schematic of equilibrium surface tension as a function of surfactant concentration with molecular picture at bulk and interface.

state<sup>1</sup> for gasses, such as the ideal gas law. The surfactant monomers at a 2D interface behave analogous to the gas molecules in a 3D space. Thus a monolayer of surfactants exhibit surface pressure,  $\Pi$  (mN/m), with the dimension of force per length; one length dimension less than the bulk pressure. A 3D equation of state relates the bulk gas pressure and the concentration; similarly, a 2D surface equation of state for surfactants is a relation between their surface pressure,  $\Pi = \gamma_0 - \gamma$  and surface excess concentration (i. e.  $\Gamma$ ).  $\gamma_0$  is the surface tension of water devoid of any surfactants. The adsorption isotherms and the surface equations of states can be derived from thermodynamics<sup>[29]</sup>.

### Adsorption isotherms

The choice of appropriate isotherm depends not only on the concentration and the molecular nature of that surfactant, but also on the presence of electrolytes. All the isotherms described here are applicable only at the pre-micellar concentrations. At dilute concentrations, the activity coefficient equals one and the chemical potential can be approximated by the concentration. This allows the use of the Gibbs isotherm in the following form,

$$\Gamma = -\frac{1}{n_1 RT} \left( \frac{d\gamma}{d \ln c} \right) \quad (2.1)$$

where  $R$  (mN.m/mol.K) is the gas constant;  $T$  (K) is the temperature.  $n_1$  is a factor accounting for adsorption of counterions. The value of  $n_1$  depends on the charges

<sup>1</sup>The equations of state intended for a comparison are the ones which relates pressure versus concentration and not between other state variables.

of the surfactant ion, the counterion, and the salt ions<sup>[26,27,30]</sup>. An isotherm must be applicable to the physical nature of adsorbed surfactants. For instance, an isotherm including the effect of charged adsorbed layer should be used for ionic surfactants. A good fit to equilibrium surface tension alone does not ensure correctness of the derived parameter,  $\Gamma$ . In the next section few isotherms which will be used later are described. The isotherms including typical effects such as the surface layer compression, ionic surface charges, and the surfactant reorientation are presented.

**Langmuir isotherm:** The Langmuir isotherm is a popular isotherm which gives a satisfactory fit for a lot of surfactants. It includes a uniform lattice-type model with no solvent or solute interactions. In principle, this assumption is incorrect for all the surfactants, but it can still provide a satisfactory fit for pure surfactants or with electrolytes in the solution (via  $n_1$ ). The corresponding surface equation of states are Szyszkowski or Frumkin (not to be confused with Frumkin isotherm)<sup>[26]</sup>,

$$\Gamma = \Gamma_{Lm} \frac{K_L c}{1 + K_L c} \quad \text{Langmuir isotherm} \quad (2.2a)$$

$$\Pi = n_1 RT \Gamma_{Lm} \ln(1 + K_L c) \quad \text{Szyszkowski equation of state} \quad (2.2b)$$

$$\Pi = -n_1 RT \Gamma_{Lm} \ln\left(1 - \frac{\Gamma}{\Gamma_{Lm}}\right) \quad \text{Frumkin equation of state} \quad (2.2c)$$

where  $\Pi$  (mN/m) is the surface pressure;  $R$  (mN.m/mol.K) is the ideal gas constant;  $\Gamma_{Lm}$  (mol/m<sup>2</sup>) is the theoretical maximum surface excess concentration and  $K_L$  (l/mM) is the Langmuir equilibrium adsorption constant.  $n_1$  is a factor accounting for the adsorption of counterions.

**Frumkin Compressibility (FC Model):** This is the classical Frumkin isotherm modified to include 2D compression of surfactants. It includes solute-solvent interactions (via  $a$ ) at the surface, but does not include effect of ionic charges.

$$bc = \frac{\theta}{1 - \theta} \exp(-2a\theta) \quad \text{FC isotherm} \quad (2.3a)$$

$$- \frac{\Pi \omega_0}{RT} = \ln(1 - \theta) + a\theta^2 \quad \text{Equation of state} \quad (2.3b)$$

$$\omega = \omega_0(1 - \varepsilon \Pi \theta) \quad (2.3c)$$

$$\theta = \Gamma \omega \quad (2.3d)$$

where  $\omega_0$  (m<sup>2</sup>/mol) is the molar area of the surfactant at  $\Pi = 0$ , that is molar area of the solvent molecule;  $a$  is the intermolecular interaction constant;  $b$  (l/mM) is the adsorption equilibrium constant; and  $\varepsilon$  (m/mN) is the 2D compression ratio of surfactant monomers in a packed surface layer. Usually  $\varepsilon \simeq 0.005 - 0.01$  m/mN<sup>[31]</sup>. This model considers that the molar area of surfactants,  $\omega$  (m<sup>2</sup>/mol), is a linear function of surface pressure and fractional surface coverage,  $\theta = \Gamma \omega$ . When  $\varepsilon = 0$ , the model is same as the classical Frumkin isotherm.

**Frumkin Ionic Compressibility (FIC Model):** This is the FC model modified for ionic surfactants and presence of electrolytes.

$$b [c(c + c_c)]^{1/2} f = \frac{\theta^{1+2\varphi}}{1 - \theta} \exp(-2a\theta) \quad \text{FIC isotherm} \quad (2.4a)$$

$$\Pi = -\frac{2RT}{\omega_0} [\ln(1 - \theta) - \varphi\theta + a\theta^2] \quad \text{Equation of state} \quad (2.4b)$$

$$\omega = \omega_0(1 - \varepsilon\Pi\theta) \quad (2.4c)$$

$$\theta = \Gamma\omega \quad (2.4d)$$

$$\log_{10} f = -\frac{0.5115\sqrt{I}}{1 + 1.316\sqrt{I}} + 0.055I \quad (2.4e)$$

where  $c_c$  (mM/l) is the counterion concentration;  $\varphi$  is the parameter to account for the fraction of surface-active ions which are not bound by counterions in the surface layer ( $0 \leq \varphi \leq 0.5$ );  $f$  is the average activity coefficient of ions in bulk solution from the Debye–Hückel equation 2.4e corrected for short-range interactions<sup>[32,33]</sup>.  $I$  (mol/l) is the ionic strength given by  $I = \frac{1}{2} \sum_{i=1}^n c_i z_i^2$ . Here  $c_i$ , (mol/l) is the concentration of ion  $i$ ;  $z_i$  is the charge number of ion  $i$ .

**Reorientation Compressibility (RC Model)** This model considers that two states of surfactant monomers coexist at the surface with molar areas  $\omega_1$  and  $\omega_2$ , which is often the case for non-ionic polyoxyethylene surfactants. For definiteness,  $\omega_2 > \omega_1$ . For instance state 1 can be the surfactant molecule adsorbed at an angle (or convoluted) to the surface. The state 2 can be the surfactant molecule adsorbed while lying flat (along) the surface.

$$b_1 c = \frac{\Gamma_1 \omega}{(1 - \theta)^{\omega_1/\omega}} \quad \text{Reorientation A isotherm} \quad (2.5a)$$

$$-\frac{\Pi\omega}{RT} = \ln(1 - \theta) \quad \text{Equation of state} \quad (2.5b)$$

$$\Gamma = \Gamma_1 + \Gamma_2 \quad (2.5c)$$

$$\Gamma\omega = \theta = \omega_1\Gamma_1 + \omega_2\Gamma_2 \quad (2.5d)$$

$$\omega_1 = \omega_{10}(1 - \varepsilon\Pi\theta) \quad (2.5e)$$

$$\frac{\Gamma_2}{\Gamma_1} = \left(\frac{\omega_2}{\omega_1}\right)^\alpha \exp\left(\frac{\omega_2 - \omega_1}{\omega}\right) \exp\left[-\frac{\Pi(\omega_2 - \omega_1)}{RT}\right] \quad (2.5f)$$

where  $\omega_{10}$  is the molar area of the surfactant in state 1 at  $\Pi = 0$ .  $\alpha$  is a constant accounting that the adsorption of the surfactant molecules in state 2 (with larger area) can be more than that of state 1. Further details can be found elsewhere<sup>[31,34]</sup>. As an example, the existence of nonionic  $C_nEO_m$  surfactants in two states of varying molar areas is justified based on the molecular structure. The hydrophilic part (that is EO) exhibits surface activity at low surface pressures<sup>[35]</sup>. At larger surface pressures, the surfactant molecule adsorption has to occupy minimal area; that is

the hydrophilic EO group reorients in the water phase to reduce the molar area. In addition, at larger surface pressures the molar area linearly decreased as observed by X-ray diffraction<sup>[36]</sup>. This effect is included by the linear compressibility of the convoluted state 1 at higher surface pressures (see Eq. 2.5e). The RC model considers these effects together with approximation for non-ideal entropy (details elsewhere<sup>[35]</sup>).

FC, FIC and RC models are complex isotherms requiring advanced numerical solving techniques. Aksenenko<sup>[37]</sup> presents an approach to solve these isotherms numerically. A collaborative project led by Dr. Reinhard Miller, *Max Planck Institute of Colloids and Interfaces* has made these isotherms available via *ISOFIT*, a free software<sup>[38]</sup>.

### 2.1.2 Dynamic surface tension

When an air-water interface is newly formed in an aqueous surfactant solution it has the surface tension of water, i. e. 72.8 mN/m<sup>[39]</sup> at 20° and atmospheric pressure. In time the surface tension will drop to its equilibrium value. The time dependant surface tension is called as the dynamic surface tension (DST). Surface tension of the surfactant solution depends on the surface excess concentration of the surfactants. Adsorption is a dynamic process which depends on the transport of the surfactant monomers from the bulk to the surface. This transport includes two steps – (i) transport of surfactants from the bulk to the subsurface (an imaginary layer below the physical surface which is few molecular diameters thick<sup>[40]</sup>,  $\mathcal{O}(\text{\AA})$ ), and (ii) exchange between the subsurface and the surface<sup>[26,39,41]</sup>.

In absence of flow, the first step consists of surfactant transfer due to diffusion towards the subsurface. Molecules reaching the subsurface will then adsorb on the surface in the second step. The adsorption can involve activation energy barriers due to effects like reorientation as shown in Fig. 2.2b. Ward and Tordai<sup>[40]</sup> modeled the first step, that is, the surfactant transfer due to diffusion from the bulk to the subsurface. Assuming that adsorption is faster than diffusion, the Ward-Tordai model can be used to determine the diffusion coefficients. In foaming the positive contribution from the convective transfer can have a big impact on the characteristic time scales of surfactant transport to the subsurface for a diffusion controlled adsorption. To be precise, the characteristic time will be lower in a diffusion-convection transport than a pure diffusion transport<sup>[42,43]</sup> which might change the rate controlling step. Chang and Franses<sup>[26]</sup>, Eastoe and Dalton<sup>[39]</sup> present a review on the diffusion-adsorption models for surfactant transport.

Rosen and Hua<sup>[8]</sup> proposed an empirical method to model a DST curve. A typical DST plot shown in Fig. 2.3a consists of four regions; (I) induction region; (II) rapid fall region; (III) meso-equilibrium region; and (IV) equilibrium region. An equation of the following type fits the first three regions,

$$\gamma_t = \gamma_m + \frac{(\gamma_0 - \gamma_m)}{[1 + (t/t^*)^n]} \quad (2.6)$$

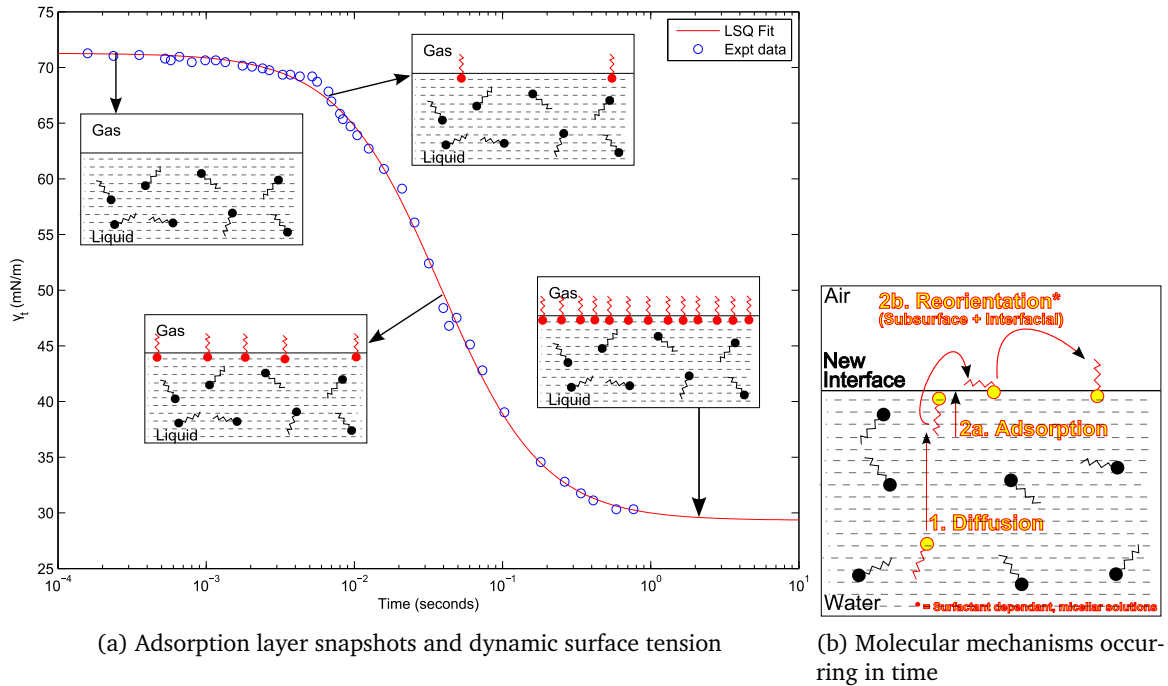


Figure 2.2: Schematic diagram of dynamic adsorption layers leading to time dependence of surface tension

where  $\gamma_t$  is the surface tension at a surface age  $t$ . Three fit parameters;  $t^*$ ,  $n$ , and  $\gamma_m$ , can be determined by using a curve fitting technique such as the method of least squares<sup>[44]</sup>.

At  $t = t^*$ ,  $\gamma_t$  has dropped by half of  $\gamma_0 - \gamma_m$  (Fig. 2.3b) and the DST curve has its maximum slope<sup>[10]</sup>.  $n$  is shown to be related to the hydrophobicity of a surfactant in a given environment. Higher hydrophobicity implies a steeper gradient (see Fig. 2.3c) in the rapid fall region and thus higher value of  $n$ <sup>[14,20,21]</sup>.  $\gamma_m$  is crudely defined as "surface tension which shows little further change with increase in time ( $< 1 \text{ mN/m}$  in  $30 \text{ s}$ )"<sup>[9]</sup> as shown in Fig. 2.3d. It is also observed that in many cases  $\gamma_m$  is approximately equal to  $\gamma_{eq}$ .

In order to make a definite three parameter curve fit, the  $\gamma_m$  should be distinctly visible in the measurement data. At low surfactant concentrations it might take very long to reach  $\gamma_m$ . If  $\gamma_m$  is not visible in the available data then a two parameter fit is performed by assuming  $\gamma_m = \gamma_{eq}$  in current work.

## 2.2 Foam structure and density

Aqueous foam is a dispersion of gas in water with a relatively large fraction of air. Foam structure is determined by the volumetric liquid fraction. Two extreme types of foams are; (i) small liquid fraction with polyhedral bubbles, or (ii) large liquid fraction with spherical bubbles. The common wall between two bubbles is called

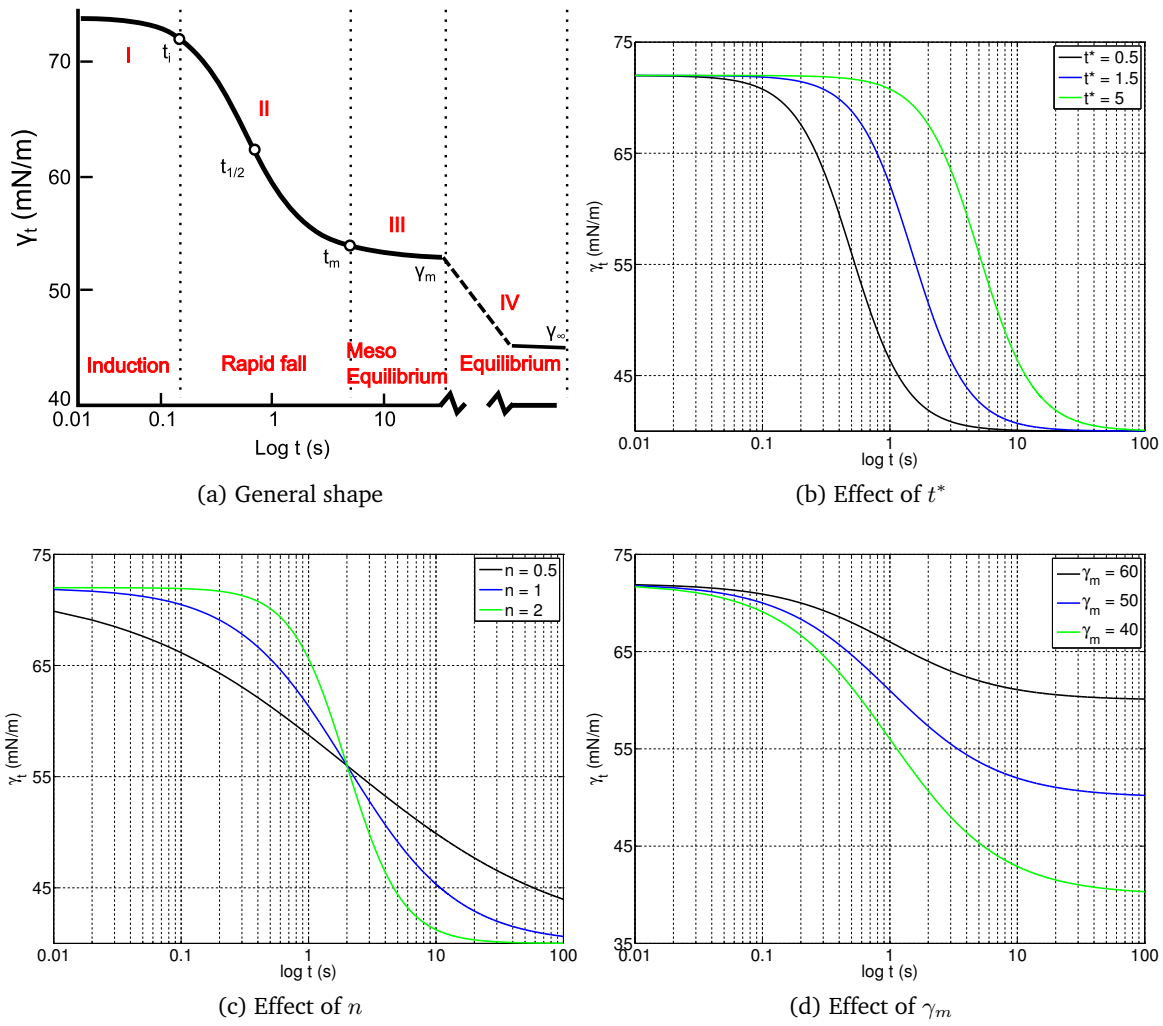


Figure 2.3: Rosen's empirical approach for DST analysis using fit parameters  $t^*$ ,  $n$  and  $\gamma_m$ .

as the foam film. A *plateau border* is where three films meet at an angle of  $120^\circ$ <sup>[1]</sup>. Four plateau borders meet at angle of  $109.47^\circ$  in a *vertex*. Any other arrangement will immediately cause structural rearrangement to meet these rules. These rules are only for dry foams. Wet foam structure can vary depending on geometry of the bubbles<sup>[45]</sup>.

A foam with polyhedral bubbles contains less water than a foam with spherical bubbles; hence is termed as dry foam and wet foam respectively. Foam wetness defined by a density term could be used as a foamer characterization parameter for current application of removal of liquids from gas wells. Higher foam density means a wet foam and *vice-versa*.

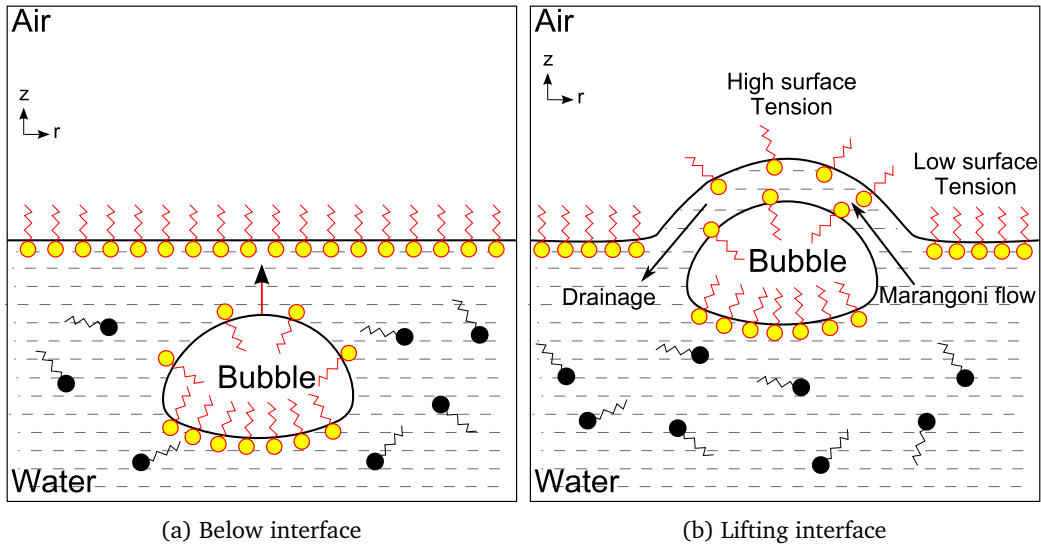


Figure 2.4: Schematic of a bubble rising in surfactant solution. Presence of surfactants creates surface tension gradients when a rising bubble stretches the interface.

## 2.3 Physiochemical theory of foaming

As foam contains immiscible phases, according to thermodynamic principles there is a driving force to reduce the interfacial area between phases. Thus all foams are inherently meta-stable. Pure liquids do not foam whereas presence of surfactants leads to foam of a certain lifetime. Thus surfactant adsorption prevents the foam from collapsing. The main surfactant induced stabilizing mechanisms will be described in this section.

### 2.3.1 Gibbs-Marangoni effect

Consider a bubble rising through a bulk surfactant solution as shown in Fig. 2.4a. As it rises surfactants get adsorbed on its surface. Surface coverage at the top of bubble is lower than at the bottom of bubble<sup>[46]</sup>. Such uneven surface coverage increases the drag force reducing bubble rise velocity. A bubble approaching the air-liquid interface will lift a film of liquid, thereby, increasing the surface area. The lifted section has a smaller surface excess concentration than the rest of the surface. Gibbs<sup>[7]</sup> discovered that a change in surface area of surfactant solutions leads to a change in the surface tension and thus defined surface elasticity as,

$$E = \frac{d\gamma}{d \ln A} \quad (2.7)$$

where,  $E$  (mN/m) is the Gibbs elasticity; and  $A$  (m<sup>2</sup>) is the surface area.

The tangential gradients in the surface tension causes convective flow of liquid towards the high surface tension region<sup>[47]</sup> (low surface pressure). Such a flow stabilizes a film lifted by the rising bubble preventing it from rupturing. Bulk motion

induced by the tangential gradients in surface tension, is known as the Marangoni effect. This effect is critical to 'stabilize' the newly formed films. Collectively these Gibbs-Marangoni effects are responsible for foam film existence.

Considering the case of an isothermal interface with adsorbed surfactants, the only way to create surface tension gradients will be through non-uniform surfactant surface excess concentration. A non-uniform surfactant surface excess concentration will relax in time. The relaxation period includes transport of surfactant due to concentration gradient, and the transport of surfactant via the Marangoni flows. As relaxation occurs, the surface tension gradients, which are the driving force for the Marangoni flow decrease. Successful film repair instance requires that sufficient liquid mass is transported to the thinned region before the surface tension gradients disappear. An estimate of the magnitude of the surface tension gradient, which is the key driving force for the Marangoni effect, can be made by experimentally measuring the dynamic surface tension. Rosen et al. suggested an approach to quantify the Marangoni effect in a given solution. Differentiating their empirical DST equation 2.6,

$$\frac{d\gamma_t}{dt} = \frac{(\gamma_0 - \gamma_m)[n(t/t^*)^{n-1}]}{t^*[1 + (t/t^*)^2]^2}$$

Evaluating this at  $t = t^*$ ,

$$\left(\frac{\partial\gamma_t}{\partial t}\right)_{t=t^*} = \frac{n(\gamma_0 - \gamma_m)}{4t^*} \quad (2.8)$$

Thus the parameter  $n(\gamma_0 - \gamma_m)/t^*$  was shown as a measure of maximum Marangoni effect for any given surfactant solution. Foaming includes creation of a large number of bubbles in a short period of time. Thus for instantaneous rapid foaming the Marangoni effect might be the rate controlling factor for foamability. Using this argument, foamability was shown to be strongly correlated with the parameter  $n(\gamma_0 - \gamma)/t^*$  (Fig. 1.6).

The gradients in surface excess concentration of surfactants cause both, Marangoni effects and surfactant transport by bulk/surface diffusion<sup>[48]</sup>. The key is that the local surface tension gradients occurring in foams must result in sufficient Marangoni flow to 'heal' the film before the surfactant transport destroys these gradients. If the adsorption is too little, then the surface tension gradients might be too low to cause any significant Marangoni effect. On the other hand, if the bulk concentration is too high then surface tension gradients might never appear. Maximum foamability is usually observed when the bulk concentration is around the critical micellar concentration<sup>[27,49]</sup>; that is the surface coverage is close to its saturation limit.

### 2.3.2 Drainage

Drainage is the loss of interstitial liquid in foams. The driving force for drainage is the gravitational force and capillary suction. Gravity effects are higher in wet

foams than dry foams whereas capillary suction contribution is larger for dry foams than wet foams. This is intuitively justified as wet foams have relatively higher mass and that the gravitational force is proportional to the mass. Capillary suction is the loss of liquid through the plateau borders due to pressure difference between the plateau border and the vertices. In a wet foam with spherical bubbles, the radius of curvature at the plateau border and at the vertices is almost the same. Thus from the Young-Laplace law (Eq. 3.1) there is almost no pressure drop between the plateau borders and the vertices; consequently capillary suction effect is negligible.

The drainage through plateau borders depends on the bulk viscosity and the water-air interfacial properties. Liquid with higher bulk and surface viscosity<sup>2</sup> will drain slower. The interfacial properties can be determined using surface rheology experiments<sup>[50]</sup>. The drainage through vertices is poorly understood currently<sup>[51]</sup>.

### 2.3.3 Micellar kinetics

A micelle is like a reservoir of neatly packed monomers. Above the c.m.c., the monomer concentration no longer increases with increasing surfactant concentration. All additional surfactants are incorporated in the micelles. When a lot of interface is created in a short time during foaming, the monomers in the bulk solution get adsorbed at the interface. In order to sustain a newly formed interface sufficient monomers must be available in the bulk. If the supply of monomers falls short while creating new interface then the interface will rupture. Thus the relative micellar break up time should be faster than the foaming process, if not, the foaming can be adversely affected.

The micellar dissolution time constant for ionic surfactants,  $\tau_2$  is  $\mathcal{O}(ms)$  whereas for nonionics,  $\tau_2 \sim \mathcal{O}(s)$ . The magnitude of  $\tau_2$  depends on the stability of micelles and it generally increases with the bulk concentration and the structure of a micelle. Micelles in 200 mM sodium dodecyl sulfate solution (literature value of c.m.c. = 8mM) are most stable (highest  $\tau_2$ ) and at that concentration the foamability was found to be lowest<sup>[52]</sup> using the Ross-Miles test. The typical concentration for gas well deliquification application is two to three times c.m.c., so micellar kinetics might have an impact.

## 2.4 Methods of foam generation

No common generally accepted test for determining the foaming ability<sup>[53]</sup> exists. This makes the results from research on foam hardly comparable, as the methods used to generate foam vary. The three most common methods of generating foams are – (i) Bartsch (shaking), (ii) Ross-Miles (pour test), and (iii) Bikermann (sparging). These methods are described below.

<sup>2</sup>Surface viscosity is 2D rheology analogous to the 2D bulk viscosity. The surface viscosity depends on the surfactant adsorption kinetics.

The Bartsch test is a simple shaking test. A fixed liquid volume is taken in a closed cylinder or a bottle such that more than 80% of the volume is occupied by air. The container is then shaken with a fixed frequency, amplitude and orientation, either mechanically or by hand. At the end of shaking the instantaneous foam height serves as a measure of foamability. The total liquid and gas volumes remain constant during foaming. The foam is formed rapidly due to the shaking motion and the foaming time scale is  $\sim \mathcal{O}(ms)$ .

The Ross-Miles test is a standard ASTM test<sup>[16]</sup>. 50 ml of the solution is taken in a cylinder. Using a pipette and a funnel fixed at a height of 90 cm, 200 ml of the same solution is allowed to fall into the cylinder. When all of 200 ml solution has fallen, the foam height is recorded (immediately) as the initial foam height. This value is a measure of foamability, while stability can be studied by measuring the rate of foam collapse. Ross-Miles test data is widely reported in literature concerning foam correlations and drainage analysis. In this method the liquid volume in the foam remains constant while the gas volume entering foam is not controlled. The foam is formed by impact of the falling liquid on the stationary solution. After a few layers of foam bubbles are created additional falling liquid can break the existing foam on impact. Thus the initial foam height already includes aspects of stability. The time scales of foaming are  $\sim \mathcal{O}(ms)$

The Bikerman test was first suggested by Foulk and Miller<sup>[54]</sup> and then used by Bikerman<sup>[55]</sup> with an aim to define foamability as a physical property of solutions. It is essentially a sparging test in which a fixed volume of air is sparged through porous septum into a fixed volume of solution. The height of foam obtained immediately after sparging gas serves as a measure of foamability. Bikerman also used the following definition as a standard<sup>[56]</sup>,

$$\Sigma = \frac{Vt}{v} \quad (2.9)$$

where  $\Sigma$  (s) is the Bikerman's unit of foamability,  $V$  ( $m^3$ ) is the volume of foam (from height),  $v$  ( $m^3$ ) is the volume of air injected in time  $t$  (s). This test was further modified<sup>[53,57]</sup> and patented<sup>[58]</sup> to include standard porous plate and automation. *KRÜSS DFA100*<sup>[59]</sup> implements this method.

The foaming mechanism in the Bikerman's method consists of three steps; (i) formation of bubbles at the gas sparger, (ii) rise of the bubbles through the bulk, and (iii) their transformation at the bulk liquid-air interface to foam. Here the gas volume in the foam is controlled but the foam is allowed to expand in volume freely, unlike the Bartsch test, in which the total volume in the closed contained remains fixed. The time scale of foaming in the Bikerman test depends on the time spend by the bubbles during its motion from the gas sparger to the height of surfactant solution in the column. Typically it is between a few seconds and less than a minute.

## 2.5 Summary

The fundamental physiochemical properties of aqueous surfactant solutions and their importance in foaming have been described. The number of parameters relevant for foams are too many for a complete analysis. Gibbs-Marangoni effect is suggested as one of the most important phenomena controlling foamability and an empirical method to quantify it has been shown. Brief sections on the drainage of foam and the importance of micellar kinetics are also included. A state-of-art on foamability study is presented to summarize the current status on the study of foams as a function of physiochemical properties.

---

## 3. Experimental setup

---

This chapter is dedicated to introduce and describe the experimental setups. These include the foam column used to measure foamability and the equipment used to measure surface tension (both dynamic and equilibrium). For each experimental setup, the reproducibility test will be shown. The chapter ends with information on chemicals used during this thesis.

### 3.1 Equilibrium surface tension

Equilibrium surface tension is measured by the *du Noüy* ring method using the *KRÜSS K9* tensiometer commercially sold by *KRÜSS* GmbH, Germany. The principle behind the du Noüy ring method is to directly measure the maximum pull on the interface. A du Noüy ring is a circular ring made of a noble metal alloy (usually Platinum-Iridium). Referring to Fig. 3.1, the ring is first immersed in the liquid sample and at this point the force is zero. As the ring is pulled up, the force increases. Due to the surface tension the ring will lift the liquid. The maximum force equals the surface tension of the interface. As the contact angle for noble metal alloy is zero, the force,  $F$  (N) is given by  $F = mg$ , where  $m$  (kg) is mass;  $g$  ( $\text{m/s}^2$ ) is the acceleration due to gravity). This maximum force per unit of the wetted length is related to the surface tension of that interface.

The ring lifts a certain mass of liquid. The contribution on the measured surface tension due to this mass is corrected by using correction factors. See Appendix A.1 for description of these correction factors and the procedure for measuring the surface tension.

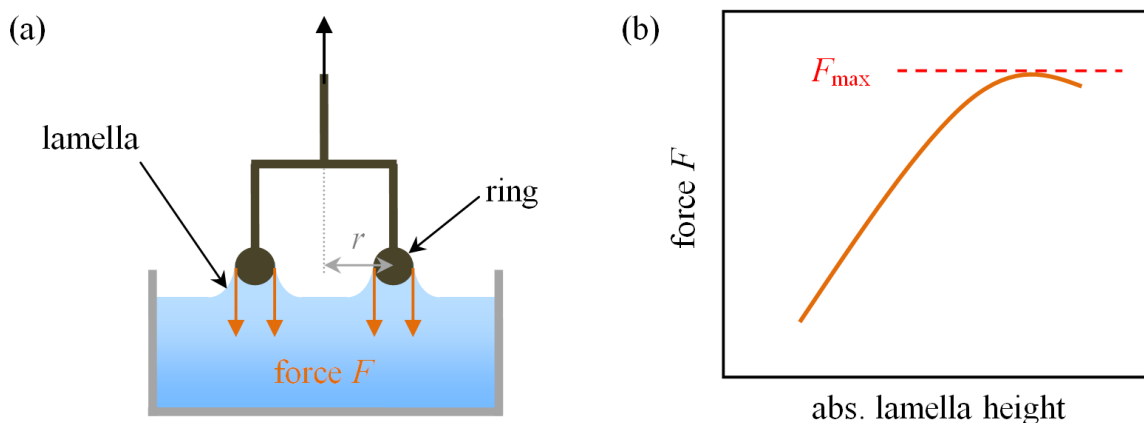


Figure 3.1: The du Noüy ring method

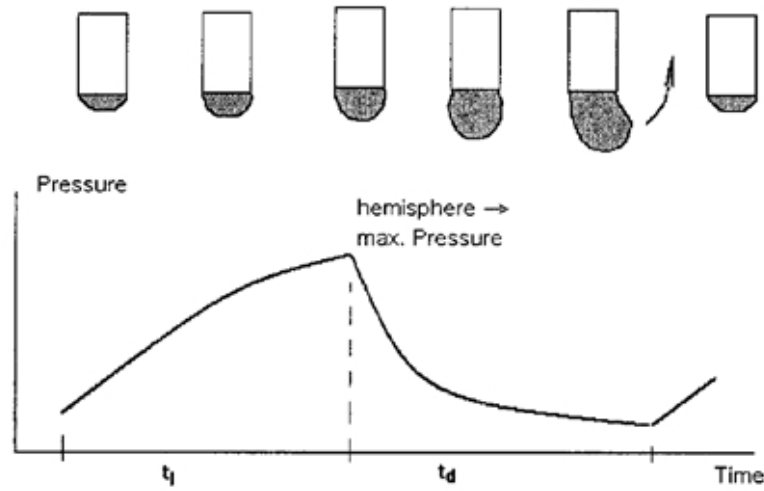


Figure 3.2: Schematic of bubble growth at tip of capillary immersed in a liquid<sup>[60]</sup>

Before measuring the surface tension every sample was stored undisturbed for 5 minutes in a temperature controlled glass vessel to ensure equilibrium at the surface and a uniform temperature. Each measurement was repeated at least three times successively while waiting for 2 minutes in between to restore the surface equilibrium.

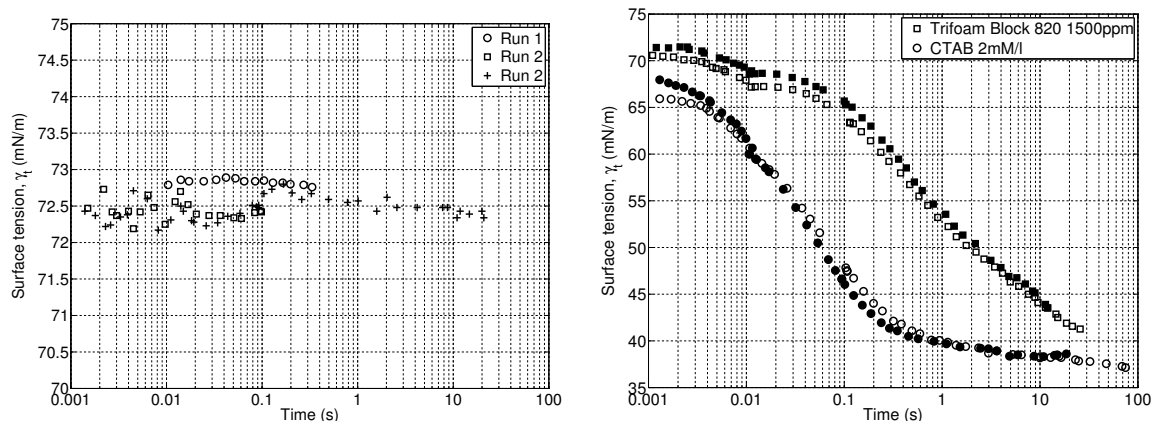
### 3.2 Dynamic surface tension

Dynamic surface tension (DST) measurements are performed using a commercially sold tensiometer *BPA-1S* by *SINTERFACE Technologies*, Germany. The tensiometer employs the maximum bubble pressure method (MPBM). It involves creating a bubble at the tip of a capillary as shown in Fig. 3.2.

The Young-Laplace law relates the surface tension of an interface with the pressure difference across that interface. It is given by,

$$\Delta P = \gamma \left( \frac{1}{R_1} + \frac{1}{R_2} \right) \quad (3.1)$$

where,  $\Delta P$  (Pa) is the pressure difference across the interface;  $\gamma$  (N/m) is the surface tension of the interface;  $R_1$  and  $R_2$  (m) are the two radii of curvature. In case of a spherical interface,  $R_1 = R_2$ . Fig. 3.2 shows the schematic of the maximum bubble pressure method. A bubble created at the tip of a capillary immersed in a liquid will grow from  $t = 0$ , when the liquid-air interface is flat. At a certain  $t = t_l$  the bubble will have same diameter as the capillary. This is the smallest possible bubble diameter. Thus, from Equation 3.1 the pressure inside the bubble will be maximum. At  $t_l < t < t_d$  the bubble grows and it finally detaches at  $t = t_l + t_d$ . Dead time,  $t_d$  (s) is the time a bubble takes to detach from the time when it has maximum pressure. By controlling the rate of bubble formation and measuring the maximum pressure inside the bubble the surface tension can be measured as a function of time.



(a) Surface tension of water shows no decrease in time indicating that the capillary is clean. Over three independent measurements (Run 1, Run 2 and Run 3) the variation is  $\leq 0.5$  mN/m.

(b) Independent dynamic surface tension measurements by *SINTERFACE* (open symbol) and self (closed symbol) showing reproducibility within  $\pm 2$  mN/m.

Figure 3.3: Reproducibility and validation of BPA-1S

BPA-1S allows measurement of the DST over a time range of 1 milliseconds to 100 seconds. The detailed routine employed to measure from the sub-millisecond time range until 100 seconds is described elsewhere<sup>[60–63]</sup>. To ensure a clean capillary, before every measurement a *control experiment* with ultra pure deionized water with a resistivity  $\rho \geq 10$  M $\Omega$ .m was performed at the temperature of  $20 \pm 0.5^\circ\text{C}$ . Fig. 3.3a shows the dynamic surface tension over the measurement range of *BPA-1S*. Decrease of the surface tension in time is an indication of the presence of surface active impurities. To ensure that the capillary is free of surface active contaminants, a control measurement with Milli-Q water is performed before each experiment. If the measured surface tension of the water is  $72.8 \pm 1$  mN/m for the entire time range covered by the device, the capillary is considered clean. If a deviation is observed, then the capillary is cleaned using the procedure described in Appendix A.2

### 3.2.1 Validation and reproducibility

From the three independent measurements with ultra pure water shown in Fig. 3.3a, it is seen that the reproducibility is within  $\pm 0.5$  mN/m. This was additionally checked by measurements by *SINTERFACE* for the same samples at their laboratory in Berlin, Germany. Fig. 3.3b shows that the agreement between the DST measurements performed at different locations and persons is within acceptable range ( $\approx 2$  mN/m). The deviation is due to unavoidable surface active impurities present due to variations in cleaning procedure and the laboratory environment.

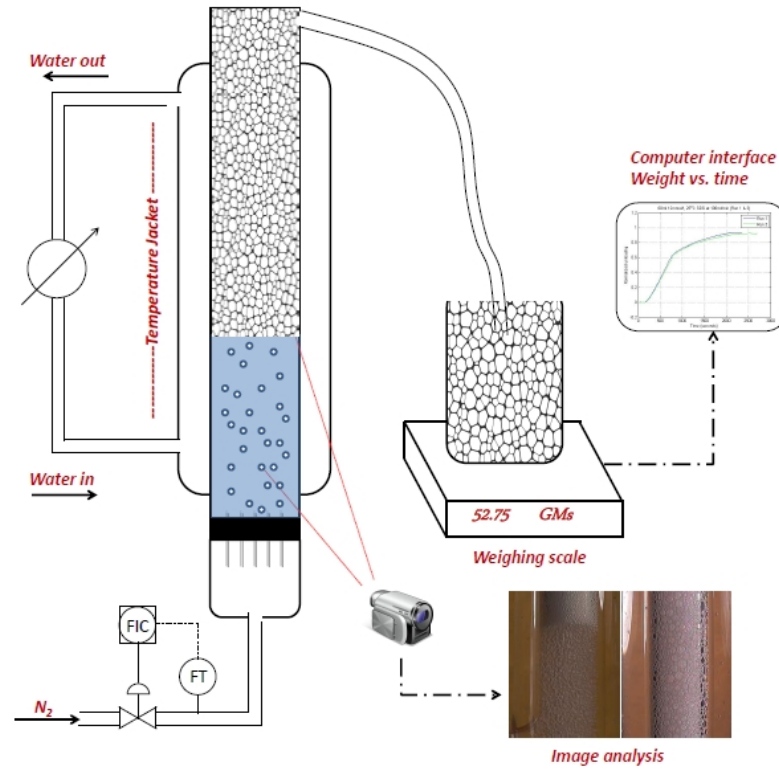


Figure 3.4: The foam column used to measure foamability. Foam is generated by (needle) gas sparger and flows upwards to collect in a bucket which is weighed. The weight of collected foam in time collected (unloading) is a measure of foamability.

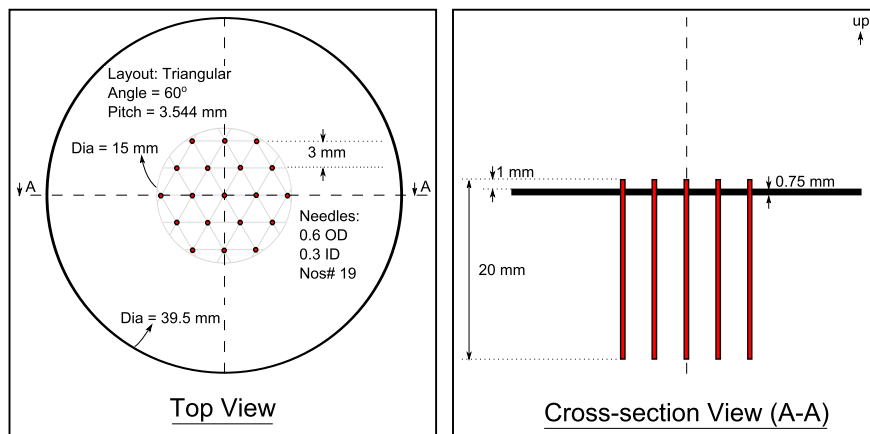


Figure 3.5: Details of the gas sparger fitted at the bottom of the foam column.

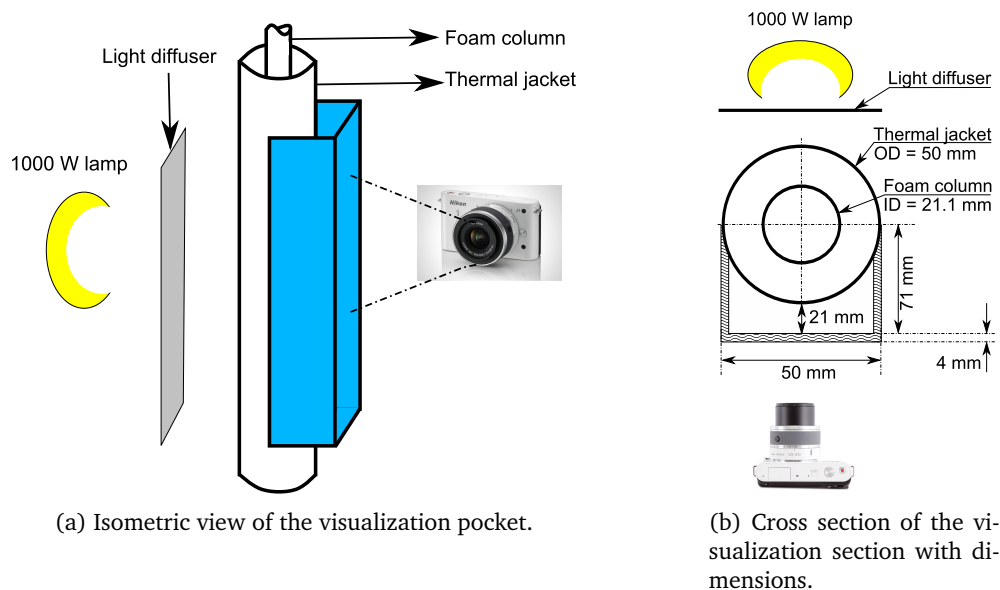


Figure 3.6: Visualization schematic.

### 3.3 Foam column

The experimental setup for generating foams is a Bikerman type sparging column modified to weigh the overflowing foam (see Fig. 3.4). It consists of a glass column  $\simeq 84$  cm high and with a 2.11 cm inner diameter. The bottom of the column is fitted with a gas sparger plate containing 19 needles, shown in Fig. 3.5. Foam is generated by sparging  $N_2$ . The top of the column contains a constriction with connection to a flexible hose. The other end of the hose is placed in a bucket on a weighing scale. The weighing scale data logging is automated to record weight each second. In time the foam created in the column flows upwards to the top of the column and through the flexible hose before collecting in the bucket. The weight of foam collected over time is analyzed to give a measure of the foamability of the test sample.

The needles are unevenly extended across the sparger plate (Fig. 3.5). Needles extend 0.1 cm from the top of the sparger; this is the side facing the column (i.e. exposed to the foaming solution). It was observed that the bubbles (formed at capillary tip) which foamed before traveling less than  $\simeq 5.5$  cm from the tip of capillary affected the foam quality. This height corresponds to a ‘dead volume’ as the bubble dynamics strongly affects foaming than the properties of the test sample. In order to compensate for this dead volume the initial volume should be increased. In current work, a sufficiently large initial volume (150 ml  $\equiv$  43 cm liquid height) is used along with the sparger design shown in Fig. 3.5.

The entire column is enclosed in a concentric column (temperature bath) through which water at fixed temperature is circulated. Thus the experiments can be performed at constant temperature. However the presence of this thermal jacket with

water introduces visual distortion while observing the foam column. A perspex rectangular pocket having same width as that of the outer concentric cylinder is glued outside of the outer concentric cylinder (Fig. 3.6). When this rectangular pocket is filled with water the visual distortion is corrected.

The rectangular pocket filled with water as shown in Fig. 3.6 corrects the visual distortion caused by the concentric thermal jacket. High speed movies of the bubbles in bulk liquid and of the foam are recorded at 400fps and at a resolution of  $640 \times 240$  pixels using the *Nikon 1 J1* consumer series camera. A 1000 W lamp is placed on the other side of the rectangular pocket with a light diffuser (sheet of translucent paper) in between.

### 3.3.1 Procedure

A typical experiment consists of placing 150 ml of test sample in the column. Nitrogen is sparged through the needles at a fixed flow rate of 200 ml/min. The nitrogen flow and the weighing scale data logging are started simultaneously. The sparger creates bubbles which rise through the bulk liquid and at the (interface) top layer of the bulk liquid, foam is formed. As foam production occurs, the bulk liquid level in the column drops. The experiment can have two possible outcomes; either all the bulk liquid transforms to foam, or the remaining liquid is unable to foam due to surfactant depletion<sup>[64]</sup>. The experimental run is terminated at either of these two outcomes. The cleaning procedure for the foam column is described in Appendix A.3.

### 3.3.2 Visualization

A typical foam column experiment yields a plot and video stills as shown in Fig. 3.7. There are three main sections associated with processes within the column. As  $N_2$  sparging begins, certain time lag is observed during which the foam generated travels through the column and then through the flexible hose. After the generated foam reaches the weighing scale a linear rise region is observed. This indicates that the liquid content in this foam does not change which is also confirmed by observing the foam structure (refer to the image stills in Fig. 3.7). Most of the liquid is unloaded during this linear rise region. In the third and last section the liquid content of foam decreases corresponding to decreasing slope in the graph. The end of third section is also the end of the experiment.

Five second long movies of the foam and the bubbles just below the foaming interface are recorded. These movies are analyzed to calculate the bubble sizes and the velocities, both, in the foam as well as in the bulk liquid. Almost all the bubbles were spherical, so their sizes were calculated by measuring the number of pixels and converting it into length units using a calibration movie of a paper with (known) metric grid line spacing. The velocities are measured by tracking the leading edge of the moving bubble over several frames (time steps).

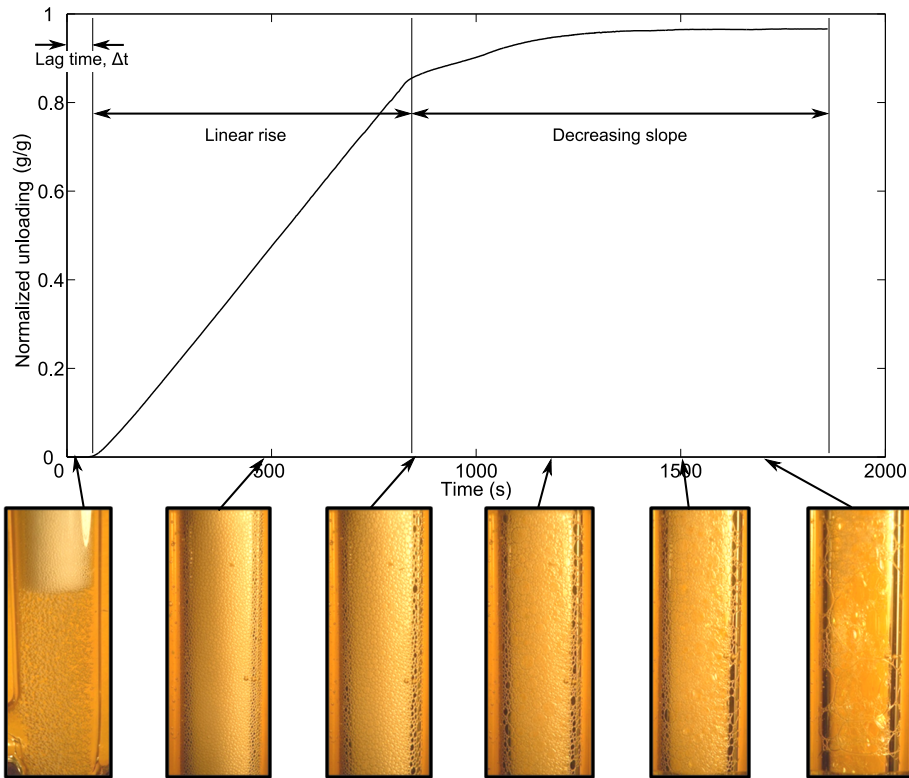
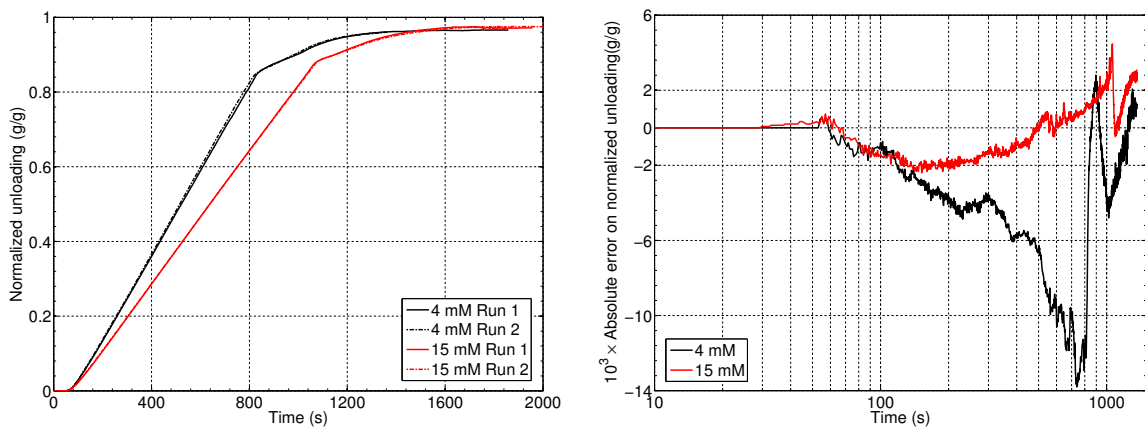


Figure 3.7: A typical result from the foam column test showing the three main sections corresponding to foam quality. The images show foam structure from the start to the end of an experiment.



(a) The unloading curves obtained for Sodium Dodecyl sulfate. The measurement runs are performed on separate days.

(b) Absolute error for the different runs shown in (a).

Figure 3.8: Reproducibility test results showing the absolute error of  $\pm 10^{-2}$ .

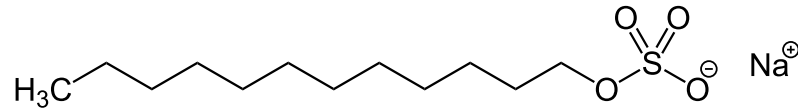
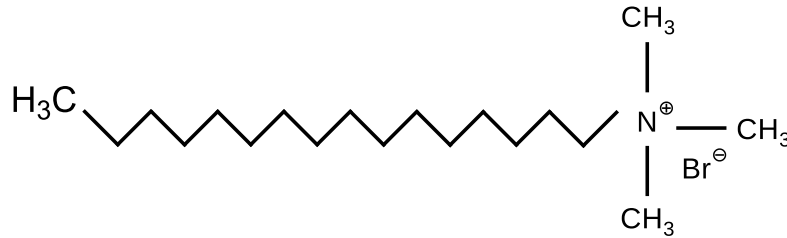
(a) Sodium dodecyl sulfate,  $(C_{12}H_{25})SO_4Na$ , (SDS)(b) Cetyltrimethylammonium bromide,  $(C_{16}H_{33})N(CH_3)_3Br$ , (CTAB)(c) Polyoxyethylene (4) lauryl ether,  $C_{12}H_{25}(OCH_2CH_2)_4OH$ , (Brij30)

Figure 3.9: Molecular structure of the pure surfactants used in the this study.

The foam density can then be calculated using,

$$\rho_{\text{foam}} = \frac{v \times nUF'}{\phi_{\text{foam}} \times \pi r_c^2} \quad (3.2)$$

where  $\rho_{\text{foam}}$  ( $\text{g}/\text{cm}^3$ ), is the density of foam;  $v$  (g), is the weight of the initial solution taken for foamability test (150 g in this thesis);  $nUF'$  (1/s), is the rate of normalized unloading (i.e.  $d(nUF)/dt$ );  $nUF$ , is the normalized unloading;  $\phi_{\text{foam}}$  (cm/s), is the velocity of the foam through column;  $r_c$  (cm), is the radius of the foam column.

### 3.3.3 Reproducibility

Fig. 3.8a shows the reproducibility for two unloading experiments over time. The absolute error over the two experiments is less than  $\mathcal{O}(10^{-2})$  (Fig. 3.8b).

## 3.4 Chemicals

A surfactant from each category (anionic, cationic and non-ionic) was chosen. The interfacial properties of all selected surfactants are well studied in past and published literature is available.

Sodium dodecyl sulfate, SDS, (Fig. 3.9a) is the most commonly studied<sup>[29,65,66]</sup> anionic surfactant. It was chosen as the anionic candidate and the BioXtra grade having a purity of  $\geq 99\%$  (GC) was purchased from Sigma-Aldrich Co. LLC. (Amsterdam). Cetyltrimethylammonium bromide, CTAB, (Fig. 3.9b) is a popular cationic surfactant whose interfacial properties are well studied<sup>[32]</sup>. Analytical grade with a

Table 3.1: Foam column specification sheet

Foam column dimensions and experiment setup parameters		
Height	(cm)	84
Diameter	(cm)	2.11
Temperature	(°C)	22
N <sub>2</sub> flowrate	(ml/min)	200
Sparger specifications		
Type	(-)	Needles
Needle length	(cm)	2
Number	(-)	19
Layout	(-)	Triangular
Pitch	(mm)	3.544
Length distribution around plate(top/bottom) <sup>a</sup>	(cm)	0.1/18.25
Rectangular visualization pocket specifications		
Height	(cm)	54
Width	(cm)	5
Minimum depth <sup>b</sup>	(cm)	2.5

<sup>a</sup> Refer to Fig. 3.5

<sup>b</sup> Refer to Fig. 3.6b

purity of  $\geq 99\%$  was purchased from VWR International, LLC. (Amsterdam). The Non-ionic surfactant, Brij 30 (Fig. 3.9c) having a purity of  $\geq 99\%$ , was chosen as it was used by Rosen et al.<sup>[11]</sup> to establish correlation for foamability. Nevertheless it has also been investigated elsewhere in the literature<sup>[67,68]</sup>. It was purchased from Sigma-Aldrich Co. LLC. (Amsterdam). All surfactants were used without any further purification. The effect of salt is studied using analytical grade NaCl. Before use, it was baked at 80°C for at least 48 hours.

Apart from the pure surfactants, Trifoam 820-Block, TB820 (by OILCHEM GmbH, Germany), a commercial foamer applied in gas-well deliquification, was also used. The chemical composition of TB820 is unknown. TB820 has been tested at the flow loop in the Kramers Laboratory, Delft University of Technology by Ir. Dries van Nimwegen.

Ultra pure deionized water having resistivity of  $\rho \geq 10 \text{ M}\Omega \text{ m}$  was used for preparing all solutions. It was produced using the *Milli-Q water purification system* by Merck MilliPore, Darmstadt, Germany.

### 3.5 Summary

The foam column used for quantifying foamability has been described and the specifications are summarized in Table 3.1. It is in principle a modified Bikerman type setup in which foam is generated by sparging  $N_2$  through 150 ml of test sample. Instead of measuring the height of foam; the weight of foam (i.e. water content) is measured in time. In addition, high speed movies at 400 fps with a resolution of  $640 \times 240$  pixels are recorded. These were used to determine bubble sizes and their velocities in the foam as well as in the bulk liquid. The test is complete when no more foam is produced. Reproducibility of foam column experiments measurements is within  $\pm 5\%$ .

The method and procedure used to measure equilibrium and dynamic surface tension of the test sample is described. Equilibrium surface tension is measured using the du Noüy ring method (*KRÜSS K9 tensiometer*) and the dynamic surface tension is measured using the maximum bubble pressure method (*SINTERFACE BPA-1S tensiometer*). Reproducibility for the *KRÜSS K9* is within  $\pm 1$  mN/m and for the *BPA-1S* it is within  $\pm 2$  mN/m.

Surfactants whose properties are well studied and published in literature are chosen as the test candidates. Commercially available purest forms of sodium dodecyl sulfate (SDS), cetyltrimethylammonium bromide (CTAB), polyoxyethylene (4) lauryl ether (Brij 30) were obtained and used without further purification. Analytical grade NaCl is used after baking it at  $80^\circ\text{C}$  for at least 48 hours. Additionally a commercial foamer used in gas well-deliquification and in the flow loop at the Kramers laboratory, Delft University of Technology<sup>[69]</sup>, has also been tested.

---

## 4. Results

---

This chapter will present the experimental results and their analysis. The sections on analysis will refer back to the theories introduced in Chapter 2 where required. The three correlations outlined in the research question will be tested for three pure surfactants, one commercial surfactant and one pure surfactant with salt. The default unit for concentration is mM/l, but for comparison in other units, please refer Table 4.1.

### 4.1 Sodium Dodecyl Sulfate (SDS)

#### 4.1.1 Preparation of the solutions

Experimental results of SDS are described in this section. The SDS solution was used within 5 hours of its preparation. Aqueous SDS auto-hydrolysis to n-dodecanol. The n-dodecanol is more surface active than SDS; thereby changing surface properties substantially<sup>[65]</sup>. Although the SDS hydrolysis to n-dodecanol can neither be prevented nor can the n-dodecanol content be precisely determined by surface tension alone; for the sake of reproducibility and to ensure comparison of data, all SDS solutions were freshly prepared every day. Thus the n-dodecanol presence is controlled to its concentration in the salt as purchased.

Table 4.1: Range of surfactant concentration in various units. See §3.4 for details on the surfactant source and chemistry

	Concentration			MW g/mol	$x \times \text{c.m.c}^c$ (-)
	mM/l	ppm wt. <sup>a</sup>	g/l		
SDS	0.1 – 50	28.8 – 14400	0.0288 – 14.4	288	0.015 – 7.7
CTAB	0.1 – 2	36.4 – 728	0.0364 – 0.728	364	0.11 – 2.2
Brij 30	0.01 – 0.5	3.62 – 181	0.00362 – 0.181	362	0.16 – 8.3
NaCl <sup>b</sup>	1 – 600	58 – 34800	0.058 – 34.8	58	N/A
TB820	N/A	100 – 3000	0.10 – 3.00	N/A	0.22 – 6.67 <sup>d</sup>

<sup>a</sup> Note for future sections: To obtain concentration in ppm by weight for any surfactant, multiply the concentration in mM/l with its respective molecular weight

<sup>b</sup> Together with fixed 1 mM/l SDS concentration

<sup>c</sup> Range in terms of the c.m.c.

<sup>d</sup> c.m.c. of TB820 = 450 ppm weight.

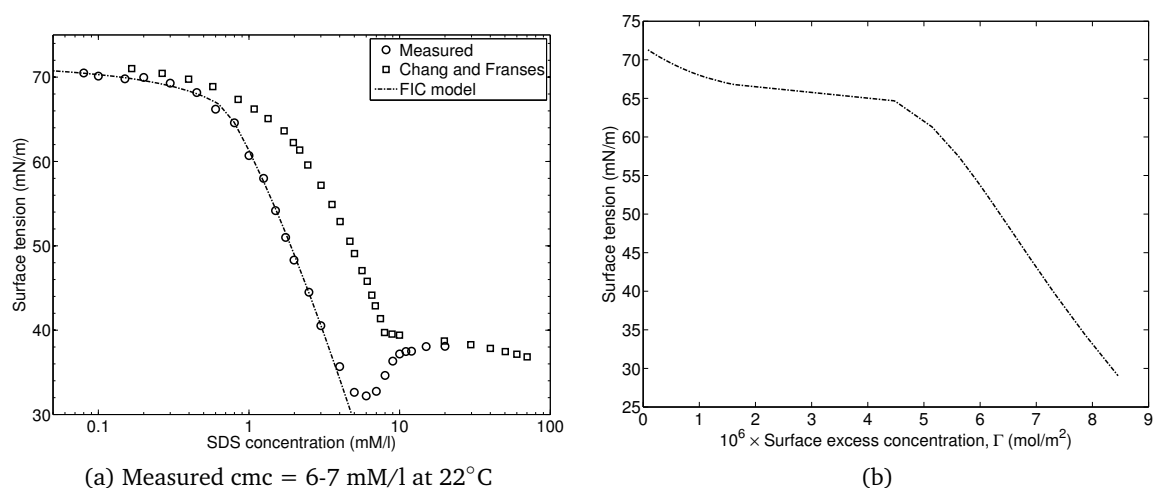


Figure 4.1: (a) Measured SDS surface tension compared to the data published by Chang and Franses<sup>[26]</sup> for pure SDS. The FIC model (Eq. 2.4) is used to obtain fit for the measured data; (b) the theoretical surface excess concentration at the surface tension for SDS according to the FIC model.

#### 4.1.2 Equilibrium surface tension

Fig. 4.1a shows the equilibrium surface tension at various SDS concentrations in ultra pure deionized water. The equilibrium surface tension was measured using the technique described in §3.1.

Even for fresh SDS solution, a minimum in surface tension at 6 mM/l can be seen (Fig. 4.1a). The data shown alongside is taken from Chang and Franses<sup>[26]</sup> for highly purified SDS. Existence of a minimum is a clear indication of presence of n-dodecanol. n-dodecanol is more surface active than SDS thus it preferentially adsorbs at the surface. Thus at 6 mM/l the surface contains n-dodecanol. Beyond 6 mM/l, as micelles are formed, the n-dodecanol is transferred from the surface to the micelles (due to higher surface activity/hydrophobicity) and the SDS surface concentration increases (increase in surface tension is observed). Thus the value of surface tension at high SDS concentrations with n-dodecanol impurity coincides with that of pure SDS.

The measured SDS data is fitted to the FIC model (Eq. 2.4). The fit parameters are summarized in Table 4.2. The compressibility of the adsorbed layer,  $\varepsilon$  (m/mN), requires the dilational rheology data. As this is not measured the value of compressibility was taken from literature<sup>[66]</sup> as 0.008. Fig. 4.1b shows the theoretical SDS surface excess concentration,  $\Gamma$  (mol/m<sup>2</sup>), at measured surface tension,  $\gamma_{eq}$  (mN/m) according to the FIC model. The FIC isotherm is a pure surfactant isotherm, it does

not include phenomena such as competitive adsorption<sup>1</sup>. The SDS data with the n-dodecanol impurity fits the FIC model, the derived parameters have a *pseudo* nature. Due to the presence of n-dodecanol, some inaccuracies will occur in the  $\Gamma$  derived by using the FIC model.

### 4.1.3 Dynamic surface tension (DST)

Fig. 4.2 shows the dynamic surface tension from 1 ms until 100 s for aqueous SDS solutions. The DST is measured using the technique described in §3.2. The SDS concentration was varied from low to high concentrations relative to its measured c.m.c. (§2.1.1), which lies between 6 – 7 mM/l. It is seen that as the concentration increases, the surface tension reduction is greater and faster. At concentrations greater than  $\approx 2 \times$  c.m.c., the DST curve shape does not change.

The solid (fit) line at each concentration in Fig. 4.2 is obtained by fitting DST to the Rosen and Hua's empirical equation described in Eq. 2.6. The variation of fit parameters with SDS concentration is shown in Fig. 4.3. We can see from Fig. 4.2 that as the concentration increases, the DST curves shift towards smaller time scale; this effect is quantified by the  $t^*$  shown in Fig. 4.3a. The SDS DST curves also become steeper with increasing concentration, which is seen visually in Fig. 4.2 and quantified in Fig. 4.3b. Parameter  $\gamma_m$  indicates the plateau value of the ST in the DST curve (Fig. 4.3c). As the minimum  $\gamma_m$  at all the studied SDS concentrations is limited to  $\approx 38$  mN/m, it can be concluded that the effect of n-dodecanol adsorption is likely to be significant at longer time scale; as shown experimentally elsewhere<sup>[66]</sup>.

Fig. 4.3d shows the variation of the Rosen parameter with SDS concentration. According to the correlation by Rosen et al.<sup>[11]</sup> (§1.3), the maximum in Rosen parameter should correspond to the maximum in foamability. The next section is dedicated to SDS foamability results.

### 4.1.4 Foamability results

The foamability test measures the weight of foam flowing out of the column over time. At the end of this test, either all liquid 'unloads' (maximum unloading) or the remaining liquid cannot foam (§3.3). Fig. 4.4 shows the results from the foam column test for SDS at 22°C. It can be seen that at low concentration (0.1 mM/l), the unloading takes a long time whereas the maximum unloading is less compared to high concentrations. The fact that at the end of the experiment, the remaining solution does not foam indicates that the surfactant is depleted. The depletion is due to adsorption at the large amount of interfacial area created during foaming. This was confirmed by measuring conductivity<sup>2</sup> of the SDS solution before and after the foam test.

<sup>1</sup>In mixed surfactant systems the adsorption of each component will depend on their individual chemical potential and also on the relative hydrophobicity. Higher surface active components may adsorb more than the lesser surface active components.

<sup>2</sup>The conductivity of 0.1 mM/l SDS was 67.7  $\mu$ S/cm whereas at the end of the foam experiment the remaining liquid had a conductivity of  $\sim 1.5$   $\mu$ S/cm; a value close to that of the water used.

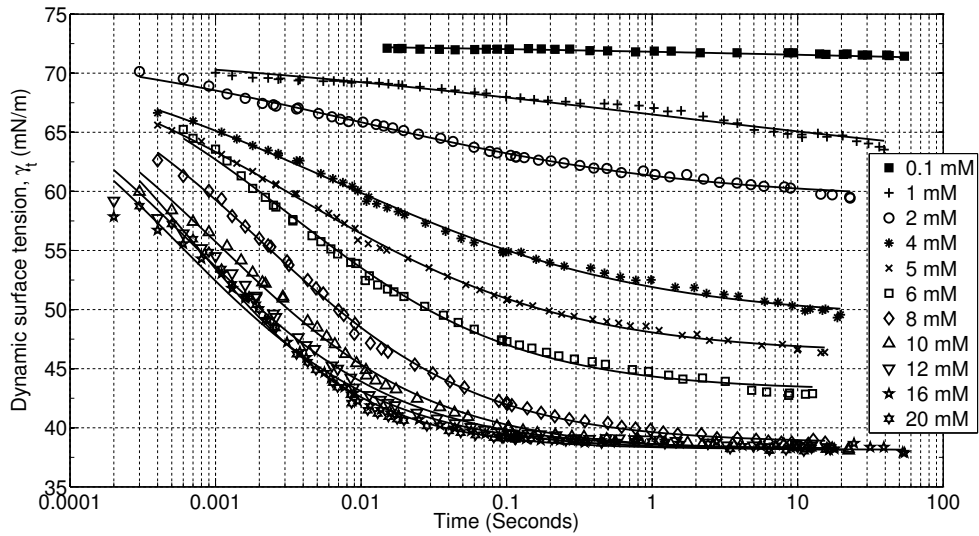


Figure 4.2: Dynamic surface tension of SDS at 22°C. The markers denote measurement points whereas the continuous line is the best fit to Rosen’s empirical Eq. 2.6

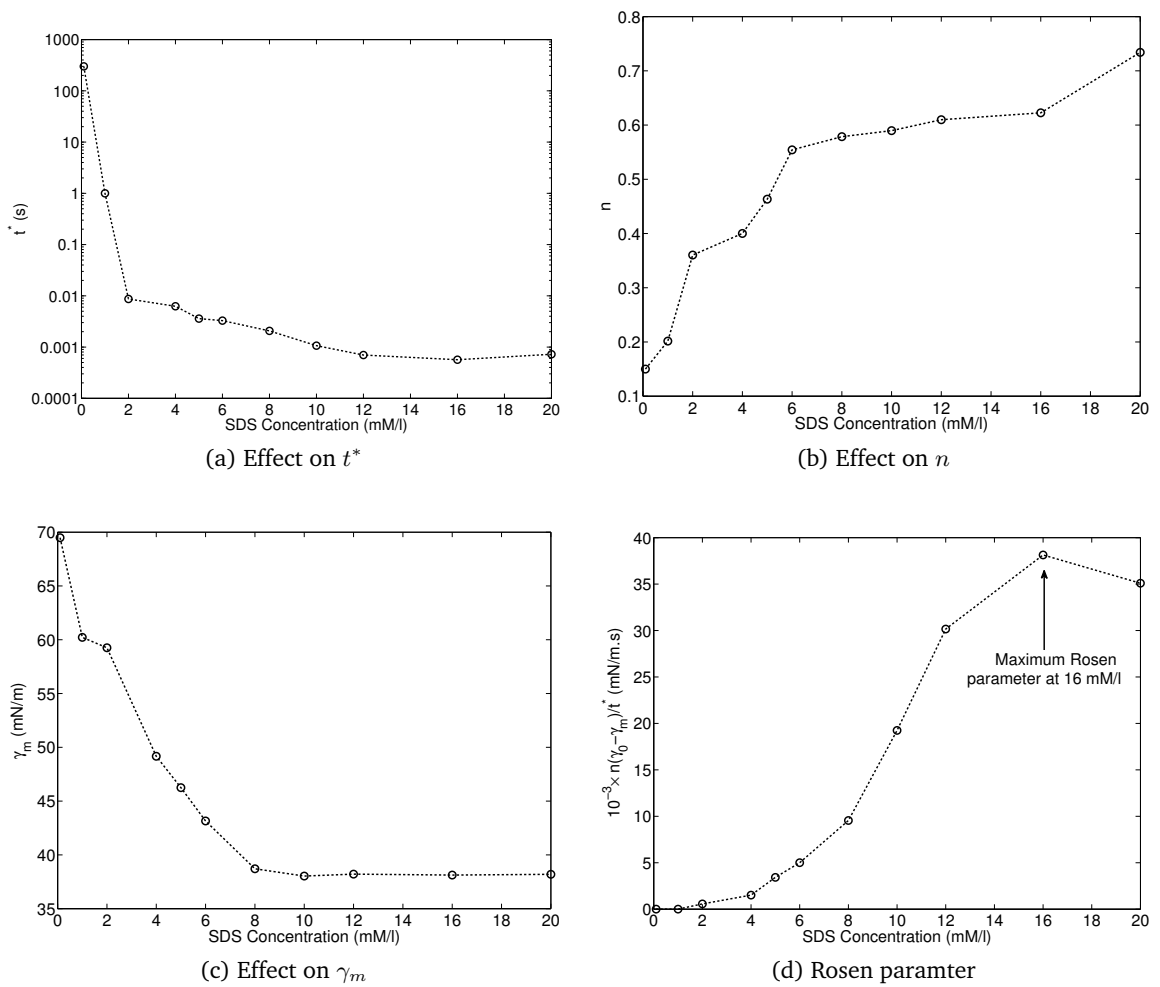


Figure 4.3: Characteristic rosen parameters of SDS DST curves.

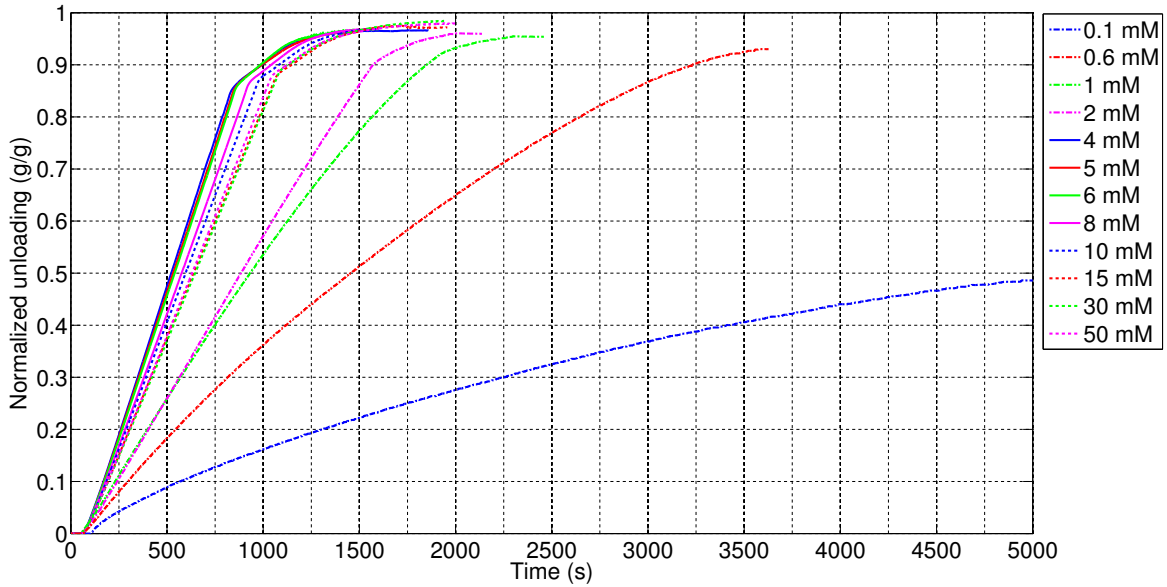


Figure 4.4: Normalized weight of foam collected for SDS at 22°C.

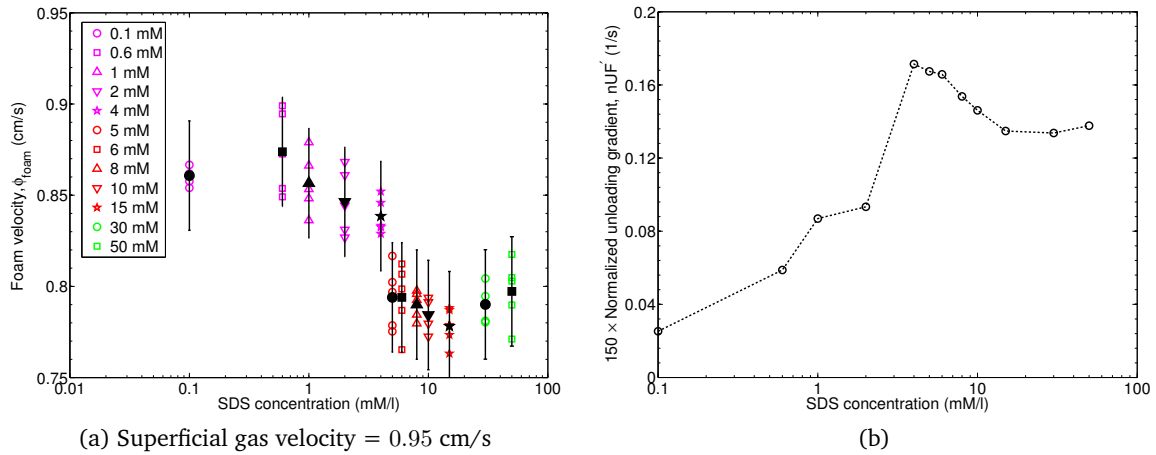


Figure 4.5: (a) Foam velocity for randomly selected bubbles of all sizes. The black marker is the average velocity whereas the corresponding error bar indicates uncertainty (see text for more details); [b] gradient of unloading curves in Fig. 4.4 between 300 s and 700 s. The gradient is calculated by a linear fit.

The normalized unloading curves can be characterized by their gradients,  $nUF'$  (1/s). A linear fit was made in the region between 300 s and 700 s to extract the gradients. These gradients are shown in Fig. 4.5b; it can be seen that the gradient varies by one order of magnitude as the SDS concentration changes from low (0.1 mM/l) to high (50 mM/l). The maximum gradient is around 4 – 6 mM/l where the equilibrium surface tension is lowest (Fig. 4.1a).

The flow visualization technique (§3.3.2) was used to determine the velocities and sizes of the bubbles in the foam and the bulk solution. Fig. 4.5a shows the foam velocity,  $\phi_{\text{foam}}$  (cm/s), for a randomly selected set of foam bubbles of all sizes. The velocity varies in a short range, 0.75 – 0.9 cm/s over three orders of magnitude change in the SDS concentration. Thus, the foam rise velocity is not a strong function of the SDS concentration. The black marker in the Fig. 4.5a at each SDS concentration is the corresponding average velocity. The error bars indicate the uncertainty<sup>3</sup> in the measured velocity due to the resolution of the high speed movies. The average foam rise velocity is used in Eq. 3.2. The velocity decreases at high SDS concentrations. This can be explained by considering the foam flow through the flexible hose from the column until the weighing scale. At low SDS concentration the foam was unstable, breaking as it passed from the column to the hose through a constriction (reduction in diameter of 2.11 cm to 0.5 cm). Thus the flow through the hose did not contain foam. On the other hand at high SDS concentrations, the foam was stable and retained its structure while flowing through the hose. Foam flow creates higher pressure drop as foams have higher viscosity than the liquids from which they are made<sup>[70]</sup>.

By combining  $nUF'$  and  $\phi_{\text{foam}}$  it is possible to calculate the foam density using Eq. 3.2,

$$\rho_{\text{foam}} = \frac{150}{\pi r_c^2} \times \frac{nUF'}{\phi_{\text{foam}}}$$

The foam density serves as a ‘unit’ of foamability. In following sections we will see how it correlates with the Rosen parameter, equilibrium surface pressure and the dynamic surface excess concentration.

#### Correlation of foam density and maximum unloading with Rosen parameter

Fig. 4.6a shows the comparison between the  $\rho_{\text{foam}}$  and the Rosen parameter; both increase until 5 mM/l, beyond which the foam density decreases while the Rosen parameter continues to increase. The magnitude of the Rosen parameter is maximum at 16 mM/l. The shape of foam density curve is not same as that of the Rosen parameter; as Rosen et al.<sup>[11]</sup> (Fig. 1.6) predicted it should be, thus, illustrating that a change in foaming method changes the measured quantities. A one to one comparison is not possible. Note that the rosen parameters varies over six orders

<sup>3</sup>The velocity is measured by tracking the leading edge of the bubble over a given time. The accuracy is in estimating the leading edge of the bubble is  $\pm 3.5\%$ ; giving an uncertainty in measured velocity of  $\pm 7\%$  (as leading edge is estimated twice, at the start and at the end of the bubble motion).

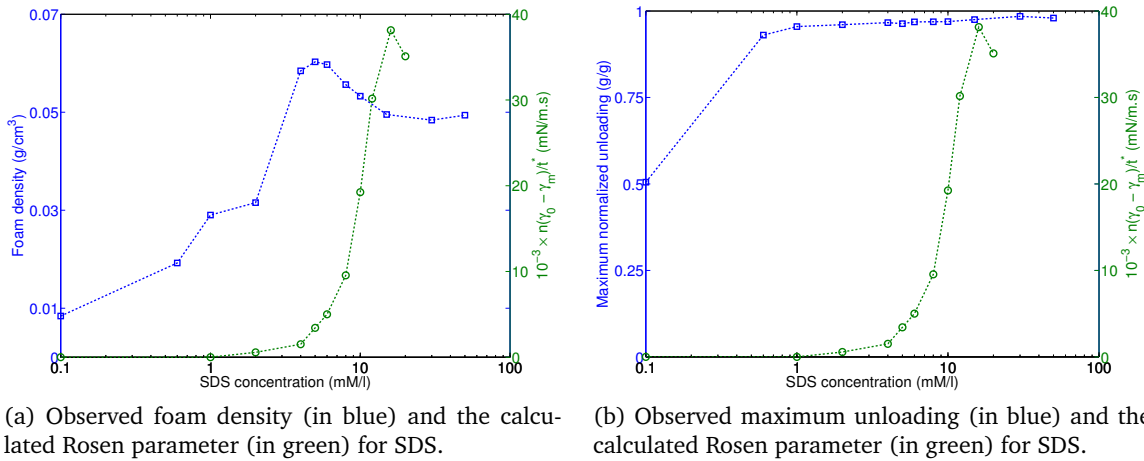


Figure 4.6: Correlation of foamability with the Rosen parameter for SDS.

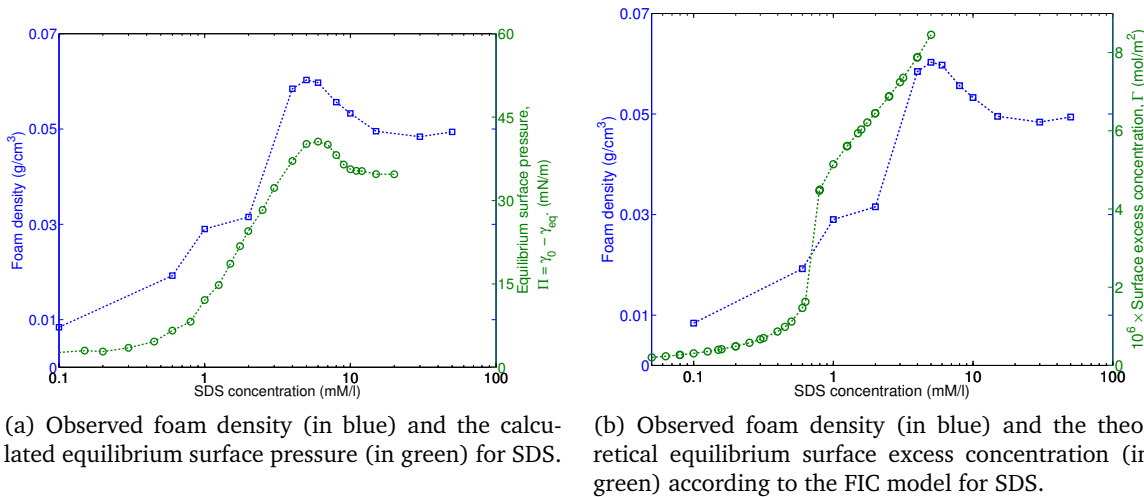


Figure 4.7: Correlation of foamability with equilibrium surface properties for SDS.

of magnitude whereas the foam density varies over a six fold magnitude. See Appendix B for a discussion on the magnitude of  $\rho_{\text{foam}}$ .

SDS is a good foamer. This is reflected in Fig. 4.6b which shows that even at low concentrations it achieves complete unloading. There appears to be no correlation between the maximum unloading and the Rosen parameter in this case.

### Correlation of foam density with equilibrium surface properties

In this section the comparison between the equilibrium surface pressure,  $\Pi$  (mN/m), and the foam density will be shown. Equilibrium surface pressure is defined as the reduction in surface tension at equilibrium due to surfactants; that is,  $\Pi = \gamma_0 - \gamma_{\text{eq}}$ . The term surface pressure indicates a ‘2D pressure’ of the adsorbed surfactants

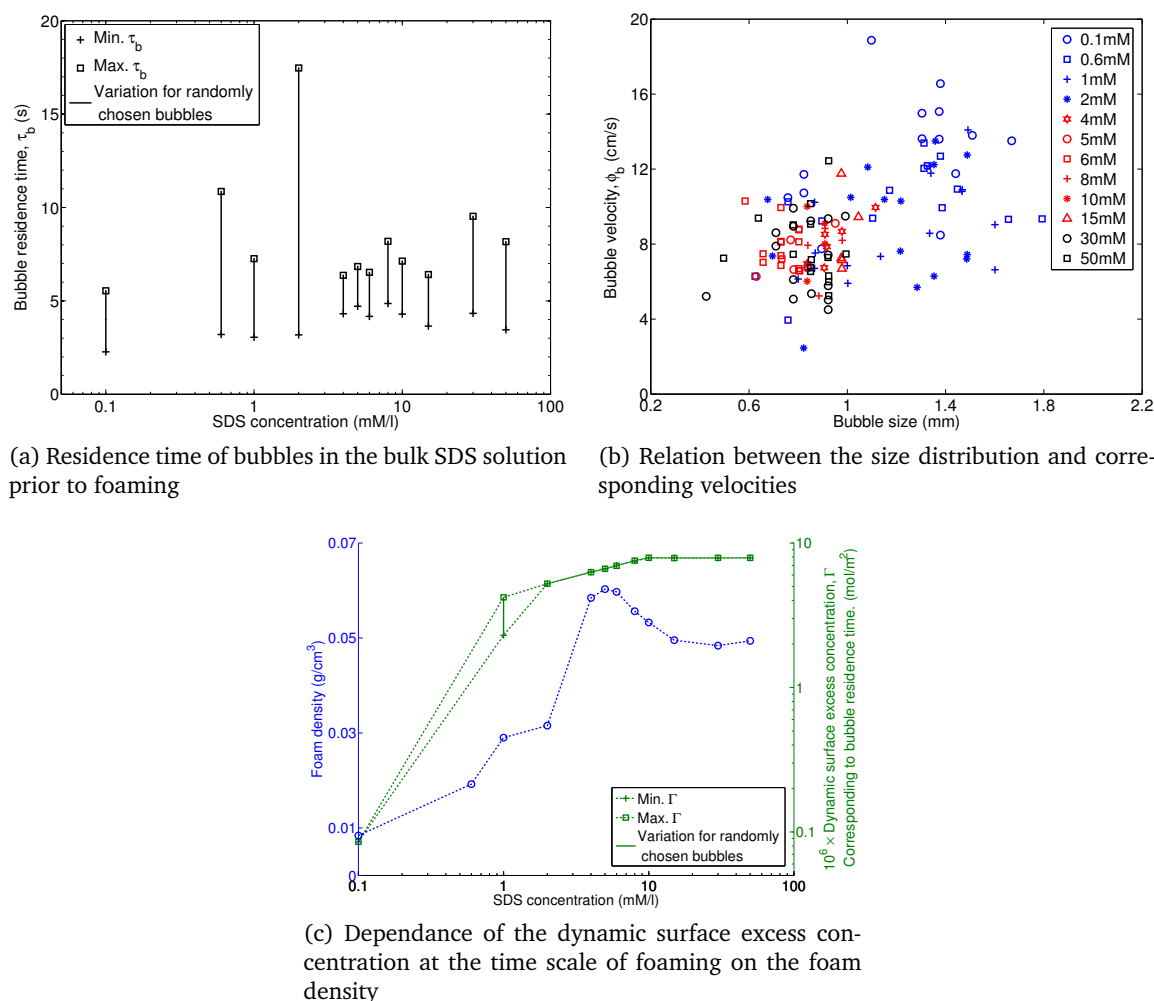


Figure 4.8: Correlation of foamability with dynamic surface excess concentration for SDS.

(§2.1.1).

Fig. 4.7a shows the comparison between  $\Pi$  and  $\rho_{\text{foam}}$  at different SDS concentrations. There is a good correlation between both these quantities. Thus given the full curve of equilibrium surface pressure and one point on the foam density curve, the foam density at other SDS concentrations can be qualitatively predicted.

Fig. 4.7b shows a comparison between the foam density and the theoretical equilibrium surface excess concentration from the FIC model for SDS. From Fig. 4.7b it is seen that a higher surface excess concentration leads to a denser foam. The comparison is only valid until 4 mM/l as beyond that micellization occurs. As described earlier (§4.1.2), the FIC model is a pre-micellar isotherm, thus it cannot be used to obtain surface excess concentration in the micellar region. Although in most cases the surface excess concentration remains constant after the c.m.c., the presence of n-dodecanol in the case of SDS creates an uncertainty. Competitive ad-

Table 4.2: Fit parameters for SDS and CTAB by the FIC model (Eq 2.4)

	$10^{-5} \times \omega_0$ (m <sup>2</sup> /mol)	$a$ (-)	$10^3 \times \varphi$ (-)	$\varepsilon$ (m/mN)	$c_c$ (mM/l)	$b$ (-)
SDS	1.70	2.00	1.2	0.008	1.82	0.107
CTAB	2.48	1.55	9.5	0.011	0.31	0.110

sorption between n-dodecanol and SDS can change their respective surface excess concentrations in the micellization region.

### Correlation of foam density with dynamic surface excess concentration

Foam formation occurs at a certain time scale. In this section the correlation of the foaming time scale with the surface excess concentration at that time scale is made. The time scale of foaming was determined by calculating the bubble residence time, that is the time spent by the bubble from its formation at the sparger until it reaches the foam. The bubble rise velocity is high at low SDS concentration and the bubble size is larger at low SDS concentration. This observation is in agreement with Malysa et al.<sup>[46]</sup>. The surface excess concentration reaches saturation from 4 mM/l onwards and this creates a narrow bubble size and velocity distribution (the red and black markers in Fig. 4.8b).

At any concentration, the velocities of bubbles vary based upon their location in a cross section of the column. The bubbles close to the wall usually had lower velocity than the bubbles located near the center of the column. These effects are also altered if the region is ‘more crowded’ or ‘less crowded’. Using the minimum and maximum velocity at each SDS concentration, the range of the bubble residence time,  $\tau$  (s), is calculated at the start of experiment. Bubbles with a small rise velocity have larger  $\tau$  and *vice-versa*.

For definiteness the maximum distance is considered which will be at the start of the experiment. With 150 ml initial solution, the height of bulk liquid for given column geometry is  $\sim 43$  cm by neglecting the gas hold up. Using the velocity of rising bubbles (measured from flow visualization) shown in Fig. 4.8b the bubble residence times shown in Fig. 4.8a.

The surface tension,  $\gamma_\tau$ , at any residence time  $\tau$  is obtained from the DST curves. This  $\gamma_\tau$  is used to estimate the dynamic surface excess concentration,  $\Gamma_\tau$ . Consider an equilibrium surface which has  $\gamma_{\text{eq}} = \gamma_\tau$ . It is assumed that the corresponding  $\Gamma_{\text{eq}}$  for such an equilibrium surface will be equal to  $\Gamma_\tau$  for a dynamic surface at the time  $\tau$ . In other words, it is assumed that  $\Gamma_\tau$  is same as the  $\Gamma_{\text{eq}}$  for a solution having  $\gamma_{\text{eq}}$  same as the  $\gamma_\tau$ . This reasonable assumption is equivalent to saying that a particular value of surface tension is due to a particular surface excess concentration of a give surfactant, irrespective of the dynamic state in which the surface exists.

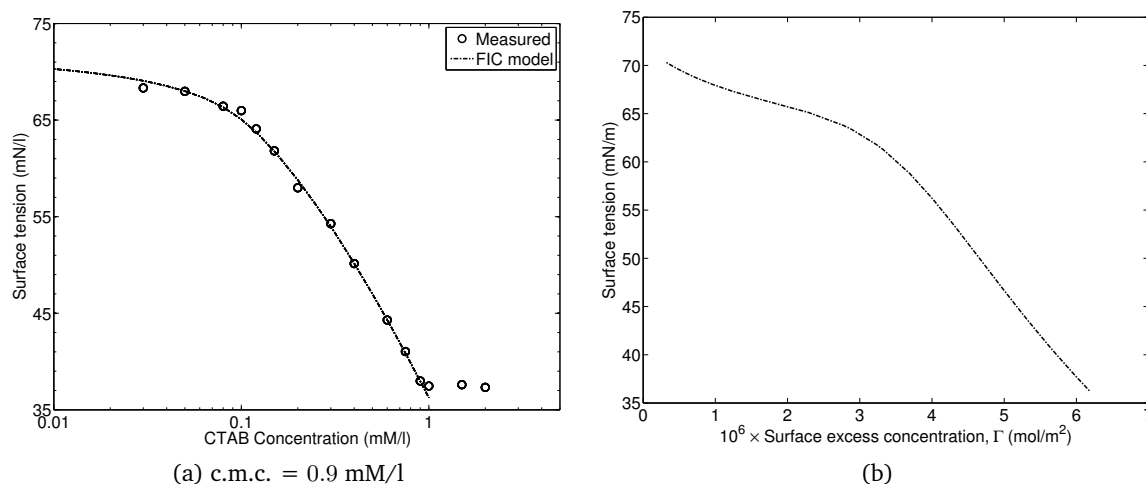


Figure 4.9: (a) Measured CTAB surface tension. The FIC model (Eq. 2.4) is used to obtain a fit for the measured data; (b) the theoretical curve from the FIC model for the dependance of surface excess concentration on the surface tension of CTAB.

Similar approach is also used in graphical method of studying dynamic adsorption explained by Chang and Franses<sup>[26]</sup>. The dynamic surface excess concentration is compared with the foam density in Fig. 4.8c. We see that as the dynamic surface excess concentration is directly proportional to the foam density until the c.m.c. Beyond this, although the surface excess concentration remains constant, the foam density decreases.

The main simplification made in estimating,  $\Gamma_\tau$ , was that  $\tau$  directly corresponds to a (uniform) surface coverage over the bubbles. The effect of bubble formation and its rise through the bulk liquid was neglected. The actual surfactant coverage will depend on the rate of bubble growth and expansion of the bubble interface at the capillary tip. The motion of a rising bubble decreases the surface coverage at the top surface of the bubble<sup>[71]</sup>.

## 4.2 Cetyltrimethylammonium Bromide (CTAB)

Experimental results for CTAB are described in this section. It was used as received.

### 4.2.1 Equilibrium surface tension

Fig. 4.9a shows the CTAB equilibrium surface tension in ultra pure deionized water. The equilibrium surface tension was measured using the technique described in §3.1. The c.m.c. is located at 0.9 mM/l. The surface tension at the c.m.c. is  $\sim 37$  mN/l.

The FIC model (Eq. 2.4) is used to fit the pre-micellar surface tension data using the parameters given in Table 4.2. The compressibility of adsorbed layer,  $\varepsilon$  (m/mN), requires the dilational rheology data. As this is not measured the value of compress-

ibility was taken from literature<sup>[32]</sup> as 0.011. The surface excess concentration,  $\Gamma$  (mol/m<sup>2</sup>), determined from the FIC model at  $\varepsilon = 0.011$  predicts a linear rise in surface excess. Stubenrauch et al.<sup>[32]</sup> also observed a linear rise in  $\Gamma$  by using neutron reflection experiments.

### 4.2.2 Dynamic surface tension (DST)

Fig. 4.10 shows the dynamic surface tension from 1 ms until 100 s for aqueous CTAB solutions. The DST is measured using the technique described in §3.2. Similar to the DST curves for SDS, it is seen that as the concentration increases, the surface tension reduction is greater and faster. Fig. 4.11 quantifies the DST curves using the Rosen's empirical Eq. 2.6. Compared to the SDS DST at its c.m.c., the value of  $t^*$  is one order of magnitude higher for CTAB at its c.m.c. The Rosen parameter increases with CTAB concentration and no maximum is observed (Fig. 4.11d).

### 4.2.3 Foamability results

Fig. 4.12 shows the results from the foam column test for CTAB at 22°C. At low concentration (0.1 mM/l), the time taken for maximum unloading is more than at higher concentrations (1 and 2 mM/l). At 0.1 mM/l surfactant depletion is observed as the normalized maximum unloading is less than one. Similar to the situation in SDS, this was confirmed by measuring conductivity<sup>4</sup> of the CTAB solution before and after the experiment.

The normalized unloading curves are characterized by their gradients,  $nUF'$  (1/s). A linear fit in the region between 100 s and 250 s was made to extract the gradients. These gradients are shown in Fig. 4.13b; it can be seen that the gradient varies by little between the low, pre-micellar CTAB concentration (0.1 mM/l), and the high, micellar CTAB concentration (2 mM/l). It seems that CTAB concentration does not have significant influence on its foamability, but rather influences the maximum unloading. Higher CTAB concentration procrastinates the influence of surfactant depletion on foamability. Fig. 4.13a shows the foam velocity,  $\phi_{\text{foam}}$  (cm/s), for a randomly selected set of foam bubbles of all sizes. Similar to SDS, the velocity varies in a short range, 0.75 – 0.9 cm/s over a one order of magnitude change in CTAB concentration. Thus, the foam rise velocity is not a strong function of the CTAB concentration. The black marker in Fig. 4.13a at each CTAB concentration is the corresponding average velocity. The error bars indicate the uncertainty<sup>5</sup> in the measured velocity arising due to the resolution of the high speed movies. The average foam rise velocity is used in Eq. 3.2 to calculate the foam density. The decrease in velocity at high CTAB concentration can be explained using the justification given for SDS.

<sup>4</sup>The conductivity of 0.1 mM/l CTAB was 10.1  $\mu\text{S}/\text{cm}$  whereas at the end of the foam experiment the remaining liquid had a conductivity of  $\sim 1.5 \mu\text{S}/\text{cm}$ ; value close to that of the water used.

<sup>5</sup>The velocity is measured by tracking the leading edge of the bubble over a given time. The accuracy in estimating the leading edge of the bubble is  $\pm 3.5\%$ ; giving an uncertainty in measured velocity of  $\pm 7\%$  (as leading edge is estimated twice, at the start and at the end of the bubble motion).

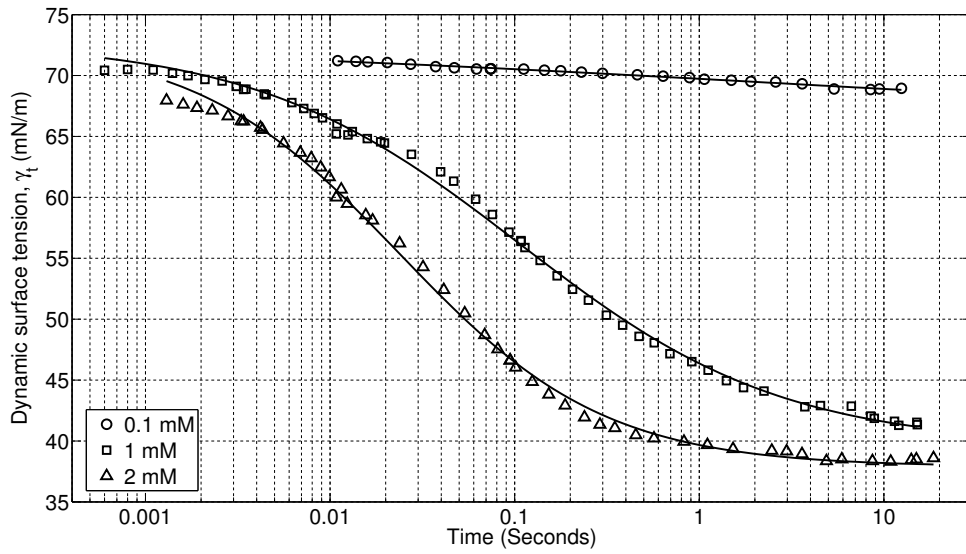


Figure 4.10: Dynamic surface tension of CTAB at 22°C. The markers denote measurement points whereas the continuous line is the best fit to Rosen's empirical Eq. 2.6

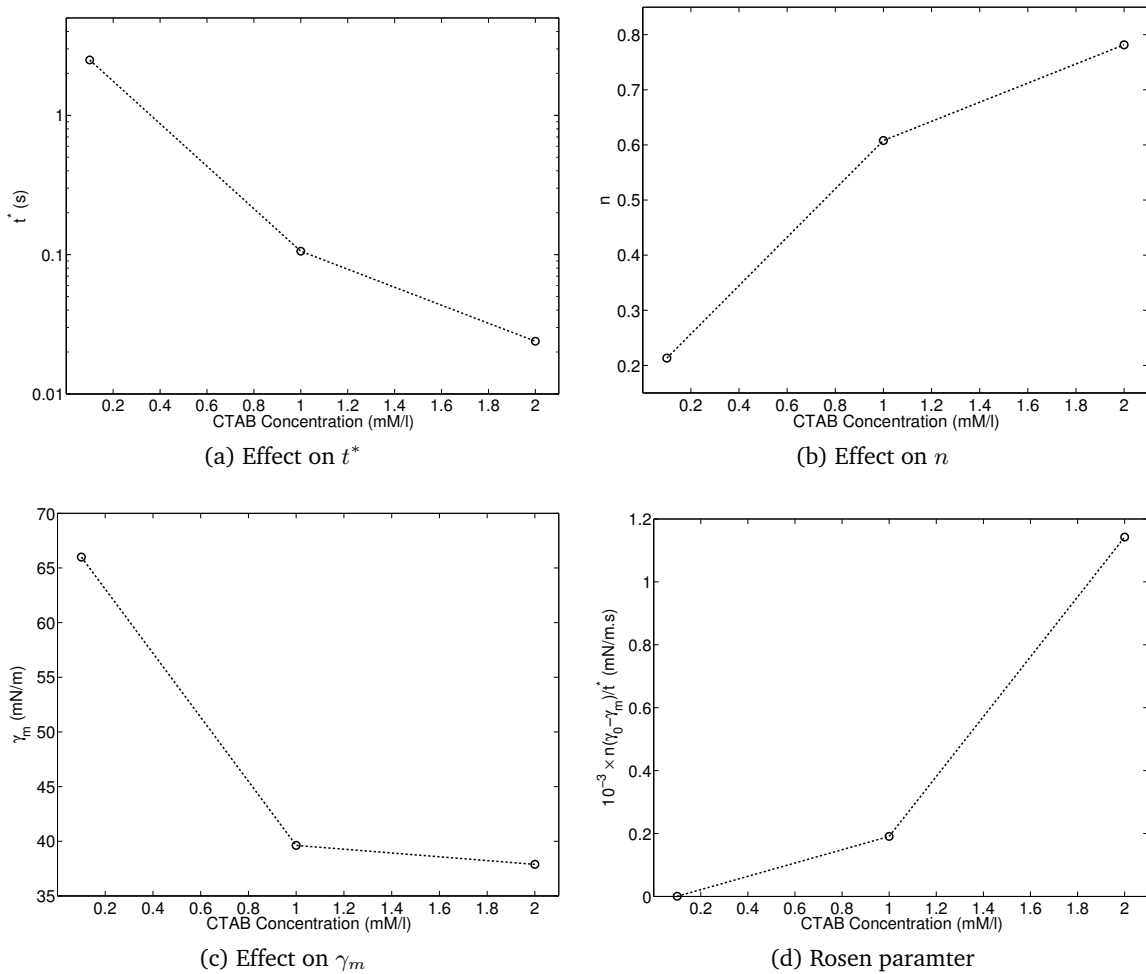


Figure 4.11: Characteristic rosen parameters of CTAB DST curves.

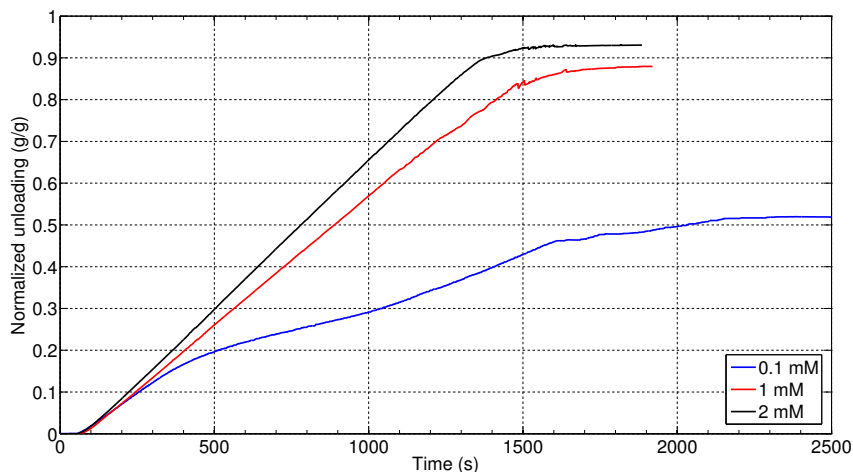


Figure 4.12: Normalized weight of foam collected for CTAB at 22°C.

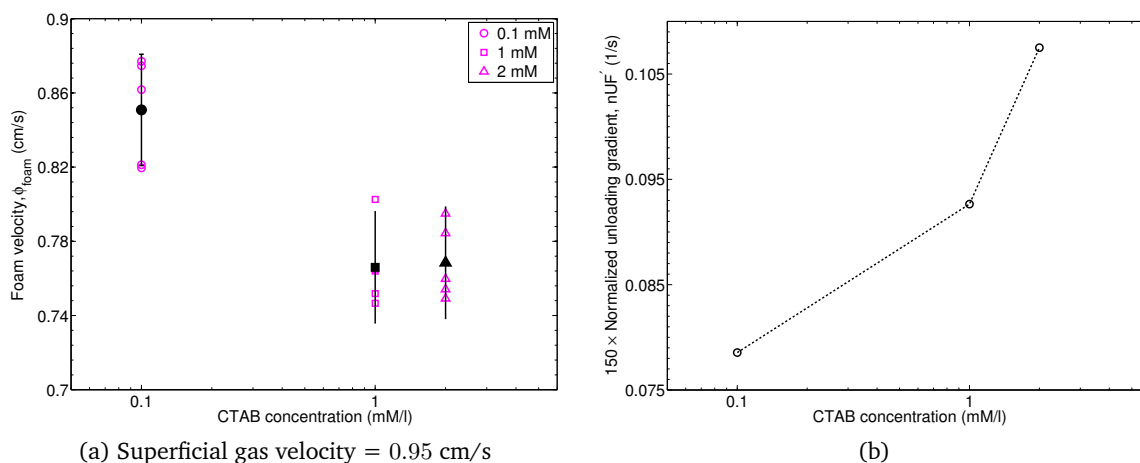
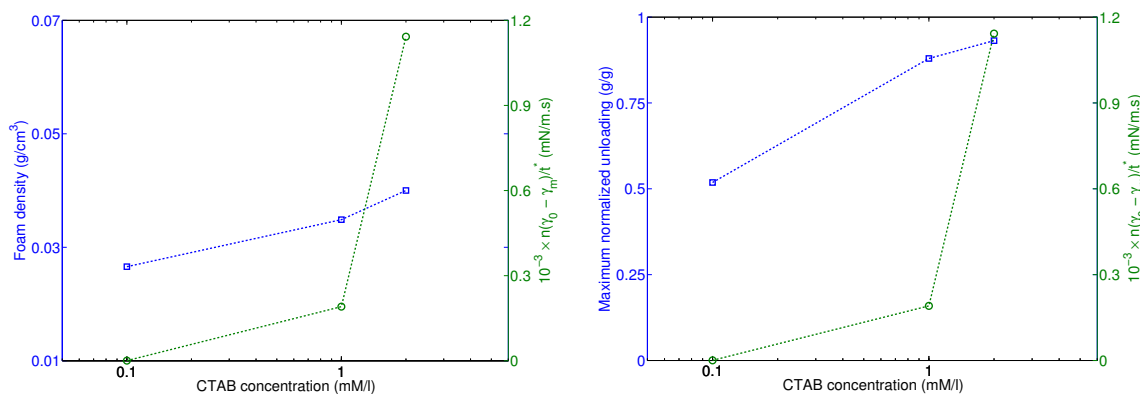


Figure 4.13: (a) Foam velocity for randomly selected bubbles of all sizes. The black marker is the average velocity whereas the corresponding error bar indicates the the uncertainty (see text for more details); (b) gradient of unloading curves in Fig. 4.12 between 100 and 250 s. The gradient is calculated by a linear fit.



(a) Observed foam density (in blue) and the calculated Rosen parameter (in green) for CTAB. (b) Observed maximum unloading (in blue) and the calculated Rosen parameter (in green) for CTAB.

Figure 4.14: Correlation of foamability with the Rosen parameter for CTAB.

The foam density serves as a ‘unit’ of foamability. In following sections we will see how it correlates with the Rosen parameter, equilibrium surface pressure and the dynamic surface excess concentration.

#### Correlation of foam density and maximum unloading with Rosen parameter

The foam density,  $\rho_{\text{foam}}$  ( $\text{g}/\text{cm}^3$ ), is calculated using Eq. 3.2; and the Rosen parameter is defined as  $n(\gamma_0 - \gamma_m)/t^*$  ( $\text{mN}/\text{m}\cdot\text{s}$ ), where  $n$ ,  $t^*$ , and  $\gamma_m$  are fit parameters from the Rosen’s empirical Eq. 2.6.

Fig. 4.14a shows the comparison between the  $\rho_{\text{foam}}$  and the rosen parameter; both increase with the CTAB concentration. Note that the Rosen parameters varies over three orders of magnitude whereas the foam density doubles. Complete unloading is achieved at micellar CTAB concentrations. The maximum unloading increases as the Rosen parameter increases.

#### Correlation of foam density with equilibrium surface properties

The foam density,  $\rho_{\text{foam}}$  ( $\text{g}/\text{cm}^3$ ), is calculated using Eq. 3.2; and the equilibrium surface pressure is defined as  $\Pi = \gamma_0 - \gamma_{\text{eq}}$  ( $\text{mN}/\text{m}$ ).  $\gamma_{\text{eq}}$  is the equilibrium surface tension of CTAB as reported in §4.2.1.

The equilibrium surface pressure and the foam density increases in the pre-micellar region (Fig. 4.15a). In the micellar region, the equilibrium surface pressure remains constant whereas the foam density continues to rise. The surface properties affecting foam density continue to change beyond the c.m.c., whereas the equilibrium surface remains almost constant. Fig. 4.15b shows that the foam density increases as the equilibrium surface excess concentration increases.

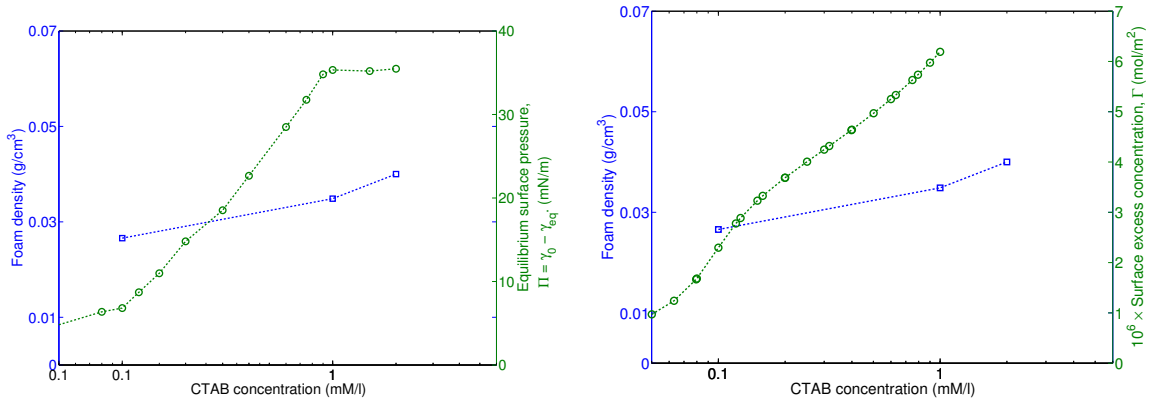
#### Correlation of foam density with dynamic surface excess concentration

The surface excess concentration of the foaming interface at the time scale of its formation is correlated with the foam density in this section. Fig. 4.16b shows the variation of the bubble size and the bubble velocity at different CTAB concentrations. Using the minimum and maximum velocities of bubbles, the residence time is calculated (See Fig. 4.16a). The residence time together with the DST curves and the FIC model gives the dynamic surface excess concentration which is shown in Fig. 4.16c. See §4.1.4 for more details on the calculation approach.

As the dynamic surface excess concentration increases, the foam density also increases. This observation holds even in the micellar region of CTAB.

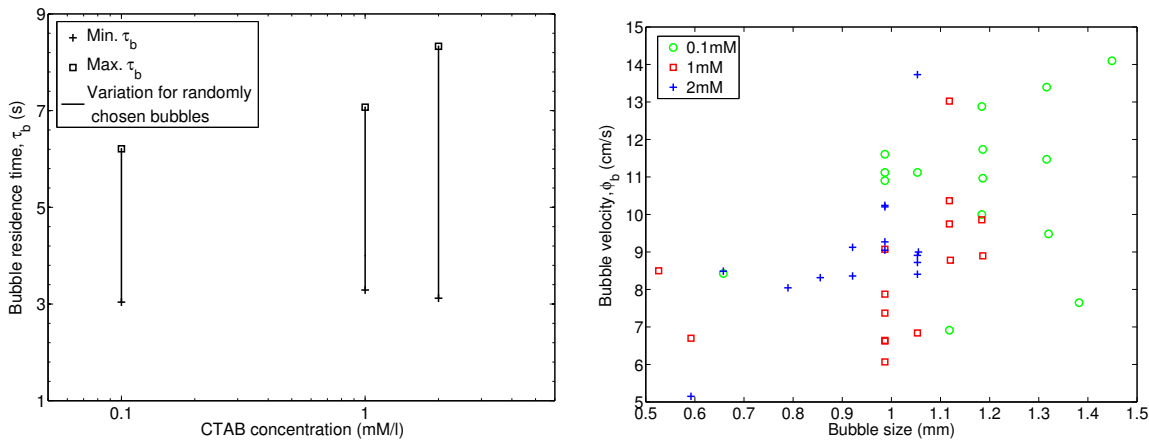
### 4.3 Polyoxyethylene (4) lauryl ether (Brij 30)

Experimental results for Brij 30 are described in this section. Brij 30 is a nonionic surfactant containing 4 polyoxyethylene groups (EO). The molecular formula is  $\text{C}_{12}\text{EO}_4$ .

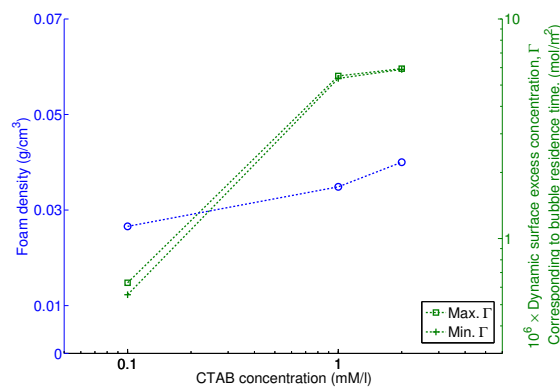


(a) Observed foam density (in blue) and the calculated equilibrium surface pressure (in green) for CTAB. (b) Observed foam density (in blue) and the theoretical equilibrium surface excess concentration (in green) according to the FIC model for CTAB.

Figure 4.15: Correlation of foamability with the equilibrium surface properties for CTAB.



(a) Residence time of bubbles in the bulk CTAB solution prior to foaming. (b) Relation between the size distribution and corresponding velocities.



(c) Dependence of the dynamic surface excess concentration at the time scale of foaming on the foam density.

Figure 4.16: Correlation of foamability with dynamic surface excess concentration for CTAB.

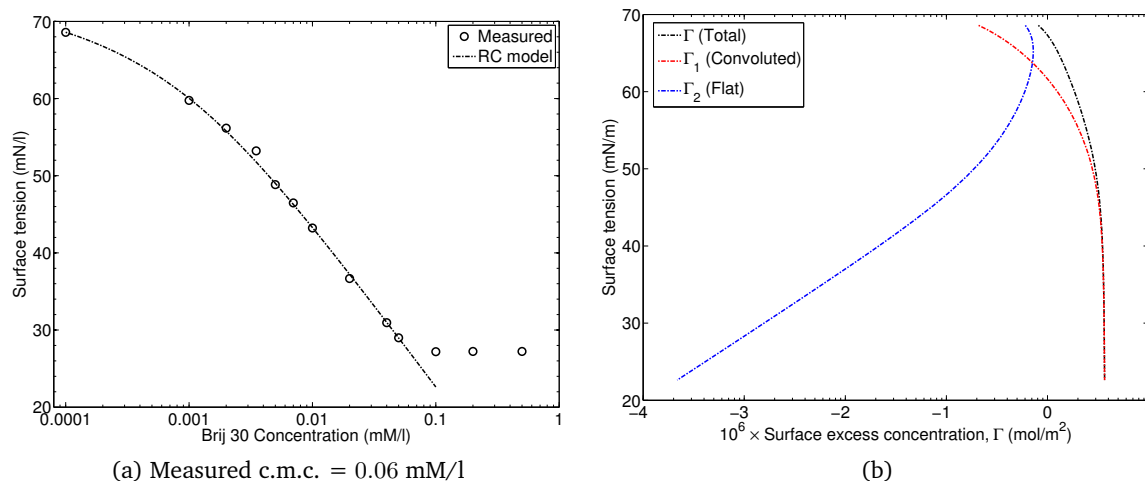


Figure 4.17: (a) Measured Brij 30 surface tension. The dotted line is a fit using the RC model (Eq. 2.5); (b) the theoretical dependance of the surface excess concentration in two states predicted by the RC model at the measured surface tension of Brij 30.

Table 4.3: RC model fit parameters for Brij 30

	$10^{-5} \times \omega_{10}$ (m <sup>2</sup> /mol)	$10^{-5} \times \omega_2$ (m <sup>2</sup> /mol)	$a$ (-)	$\varepsilon$ (m/mN)	$b$ (-)
Brij 30	2.77	9.326	0.855	0.000425	2260

The maximum concentration Brij 30 used was 0.5 mM/l. It was not possible to increase the concentration much beyond 0.5 mM/l as the Brij 30 precipitated into a cloudy surfactant rich layer (cloud point).

### 4.3.1 Equilibrium surface tension

Fig. 4.17a shows the Brij 30 equilibrium surface tension in ultra pure deionized water. The equilibrium surface tension was measured using the technique described in §3.1.

The c.m.c. is located at 0.06 mM/l. The surface tension at the c.m.c. is  $\sim 27$  mN/l. The RC model (Eq. 2.5) is used to fit the pre-micellar surface tension data (dotted line in Fig. 4.17a). The fit parameters are given in Table 4.3. The RC model includes surfactant adsorption in two states (state 1 and state 2) having different molar areas,  $\omega_1$  and  $\omega_2$  (m<sup>2</sup>/mol). For definiteness,  $\omega_2 > \omega_1$ . This can be imagined as the flat surfactant monomer having an adsorbed molar area of  $\omega_2$ , whereas a convoluted (or reoriented) state which has a molar area of  $\omega_1$ . (See §2.1.1 for further details on the RC model)

Fig. 4.17b shows the theoretical surface excess concentration of Brij 30 in two

states. At a surface pressure of 20 and higher (i.e. ST of  $\sim 50$  mN/m and lower), the adsorbed layer consists of convoluted surfactant. This corresponds to 0.004 mM/l (and higher) bulk concentration.

### 4.3.2 Dynamic surface tension (DST)

Fig. 4.18 shows the dynamic surface tension from 1 ms until 100 s for aqueous Brij 30 solutions. The DST is measured using the technique described in §3.2. Similar to the DST curves for SDS and CTAB, it is seen that as the concentration increases, the surface tension reduction is greater and faster. Fig. 4.19 quantifies the DST curves using the Rosen's empirical Eq. 2.6. Compared to SDS DST at its c.m.c., the value of  $t^*$  is three orders of magnitude higher for Brij 30 at its c.m.c. The Rosen parameter increases with Brij 30 concentration and no maximum is observed (Fig. 4.19d).

### 4.3.3 Foamability results

As Brij 30 is a bad foamer, only micellar concentrations were used for the foamability test. Fig. 4.20 shows the results from the foam column test for Brij 30 at 22°C. The maximum unloading increases with the Brij 30 concentration. Even at 10 times of the micellar concentration, the normalized maximum unloading is  $\sim 0.5$ . Thus due to these low bulk concentrations the effects of depletion are noticeable.

The normalized unloading curves are characterized by their gradients,  $nUF'$  (1/s). A linear fit in the region between 100 s and 250 s was made to extract the gradients. These gradients are shown in Fig. 4.21b; it can be seen that the gradient hardly changes even when the concentration increases by a factor of 5. It seems that similar to the observation for CTAB, the Brij 30 concentration does not have a significant influence on its foamability, but it rather influences the maximum unloading. Higher Brij 30 concentration postpones the influence of surfactant depletion on foamability.

Fig. 4.21a shows the foam velocity,  $\phi_{\text{foam}}$  (cm/s), for a randomly selected set of foam bubbles of all sizes. Similar to SDS and CTAB, the velocity varies in a short range, 0.7–0.9 cm/s over a 5 fold change in the CTAB concentration. Thus, the foam rise velocity is not a strong function of the Brij 30 concentration. The black marker in Fig. 4.21a at each Brij 30 concentration is the corresponding average velocity. The error bars indicates the uncertainty<sup>6</sup> in the measured velocity arising due to the resolution of the high speed movies. The average foam rise velocity is used in Eq. 3.2 to calculate the foam density. The decrease in velocity at high Brij 30 concentration can be explained using the justification given for SDS.

The foam density serves as a 'unit' of foamability. In following sections we will see how it correlates with the Rosen parameter, equilibrium surface pressure and the dynamic surface excess concentration.

<sup>6</sup>The velocity is measured by tracking the leading edge of the bubble over a given time. The accuracy in estimating the leading edge of the bubble is  $\pm 3.5\%$ ; giving an uncertainty in measured velocity of  $\pm 7\%$  (as leading edge is estimated twice, at the start and at the end of the bubble motion).

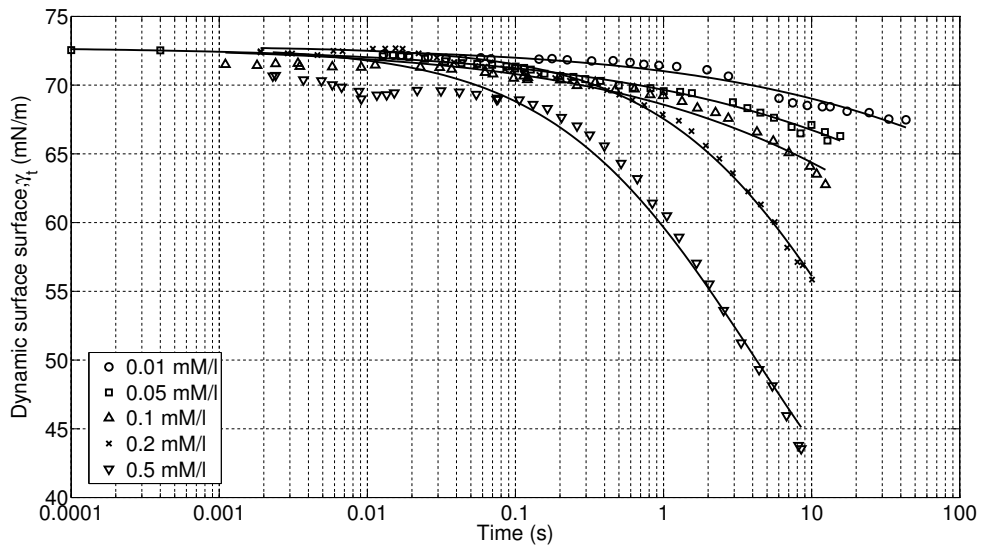


Figure 4.18: Dynamic surface tension of Brij 30 at 22°C. The markers denote measurement points whereas the continuous line is the best fit to Rosen's empirical Eq. 2.6

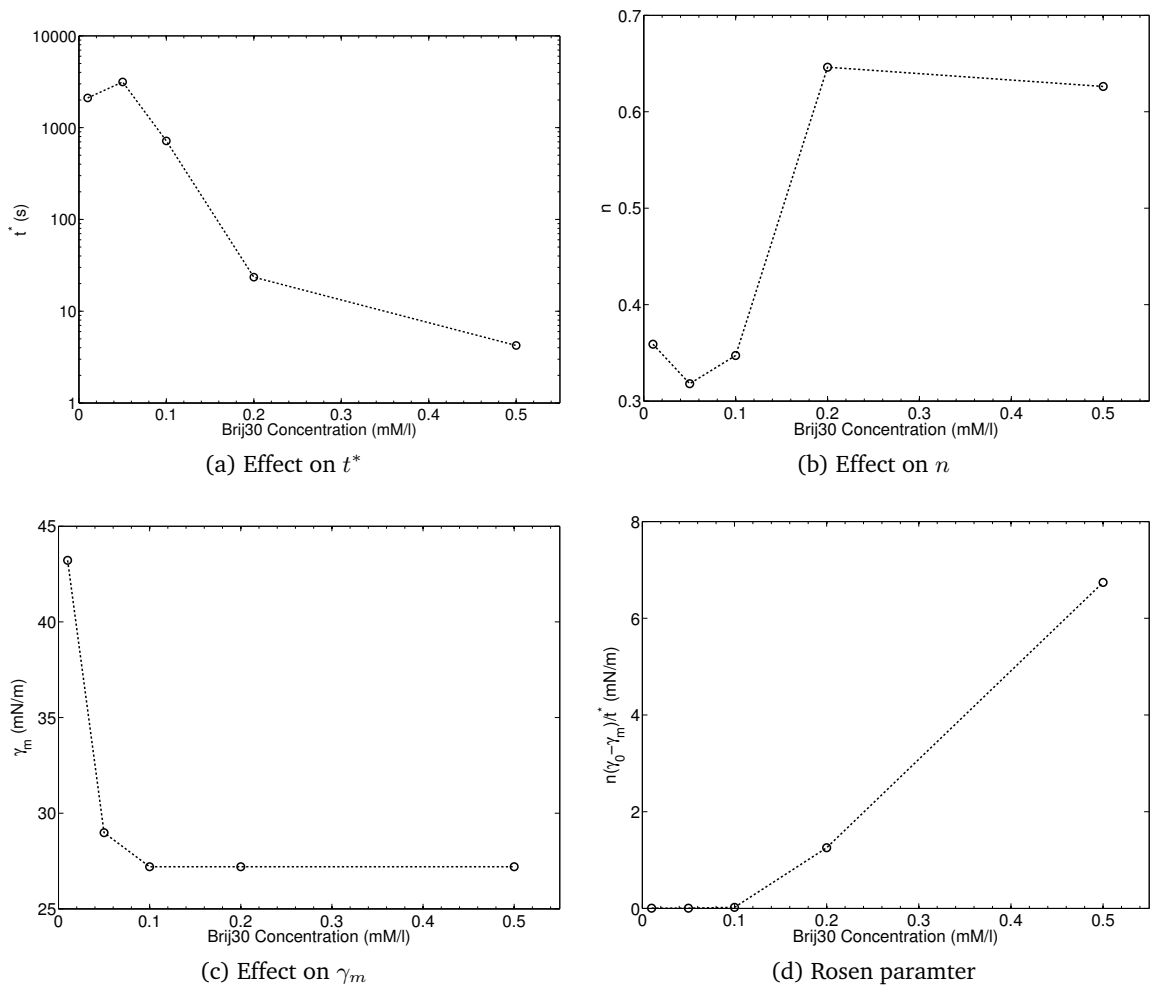


Figure 4.19: Characteristic rosen parameters of Brij 30 DST curves.

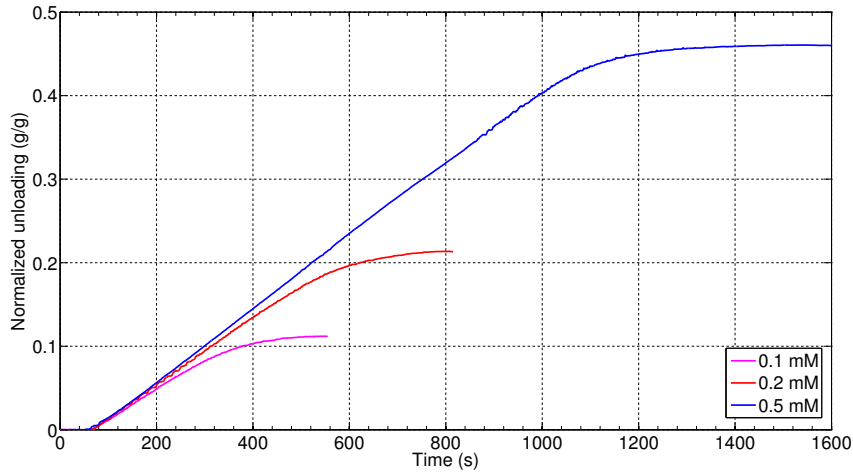


Figure 4.20: Normalized weight of foam collected for Brij 30 at 22°C.

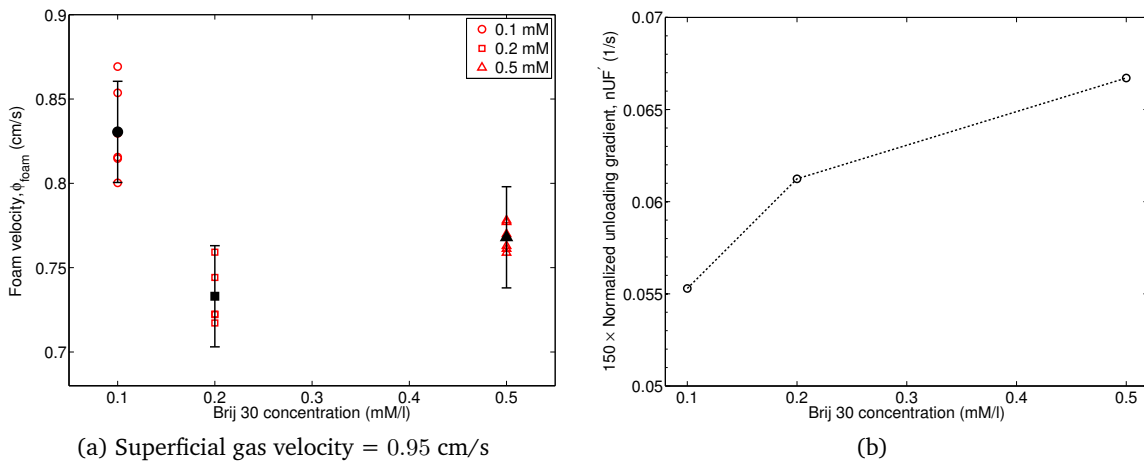
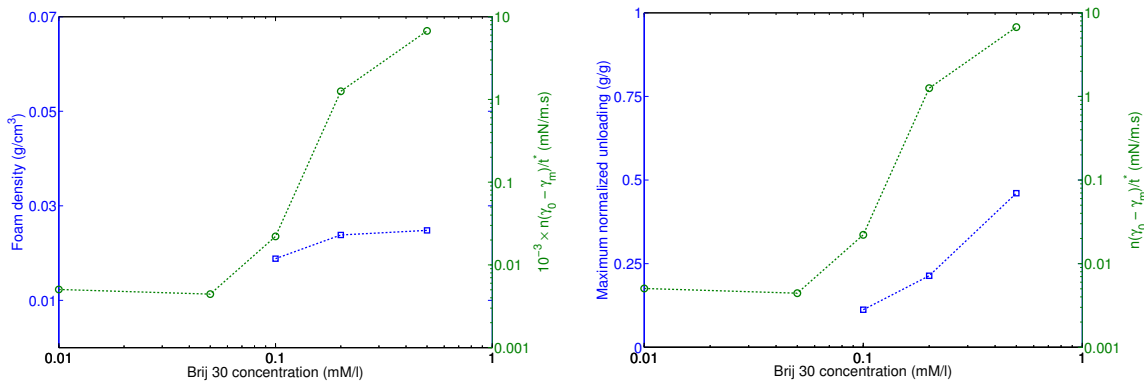


Figure 4.21: (a) Foam velocity for randomly selected bubbles of all sizes. The black marker is the average velocity whereas the corresponding error bar indicates the the uncertainty (see text for more details); (b) gradient of unloading curves in Fig. 4.20 between 100 and 250 s. The gradient is calculated by a linear fit.



(a) Observed foam density (in blue) and the calculated Rosen parameter (in green) for Brij 30 (b) Observed maximum unloading (in blue) and the calculated Rosen parameter (in green) for Brij 30

Figure 4.22: Correlation of foamability with the Rosen parameter for Brij 30.

### Correlation of foam density and maximum unloading with Rosen parameter

Fig. 4.22a shows the comparison between the  $\rho_{\text{foam}}$  and the Rosen parameter. The foam density increases slightly for a three order of magnitude increase in the Rosen parameter. The maximum unloading and the Rosen parameters increase with the Brij 30 concentration (Fig. 4.22b). The maximum unloading is incomplete for all the Brij 30 concentration studied.

### Correlation of foam density with equilibrium surface pressure

As all studied concentrations are in the micellar region, the equilibrium surface pressure remains constant. The foam density however increases by little. Thus the surface properties affecting the foam density continue to change in the micellar region.

### Correlation of foam density with dynamic surface excess concentration

The surface excess concentration of the foaming interface at the time scale of its formation is correlated with the foam density in this section. Fig. 4.24b shows the variation of the bubble size and the bubble velocity at different Brij 30 concentrations. Using the minimum and maximum velocity of bubbles, the residence time is calculated (See Fig. 4.24a). The residence times together with the DST curves and the RC model gives the dynamic surface excess concentration which is shown in Fig. 4.24c. See §4.1.4 for more details on the calculation approach.

Fig. 4.24c shows only the total (minimum and maximum) surface excess concentration. Both, the dynamic surface excess concentration and the foam density change by little over the Brij 30 concentration.

## 4.4 Sodium Dodecyl Sulfate (SDS) + Sodium Chloride (NaCl)

The effect of salt is considered by varying the NaCl concentration in 1 mM/1 SDS. The NaCl concentration is varied from very low (0.001 M) to very high (0.6 M). The sea water contains  $\sim 3.1\%$  salts which corresponds to 0.53 M of NaCl. The DST and foamability results will be shown in the next section.

### 4.4.1 Dynamic surface tension (DST)

Fig. 4.25 shows the dynamic surface tension from 1 ms until 100 s for aqueous 1 mM/1 SDS + NaCl solution. The DST is measured using the technique described in §3.2.

As the NaCl concentration increases, the time scale at which surface tension reduces is increased (quantified by  $t^*$ , Fig. 4.26a). The increase in NaCl concentration causes the surface tension to decrease, at constant surfactant concentration. This is quantified by  $\gamma_m$  in Fig. 4.26c. The Rosen parameter decreases marginally even at large NaCl concentration (Fig. 4.26d).

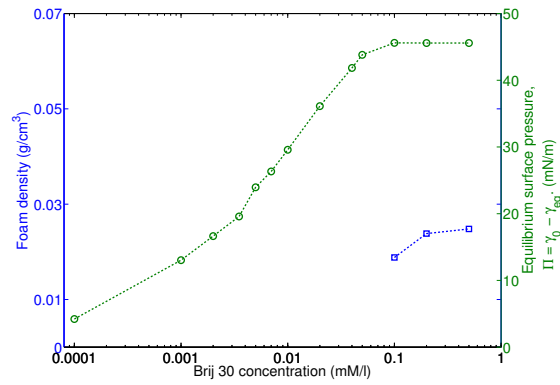
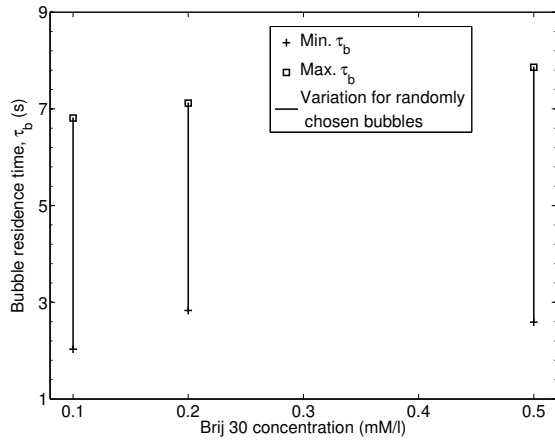
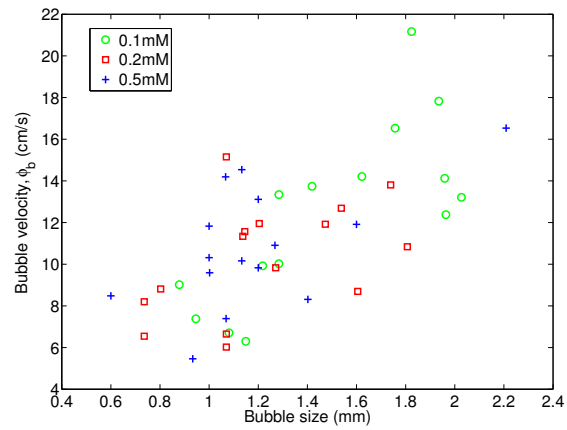


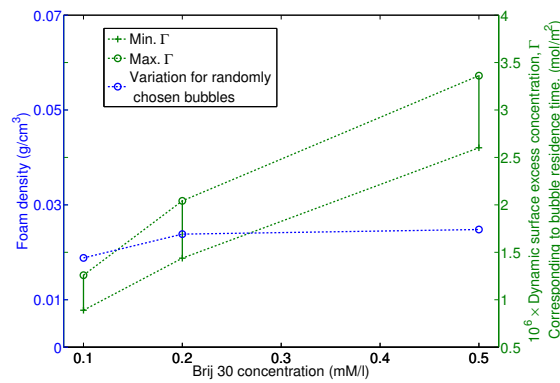
Figure 4.23: Observed foam density (in blue) and the calculated equilibrium surface pressure (in green) for Brij 30.



(a) Residence time of bubbles in the bulk Brij 30 solution prior to foaming.



(b) Relation between the size distribution and corresponding velocities.



(c) Dependence of the dynamic surface excess concentration at the time scale of foaming on the foam density.

Figure 4.24: Correlation of the foamability with dynamic surface excess concentration for Brij 30.

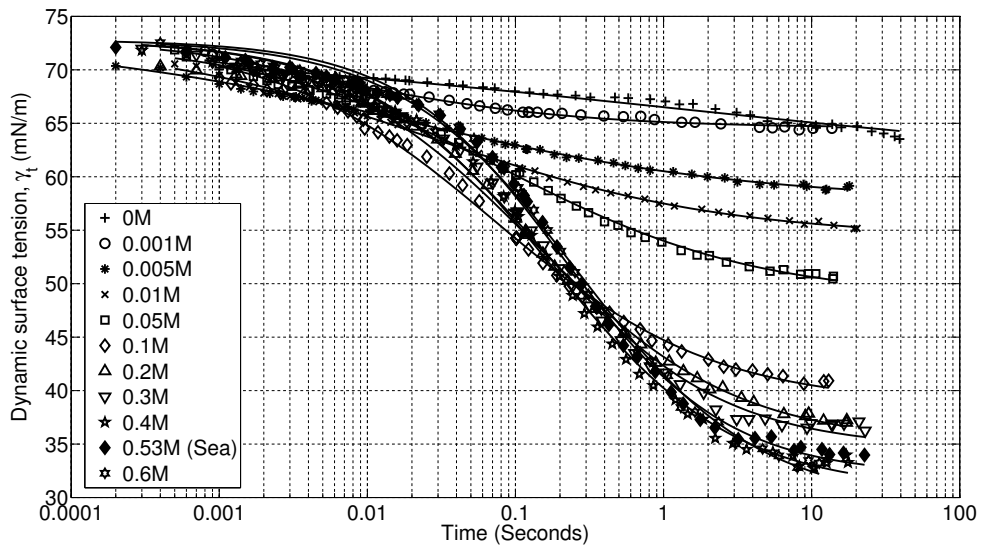


Figure 4.25: Dynamic surface tension curves of 1 mM/1 SDS with varying NaCl concentrations at 22°C. The markers are the actual measurements while the continuous lines are best fit to the measured data using the Rosen's empirical Eq. 2.6.

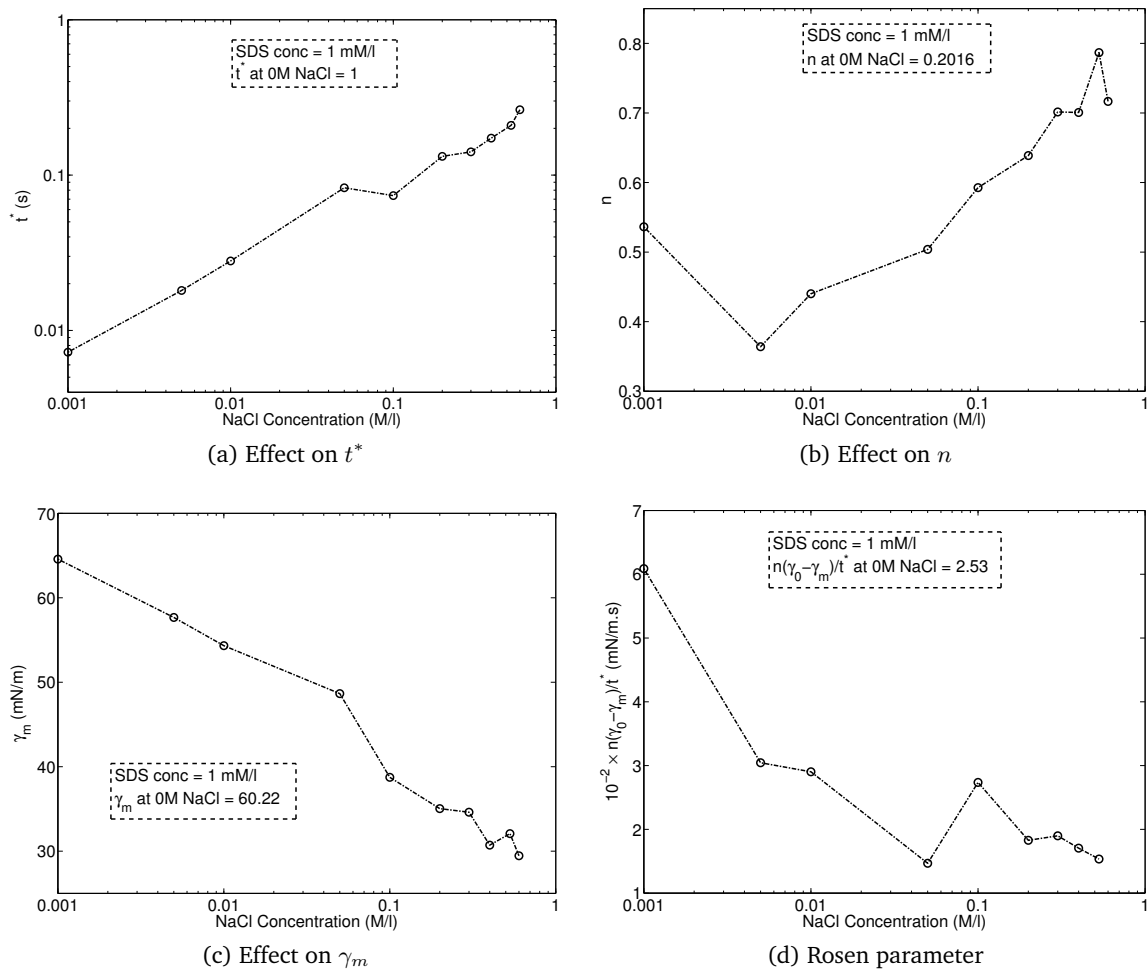


Figure 4.26: Characteristic rosen parameters of SDS + NaCl DST curves.

### 4.4.2 Foamability results

Fig. 4.27 shows the the normalized unloading weight of foam collected over time for 1 mM/l SDS + NaCl. The normalized unloading curves are characterized by their gradients,  $nUF'$  (1/s). A linear fit in the region between 100 s and 1000 s was made to extract the gradients. These gradients are shown in Fig. 4.28b. We can see that the presence of NaCl has no effect in the unloading gradients.

Fig. 4.21a shows the foam velocity,  $\phi_{\text{foam}}$  (cm/s), for a randomly selected set of foam bubbles of all sizes. Similar to SDS, CTAB and Brij 30, the velocity varies in a short range, 0.65 – 0.9 cm/s over three orders of magnitude change in the concentration. Thus, the foam rise velocity is not a strong function of the NaCl concentration. The black marker in Fig. 4.21a at each NaCl concentration is the corresponding average velocity. The error bars indicates the uncertainty<sup>7</sup> in the measured velocity arising due to the resolution of the high speed movies. The average foam rise velocity is used in Eq. 3.2 to calculate the foam density. The decrease in velocity at high NaCl concentration can be explained using the justification given for SDS.

The foam density serves as a ‘unit’ of foamability. In the following section we will see how it correlates with the Rosen parameter.

#### Correlation of foam density and maximum unloading with Rosen parameter

Fig. 4.29a shows the comparison between the  $\rho_{\text{foam}}$  and the Rosen parameter. The foam density increases slightly whereas the Rosen parameter decreases with the NaCl concentration. The maximum unloading and the Rosen parameter decrease with increasing NaCl concentration (Fig. 4.29b). The maximum unloading is incomplete at high NaCl concentration. Presence of salt at the adsorbed layer increases the surface concentration (thus a lower  $\gamma_m$  in Fig. 4.26c), leading to faster depletion.

## 4.5 Trifoam Block 820 (TB820)

Trifoam Block 820 (TB820) is a commercial foamer applied in gas well deliquification. It’s chemical composition is unknown. In this section, the dynamic surface tension data will be characterized by using maximum gradients and compared with observed foam density.

### 4.5.1 Dynamic surface tension (DST)

Fig. 4.30 shows the dynamic surface tension from 1 ms until 100 s for aqueous TB820 solution. The DST is measured using the technique described in §3.2.

TB820 DST shows two gradients separated by the red line in Fig. 4.30. TB820 is likely to be a mixture of surfactants. These gradients will be characterized as the

<sup>7</sup>The velocity is measured by tracking the leading edge of the bubble over a given time. The accuracy is in estimating the leading edge of the bubble is  $\pm 3.5\%$ ; giving an uncertainty in measured velocity of  $\pm 7\%$  (as leading edge is estimated twice, at the start and at the end of the bubble motion).

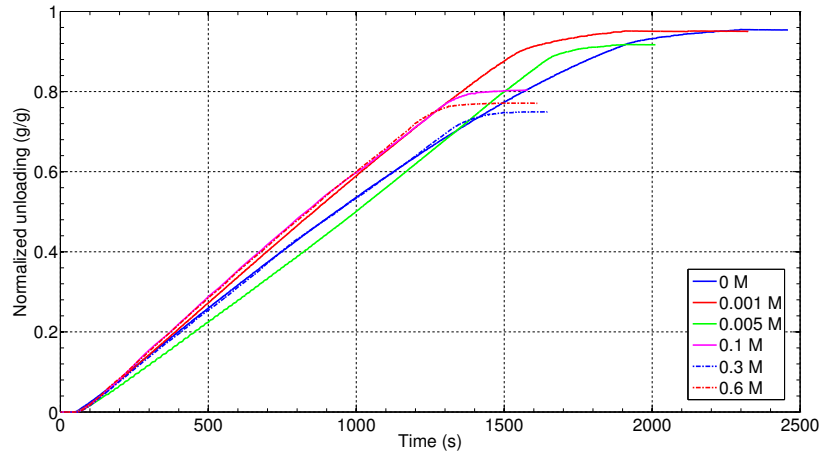


Figure 4.27: Normalized weight of foam collected for 1 mM/l SDS + NaCl at 22°C.

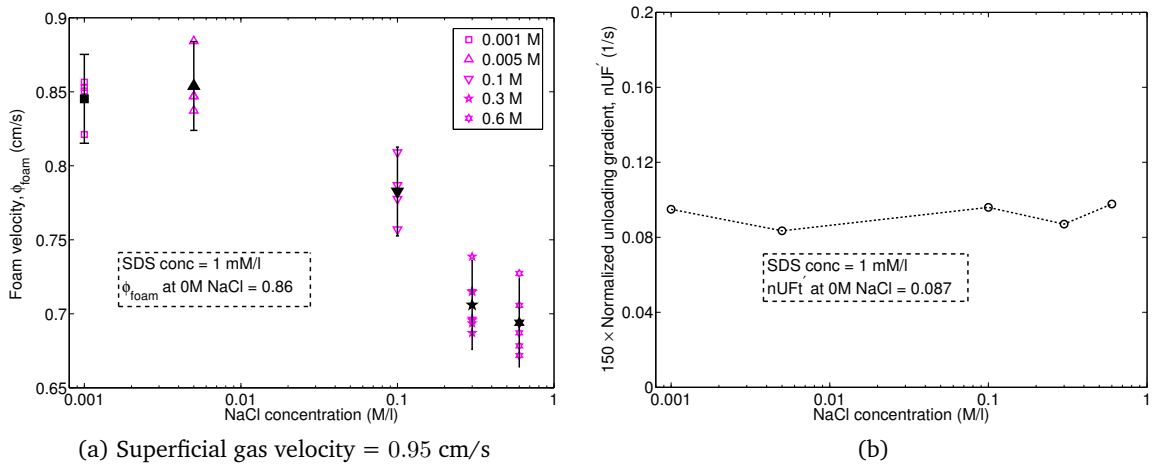


Figure 4.28: (a) Foam velocity for randomly selected bubbles of all sizes. The black marker is the average velocity whereas the corresponding error bar indicates the uncertainty (see text for more details); (b) gradient of unloading curves in Fig. 4.27 between 100 and 1000 s. The gradient is calculated by a linear fit.

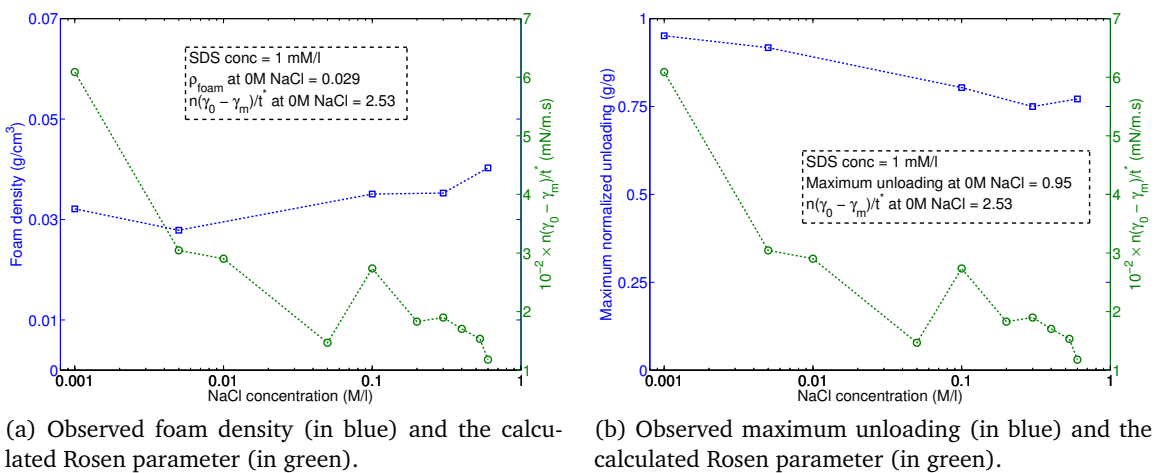


Figure 4.29: Correlation of foamability with the Rosen parameter for 1 mM/l SDS + NaCl.

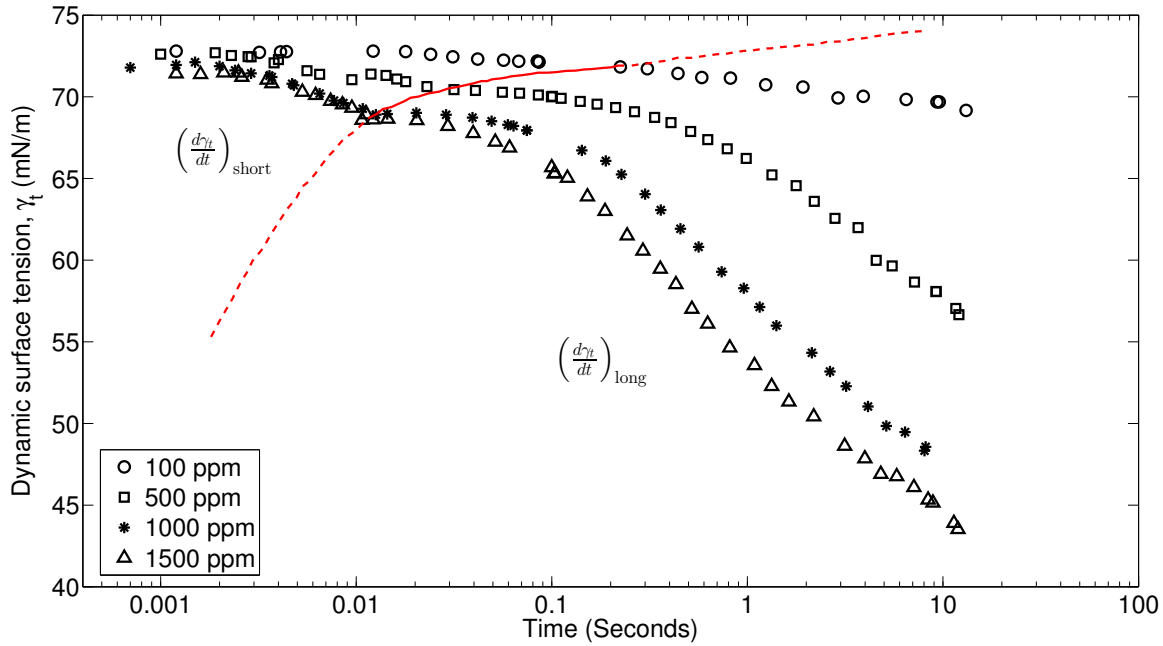


Figure 4.30: Dynamic surface tension of TB820 at 22°C. The markers denote measurement points. Two gradients are seen (separated by the red line) and they can be characterized in the short and the long time scale. See text for details on characterization.

short time gradient and the long time gradient as shown in the figure. The gradient is calculated by fitting a logarithmic curve of type,

$$\gamma_t = m \log t + c$$

where  $m$  is the slope and  $c$  is the y-intercept. The Rosen parameter is the slope at  $t^*$ , which is the time when  $\gamma_t = (\gamma_0 - \gamma_m)/2$ . Similarly the logarithmic equation was differentiated and evaluated at  $t_{\text{short}}^*$  and at  $t_{\text{long}}^*$ ,

$$\left(\frac{d\gamma_t}{dt}\right)_{\text{short}} = \frac{m}{t_{\text{short}}^*}$$

$$\left(\frac{d\gamma_t}{dt}\right)_{\text{long}} = \frac{m}{t_{\text{long}}^*}$$

$t_{\text{short}}^*$  and  $t_{\text{long}}^*$  is defined similar to the Rosen's  $t^*$  in its region. These gradients will be shown alongside the foam density in the next section.

#### 4.5.2 Foamability results

Fig. 4.31 shows the the normalized unloading weight of foam for TB820. The normalized unloading curves are characterized by their gradients,  $nUF'$  (1/s). A linear fit in the region between 100 s and 1000 s was made to extract the gradients. These gradients are shown in Fig. 4.32b. We can see that they increase marginally over a three fold increase in TB820 concentration.

Fig. 4.32a shows the foam velocity,  $\phi_{\text{foam}}$  (cm/s), for a randomly selected set of foam bubbles of all sizes. The velocity is 0.75 cm/s for all the studied concentrations. The black marker in Fig. 4.32a at each TB820 concentration is the corresponding average velocity. The error bars indicate the uncertainty<sup>8</sup> in the measured velocity arising due to the resolution of the high speed movies. At a lower TB820 concentration the velocity might be higher as observed for SDS, CTAB and SDS + NaCl. Due to lack of time these measurements could not be performed. The average foam rise velocity is used in Eq. 3.2 to calculate the foam density.

The foam density serves as a ‘unit’ of foamability. In the next section we will see how it correlates with the analogous of the Rosen parameter.

### Correlation of foam density with the maximum DST gradient

The foam density,  $\rho_{\text{foam}}$  (g/cm<sup>3</sup>), is calculated using Eq. 3.2, and the maximum DST gradient is calculated as described earlier.

Fig. 4.33a compares the maximum DST gradient with the calculated foam density. Both the short and the long time gradient increase with the TB820 concentration. From 1000 ppm onwards the rise in gradient is less than at the lower concentrations. As not enough common measurements are available between the DST and the foam density, a comparison cannot be made. However, an overall comparison of foam density with Rosen parameters will be made in the next section.

Fig. 4.33b compares the maximum DST gradient with the maximum unloading. The maximum unloading is incomplete at the measured concentration indicating depletion of surfactant. As the TB820 concentration increases, the maximum unloading also increases. There is not enough experimental data to compare the effect of maximum DST gradients with the maximum unloading due to time constraints.

## 4.6 Overall comparisons

In the previous sections three correlations were tested; (i) correlation of the foam density with the Rosen parameter, (ii) correlation of the foam density with equilibrium surface pressure, and (iii) correlation of the foam density with the dynamic surface excess concentration. Varying extent of interdependence was found, but there was no single relation satisfying all studied surfactants. All surfactant concentrations could be divided into two sections, pre-micellar and micellar. Across the c.m.c., the nature of trends changed. A summary of the partial trends is given in Table 4.4. In this section, a broader picture is considered, that is, all the foam densities are compared with all Rosen parameters, equilibrium surface pressures and the dynamic surface excess concentrations.

<sup>8</sup>The velocity is measured by tracking the leading edge of the bubble over a given time. The accuracy in estimating the leading edge of the bubble is  $\pm 3.5\%$ ; giving an uncertainty in measured velocity of  $\pm 7\%$  (as leading edge is estimated twice, at the start and at the end of the bubble motion).

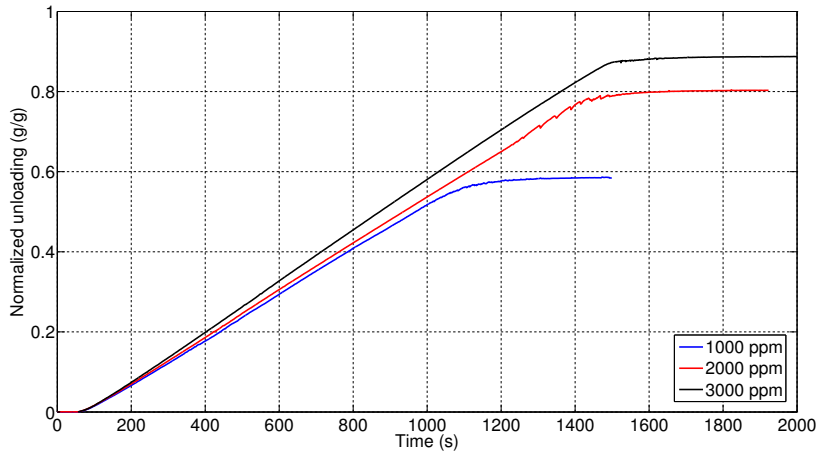


Figure 4.31: Normalized weight of foam collected for TB820

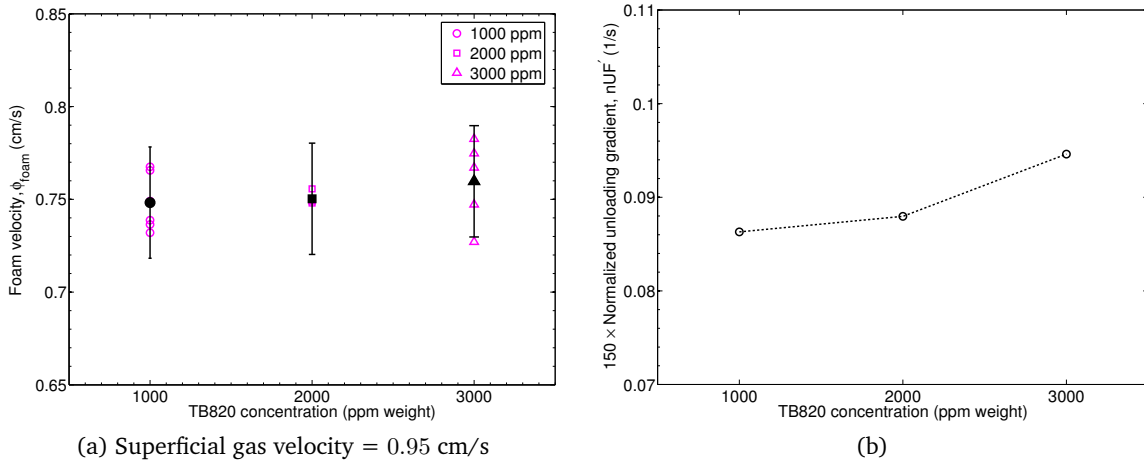
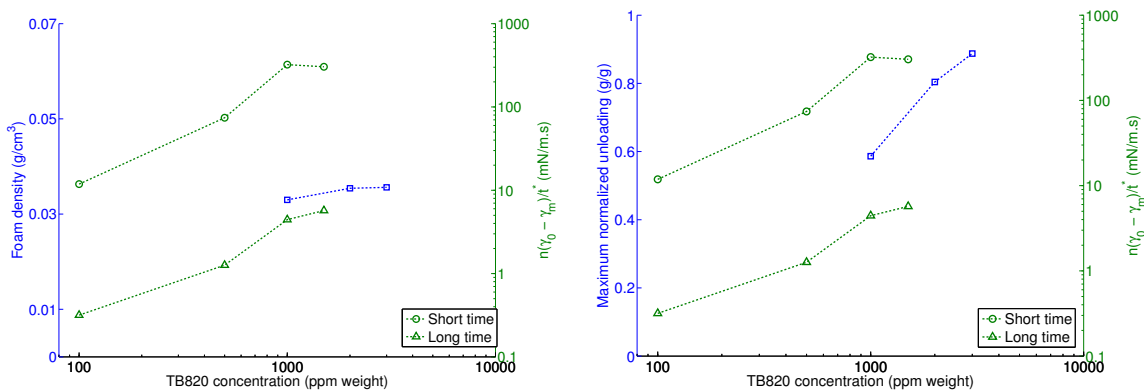


Figure 4.32: (a) Foam velocity for randomly selected bubbles of all sizes. The black marker is the average velocity whereas the corresponding error bar indicates the the uncertainty (see text for more details); (b) gradient of unloading curves in Fig. 4.31 between 100 and 1000 s. The gradient is calculated by a linear fit.



(a) Observed foam density (in blue) and the calculated (analogous) Rosen parameter (in green) for TB820.

(b) Observed maximum unloading (in blue) and the calculated (analogous) Rosen parameter (in green) for TB820.

Figure 4.33: Correlation of foamability with the (analogous) Rosen parameter for TB820.

#### 4.6.1 Foam density with Rosen parameter

Fig. 4.34 shows overall relation of the foam density with the Rosen parameter. We see that for a higher foam density a larger Rosen parameter is required. A change in eight order of magnitude of the Rosen parameter causes a seven fold increase in the foam density. The influence of DST on the foam density seems rather weak. A logarithmic curve of following type fits this trend. This relation is valid for the current experiment conditions, that is,  $N_2$  flow rate of 200 ml/min and an initial solution volume of 150 ml. The slope of this fit should change with the experiment conditions. Further experiments are needed to verify this.

The logarithmic trend between the Rosen parameter and the foam density was not seen for some measurements with SDS at high Rosen parameters ( $\mathcal{O}(10^3 - 10^4)$ ). It is unclear if the reason is due to the (n-dodecanol) impurity in SDS or due to the high Rosen parameter.

#### 4.6.2 Foam density with dynamic surface excess concentration

Fig. 4.35 shows the overall relation of the foam density with the dynamic surface excess concentration. It is clear that for a higher foam density a larger surfactant surface coverage is required at the time scale of foaming. Both, the foam density and the dynamic surface excess concentration varies seven fold over the measurements. There is a linear trend between these two quantities. This relation is valid for the current experiment conditions, that is,  $N_2$  flow rate of 200 ml/min and an initial solution volume of 150 ml. The slope of fit should change with the experiment conditions. Further experiments are needed to verify this.

The dynamic surface excess depends on the time scale of foaming. The time scale of foaming depends on the setup used to produce the foam, thereby linking such a trend with the method used to produce foam.

#### 4.6.3 Foam density with equilibrium surface pressure

Fig. 4.36 shows the overall relation of the foam density with the equilibrium surface pressure. We see that there is a linear correlation at low surface pressure. These low surface pressures are obtained (often) in the pre-micellar region. In the micellar region, the equilibrium surface pressure does not change whereas the foam density continues to change. Thus the parameters affecting the foam density are not constant beyond the c.m.c.

In the case of SDS, there seems to be a linear trend, but this is unique to SDS. It is unclear if the n-dodecanol impurity caused this linearity, but comparing with the Brij 30 measurements ( $\Pi = 45$  mN/m), the general dependence clearly fails.

#### 4.6.4 Maximum unloading with dynamic surface excess concentration

Fig. 4.37 shows the overall relation of the maximum unloading with the dynamic surface excess concentration. We see that there is no trend between these two quan-

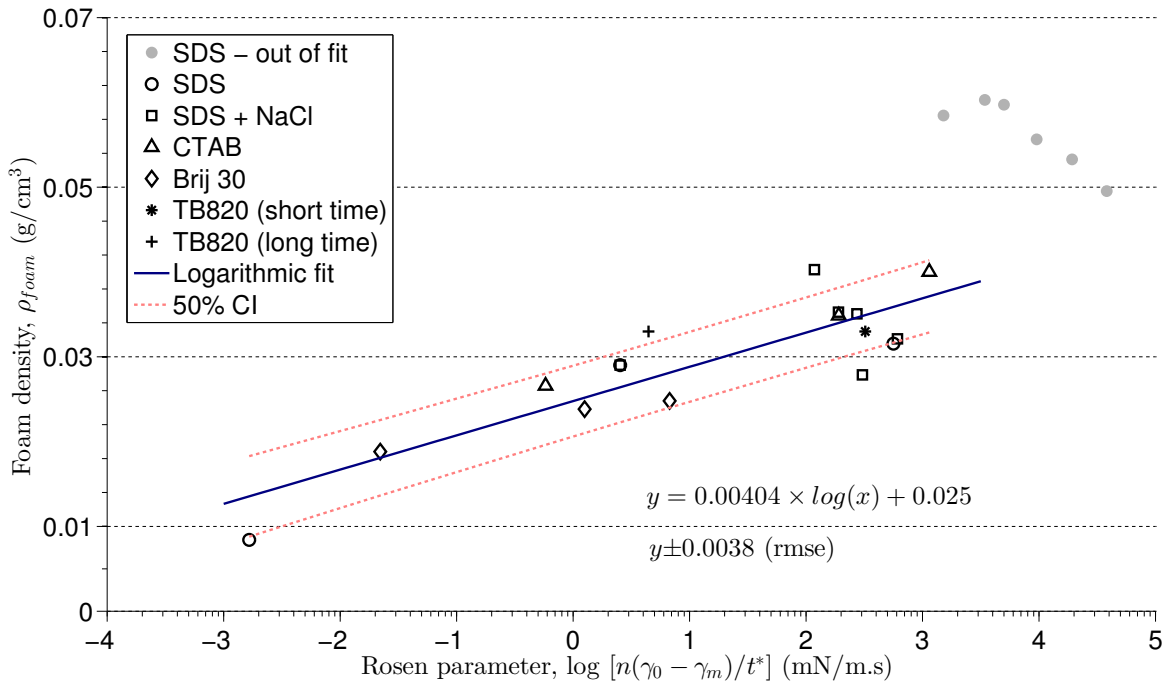


Figure 4.34: Overall relation between the foam density and Rosen parameter

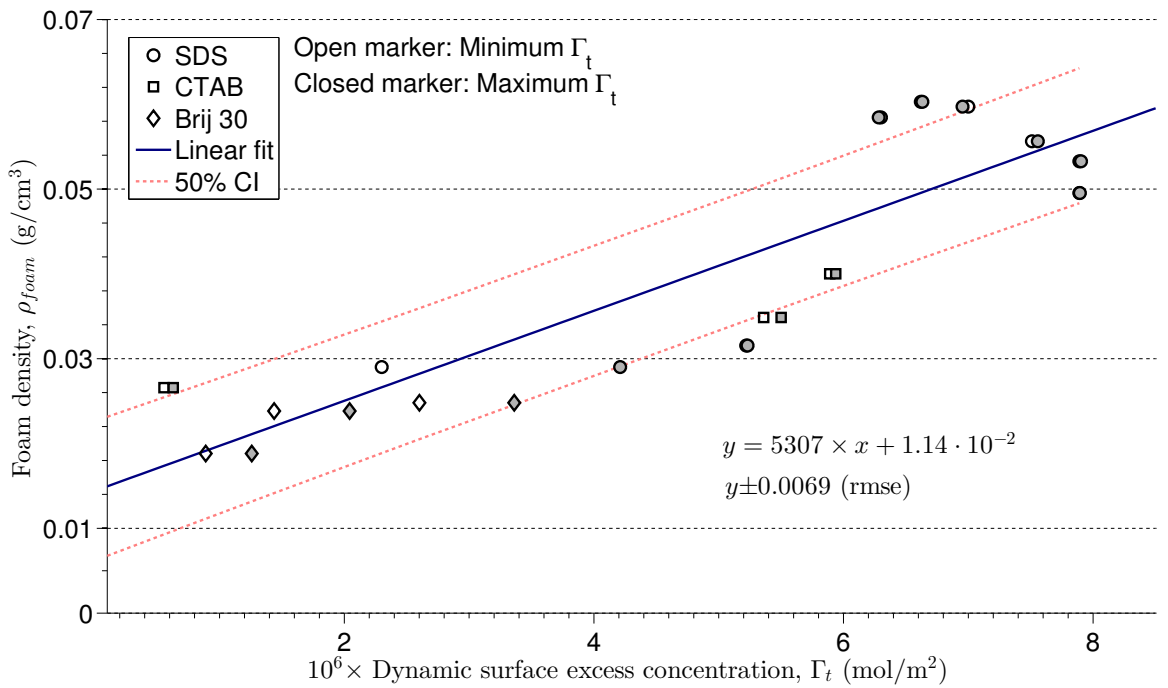


Figure 4.35: Overall relation between the foam density and the dynamic surface excess concentration

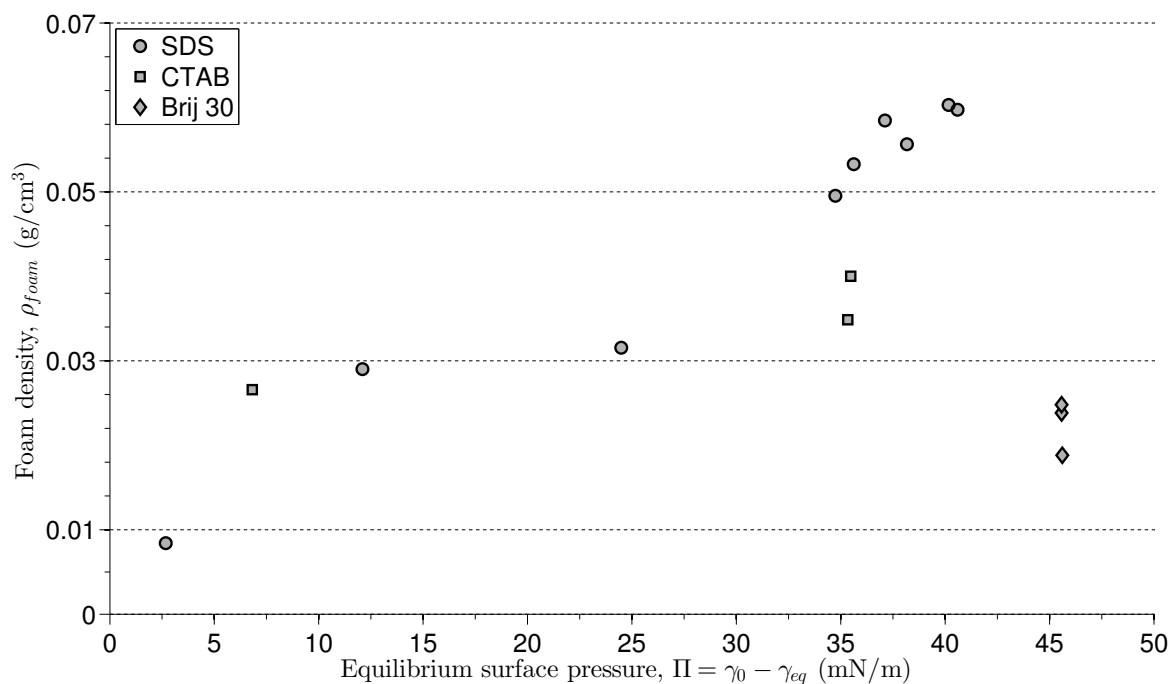


Figure 4.36: Overall relation between the foam density and the equilibrium surface pressure

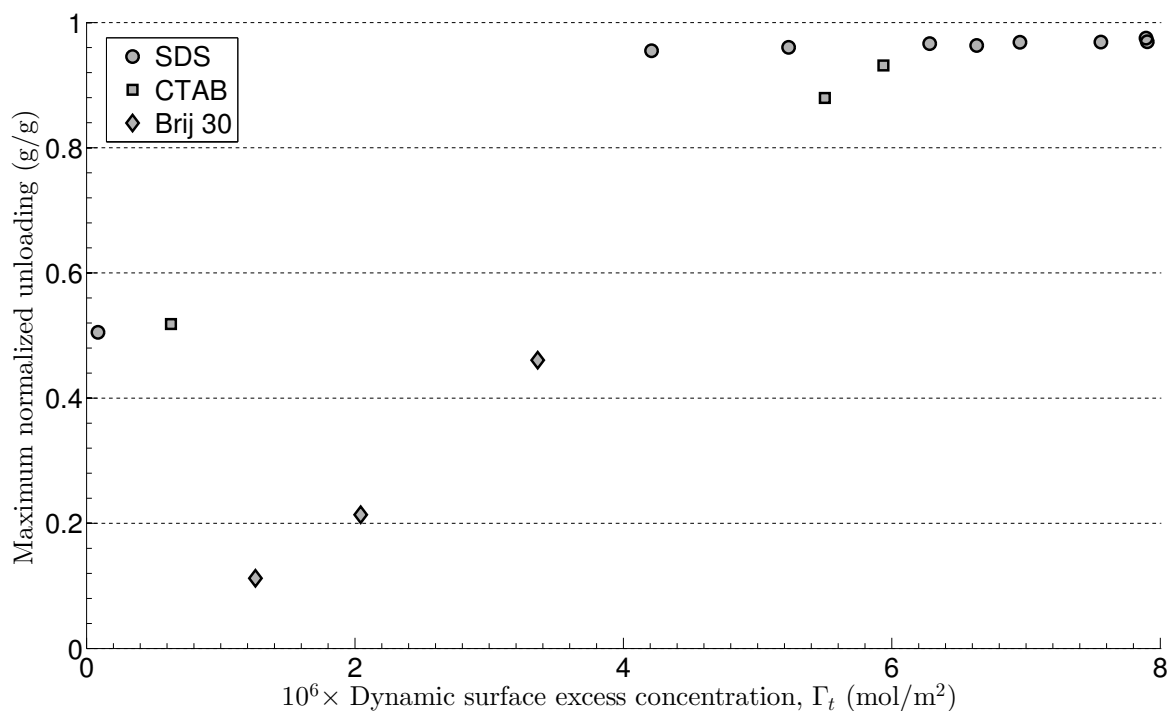


Figure 4.37: Overall relation between the maximum unloading and the dynamic surface excess concentration. We see that for individual surfactants, a higher maximum unloading is obtained for higher  $\Gamma_t$  whereas an overall comparison shows no general trend. Effect of initial surfactant concentration, mass and total interface of foam should be considered.

tities. Maximum unloading is related to the depletion of surfactant. It depends on the initial surfactant concentration, the mass and the total interfacial area of the produced foam.

## 4.7 Summary

In this chapter the experimental results were shown together with their analysis. The equilibrium surface tension is fitted to appropriate isotherms which were described earlier in §2.1.1. The theoretical equilibrium surface excess concentration can be calculated from the adsorption isotherms. The dynamic surface tension curves are characterized by fitting them to the Rosen's empirical Eq. 2.6. The Rosen parameter is defined as  $n(\gamma_0 - \gamma_m)/t^*$  (mN/m.s); where  $n$ ,  $t^*$  (s), and  $\gamma_m$  (mN/m), are the fit parameters.

The experiments from the foam column tests gave the unloading curves. These unloading curves were characterized by the linear gradient. Flow visualization of the rising foam and the rising bubbles in the surfactant solutions enabled calculation of the size and velocity distribution of the rising bubbles and the rising foam. The foam density is calculated by combining the foam velocity and the normalized unloading gradient.

The analysis revealed that there is an overall correlation of the foam density with the Rosen parameter and the dynamic surface excess concentration. For a denser foam, a larger Rosen parameter and a larger surfactant surface coverage at the time scale of foaming is required. The foam density for all studied surfactants changed seven fold, whereas the Rosen parameter changed over eight orders of magnitude. The correlation had a logarithmic trend, which (see Fig. 4.34) is believed to be a function of experimental conditions (that is  $N_2$  flow rate and initial volume of surfactant solution). This hypothesis could not be verified due to lack of time.

In the case of dynamic surface excess concentration, the variation was seven fold for a seven fold change in the foam density. The correlation has a linear trend, whose (see Fig. 4.35) is also believed to be a function of experiment conditions (that is  $N_2$  flow rate and initial volume of surfactant solution). This hypothesis could not be verified due to lack of time.

The foam density variations for changes in the concentration of single surfactants could not be explained by any of the tested correlations. Partial correlations were found in some cases. These findings are summarized in Table 4.4. From this table, we can say that DST can qualitative predict foamability at the pre-micellar concentrations. However, in micellar solutions, DST alone is insufficient.

Table 4.4: Summary of the partial trends for the foam density,  $\rho_{\text{foam}}$  ( $\text{g}/\text{cm}^3$ ), and the maximum unloading (max. nUF) with the (i) Rosen parameter, (ii) equilibrium surface pressure,  $\Pi$  ( $\text{mN}/\text{m}$ ), and (iii) dynamic surface excess concentration,  $\Gamma_r$  ( $\text{mol}/\text{m}^2$ )

		Rosen parameter			$\Pi$			$\Gamma_r$		
		Pre-micellar	Micellar	Pre-micellar	Micellar	Pre-micellar	Micellar	Pre-micellar	Micellar	
SDS	$\rho_{\text{foam}}$	Direct	Inverse	Direct	Direct	Direct	Direct	None		
	Max. nUF	Direct	<sup>a</sup>	Direct <sup>b</sup>	None <sup>b</sup>	Direct <sup>b</sup>	None	Direct <sup>b</sup>		
CTAB	$\rho_{\text{foam}}$	Direct	Direct	Direct	None	Direct	Direct			
	Max. nUF	Direct	Direct	Direct <sup>b</sup>	None <sup>b</sup>	Direct <sup>b</sup>	Direct <sup>b</sup>			
Brij 30	$\rho_{\text{foam}}$	N/A	Direct	N/A	None	N/A	Direct			
	Max. nUF	N/A	Direct	N/A	None	N/A	Direct			
Rosen parameter										
NaCl	$\rho_{\text{foam}}$	Inverse			N/A			N/A		
	Max. nUF	Direct			N/A			N/A		

<sup>a</sup> Achieved complete unloading

<sup>b</sup> Explicit plots not given in the report.

---

## 5. Conclusions and recommendations

---

This chapter summarizes the conclusions from this study. Based on these conclusions, recommendations for further work are made.

### 5.1 Conclusions

Surfactants can postpone liquid loading in the gas wells, thereby increasing the total recovery of gas from the reservoir. The exact deliquifying mechanism of the surfactants is poorly understood. A mechanistic foam flow model is currently being developed. Such a model requires the input of ‘foamability’ (foaming ability) for a given surfactant physiochemical properties. This research makes the first step in understanding the correlation of the foamability of surfactants with their dynamic and equilibrium surface tension in a customized setup.

Foamability was tested experimentally by a modified Bikerman test in which the weight of the overflowing foam is measured in time. Flow visualization allowed the calculation of  $\rho_{\text{foam}}$  ( $\text{g}/\text{cm}^3$ ), which served as a measure of foamability. In addition to  $\rho_{\text{foam}}$ , maximum unloading is defined as the total amount of foam unloaded in each experiment. The foam density,  $\rho_{\text{foam}}$ , and the maximum unloading were compared with three physio-chemical properties of aqueous surfactant systems; (i) the dynamic surface tension (through the Rosen parameter), (ii) the dynamic surface excess concentration, and (iii) the equilibrium surface tension. The DST curves over a time range of 1 ms to 100 s were characterized using the Rosen parameter, which quantifies the maximum slope. The dynamic surface excess concentration includes the surface coverage of the foaming interface at the time scale of its formation. The equilibrium surface tension is compared via the corresponding surface pressure,  $\Pi = \gamma_0 - \gamma_{\text{eq}}$ , ( $\text{mN}/\text{m}$ ).

Several previous attempts in finding the relation between the dynamic surface tension (DST) and the foamability have ended with contradicting results (see §1.4). Rosen et al. obtained the strongest relation using a Ross-Miles test to quantify the foamability. The current study was started by applying the technique proposed by Rosen et al.<sup>[11]</sup> to characterize the DST and determining the relation with the mass density of foam in a completely different setup.

Previously well studied surfactant candidates of each type (ionic, cationic, and nonionic) were selected for the experiments. The chosen ionic surfactant was sodium dodecyl sulfate (SDS) in the concentration range<sup>1</sup> of 0.1 – 50 mM/l. The chosen cationic surfactant was cetyltrimethylammonium bromide (CTAB) in the concentra-

---

<sup>1</sup>Refer Table 4.1 on page 31 for the concentration ranges in ppm by weight and g/l.

tion range<sup>1</sup> of 0.1 – 2 mM/l. The chosen nonionic surfactant was polyoxyethylene-4 lauryl ether (Brij 30) in the concentration<sup>1</sup> range of 0.01 – 0.5 mM/l. In addition to pure surfactants, Trifoam Block 820, a commercial foamer which is used in gas well deliquification was also used. Its concentration<sup>1</sup> was varied from 100 – 3000 ppm by weight. As salt is always present in gas wells, the effect of salt was studied by using sodium chloride (NaCl) in combination with 1 mM/l SDS. The salt concentration was changed from 0.001 – 0.6 M, where a concentration<sup>1</sup> of 0.53 M corresponds to the salt in sea water.

### 5.1.1 Total produced foam mass

The total produced foam mass (maximum unloading) did not have an overall dependence on the Rosen parameter, dynamic surface excess concentration (Fig. 4.37), and equilibrium surface tension. Maximum unloading is related to the depletion of surfactant. It depends on the initial surfactant concentration, the mass and the total interfacial area of the produced foam.

For individual surfactants, the maximum unloading is higher if the corresponding dynamic surface excess concentration is higher. Increasing initial concentration of surfactant led to higher production of foam, and also higher dynamic surface excess concentration. The increased loss by adsorption is compensated by the higher bulk concentration of the surfactant.

### 5.1.2 Foam density

#### Equilibrium surface pressure

Foam density increases with increasing equilibrium surface pressure for pre-micellar solutions. The equilibrium surface pressure does not (usually) change much after the c.m.c., but the dynamic surface properties still change, affecting the foam density. It must be noted that in the case of SDS, the equilibrium surface pressure has excellent qualitative agreement with the foam density at all concentrations. This observation is not fully understood, but could be related due to n-dodecanol impurity in the SDS.

#### Rosen parameter

A surfactant solution with a larger Rosen parameter was found to produce a denser foam (Fig. 4.34). The trend is logarithmic. A change of eight orders of magnitude of the Rosen parameter caused a mere seven fold increase in the foam density. The relation is very weak. The logarithmic trend holds even for large salt concentrations. At different experimental conditions in the current setup, the slope of this logarithmic trend should change.

This trend is unable to capture changes in the foam density as the initial surfactant concentration was varied from pre-micellar to micellar solutions. The foam density and the Rosen parameter always increased with the concentration until the corresponding c.m.c. was reached for all the studied surfactants. Pure (micellar)

SDS and SDS+ NaCl were exception to this trend. In the case of pure SDS near and above the c.m.c., the foam density decreased while the Rosen parameter increased. This behaviour is not understood fully; it might be related due to the micellar kinetics or rigidity of the SDS/n-dodecanol adsorbed layer.

#### Dynamic surface excess concentration

In all the studied systems, the dynamic surface excess concentration,  $\Gamma_\tau$  (mol/m<sup>2</sup>), at the time scale of foaming increased with the surfactant concentration. As the foam density also usually increased with the concentration it can be concluded that for higher foam density a larger dynamic surface excess concentration is required. When comparing over three surfactants; SDS, Brij 30 and CTAB, a clear linear trend (Fig. 4.35) can be seen. The surfactant which has a larger dynamic surface excess concentration was found to produce a denser foam.

The time scale of foaming for different foaming methods varies, and so does their corresponding dynamic surface excess concentration. The surfactant adsorption when a foam film is formed will determine the stability of that film, thereby, affecting measurements of foamability by different methods.

#### 5.1.3 Limitations and opportunities

In all the foam column tests the experimental conditions remained same; that is, 150 ml initial solution and 200 cm<sup>3</sup>/min N<sub>2</sub> flow rate. Preliminary tests at different experimental conditions strongly affected the unloading gradients (and thus foam density). It seems that the method of generating foam has a strong effect on the foamability. Further work is needed to study exact differences.

This dependance of the foam density on DST could assist in choosing the ideal surfactant for a particular gas well deliquification application. A denser foam would potentially be more effective in removing liquids (owing to higher liquid content). Whether such a potential can be realized requires knowledge of foam flow though the gas well. The mechanistic foam flow model being developed for real life applications should benefit from this qualitative trend.

## 5.2 Recommendations

Foams are extremely complex systems to study. Many individual facts essential for foaming are known, but there is no single coherent theory to describe any given foam. Nevertheless, two correlations between physiochemical parameters and foams were found in this thesis. The recommendations are divided based on the focus areas, that is, (i) continuing the current approach, (ii) establishing the effect of foaming methods, and (iii) isolating steps in foam formation.

### Continuing current approach

The logarithmic trend between the Rosen parameter and the foam density was not seen for some measurements with SDS at high Rosen parameters ( $\mathcal{O}(10^3 - 10^4)$ ). It is unclear if the reason is due to the (n-dodecanol) impurity in SDS or due to the high Rosen parameter. In order to check if this is due to such high Rosen parameter, further experiments (at same conditions) are needed for surfactant solutions with a high Rosen parameter. Surfactants with  $t^*$  in the millisecond range have a high Rosen parameter. As a suggestion, Zonyl FS-50, a perfluoro surfactant by DuPont chemicals, can be used. Zonyl FS-50 is a good foamer like SDS; it might also have a high Rosen parameter. This surfactant was purchased during the thesis but could not be used due to lack of time.

In the current work, experimental conditions were kept fixed at 200 ml/min  $N_2$  flow rate and 150 ml initial volume. It is recommended that, tests with (same) set of surfactants should be performed while systematically varying the  $N_2$  flow rate and the initial volume. The coefficients of (both) the correlations, Fig. 4.34 and 4.35, are expected to be a function of the experimental conditions. Using such additional test, the variations in these coefficients can be studied. It might also be possible to include a function for the experimental conditions in the fits for the trend.

### Effect of foaming methods

The current method of characterizing DST can be tested for the Ross-Miles test and the Bartsch test. The objective is to determine if the observed foam density dependence is unique to the foaming method. The correlation of foam height with the Ross-Miles test has already been established<sup>[11]</sup>, but a method to estimate the foam density is needed. As a first suggestion, a total liquid balance can give the liquid quantity in the foam structure whereas the foam height can be used to calculate the gas volume. Together, a density term ( $g/cm^3$ ) can be defined for the correlation. Calculating foam density for the Bartsch test is trivial.

### Isolating steps in foam formation

This study is recommended to study the dynamic surface excess concentration in greater detail by focussing on the mechanical process of the bubble formation at the sparger. A study on the influence of bubble formation time scale at the sparger and its travel through the bulk surfactant solution is recommended. Jachimska et al.<sup>[71]</sup> showed that the foam film formed by bubble which traveled longer distance was ruptured faster than the film formed by bubble traveling over short distances. The author suggested that uneven surfactant coverage on a bubble surface caused the foam film to rupture. Analogous to this study, the effect on foam density can be studied. This would require that the bubble formation at the capillaries is visible, requiring some changes in the foam column. If the time scale of bubble formation is indeed important then this result can be used in analysis of foaming mechanism in the large scale foam flow loop. In the large scale setup, foam is formed by shear at

air-liquid interface. The shearing air creates satellite drop/bubble in a certain time scale. This time scale can be used to estimate the (uniform) surfactant coverage at formation; following which, the surfactant coverage becomes nonuniform due to motion of the drop.

#### **On foam characterization for a foam flow model**

Quantifying the precise influence of physiochemical properties of a surfactant solution on the foam density still seems a difficult task. For the sake of the foam flow model in development, an empirical method to characterize foam is suggested. For instance, a given foam structure can be considered as a function of the bubble size and of plateau border length<sup>[51,72]</sup>. Neethling et al.<sup>[51]</sup> showed that the liquid content in foam overflowing from a column can be estimated accurately by considering interfacial rheology and bulk viscosity. Two empirical parameters were used to characterize drainage through the plateau borders and the vertices. Further analysis on using their approach in current work seems promising.



## Acknowledgements

During this project, lots of people have contributed towards the results. Many thanks to my supervisors: Dries, Luis, Menno and Ruud for guiding me throughout the project. Their guidance helped in organizing my ideas which at first seemed simply random. I would like to thank Dries, especially for the Skype meetings we had to improve the report while I was away for an internship in Norway. Automatic measurements from a 20 year old weighing scale was made possible due to Dries's LabVIEW skills, thanks for your unparalleled help.

Menno's philosophy on de-mystifying mother nature's secrets convinced me to accept certain deviations (and move on) in the dynamic surface tension measurements during the days when all experimental setups seemed to fall apart. He also arranged a high speed camera which enabled measurement of velocities and bubble sizes. His contributions in this project are appreciated.

Many thanks to Ger Koper, DelftChemTech for the discussions on the chemistry within foams. I learnt of various researchers working on surfactant adsorption which greatly helped in finding relevant literature.

In the STCA lab, I would like thank Rien, Albert and Arlette for their assistance in getting started. Rien Oskam gave valuable ideas on improving the experimental setup and simplified navigating through the complex Shell protocols. I am thankful to the people at the instrumentation workshop for fixing the du Noüy ring (which had a notorious habit of distorting often) always at a short notice.

Dr. Eugene Aksenenko at the Institute of Colloid Chemistry & Chemistry of Water, (Ukrainian National Academy of Sciences) is thanked for sharing literature references on adsorption models and providing prompt support on the adsorption software.

I had several discussions with Alexander Makievski, SINTERFACE Technologies (Germany) regarding the working principle of the maximum bubble pressure tensiometer. He helped in fixing the tensiometer and validating measurements. Thanks for your close cooperation.

I am thankful to Vipul for sharing his technique of image analysis. I was able to save considerable amount of time by partially automating the image analysis.

Lastly I would like to thank all my friends and family who were always there for me. I could always count on them when I needed to socialize and when I sought motivation.



---

# List of symbols

---

## Roman Symbols

Symbol	Description	Units
$a$	Intermolecular interaction constant	[-]
$b$	Adsorption equilibrium constant	[-]
$c$	Concentration	[mM/l]
$c_c$	Counterion concentration	[mM/l]
$f$	Activity coefficient	[mM/l]
$g$	Acceleration due to gravity	[m/s <sup>2</sup> ]
$m$	mass	[kg]
$n$	Rosen fit parameter	[-]
$n_1$	Factor for adsorption of counterions	[-]
$r_c$	Radius of the foam column	[cm]
$t$	Time	[s]
$t^*$	Rosen fit parameter	[s]
$t_l$	Bubble life time	[s]
$t_d$	Bubble dead time	[s]
$v$	Weight of initial solution	[g]
$z$	Charge number	[-]
$A$	Surface area	[m <sup>2</sup> ]
$E$	Gibbs elasticity	[mN/m]
$F$	Force	[N]
$\dot{F}$	Zuidema and Waters correction factor	[-]
$I$	Ionic strength	[mol/l]
$K_L$	Langmuir equilibrium adsorption constant	[l/mM]
$P$	Pressure	[Pa]
$R$	Radius of curvature	[m]
$R$	Gas constant	[mN.m/mol.K]
$R_{1/2}$	Dynamic surface activity	[mN/m.s]
$R_1$	Radius of curvature	[m]
$R_2$	Radius of curvature	[m]
$T$	Temperature	[K]
$V$	Volume of foam	[m <sup>3</sup> ]

## Greek Symbols

Symbol	Description	Units
$\alpha$	Constant for adsorption in state 2	[-]
$\gamma$	Surface tension	[mN/m]
$\gamma_0$	Surface tension of water	[mN/m]
$\gamma_{eq}$	Equilibrium surface tension	[mN/m]
$\gamma_m$	Mesoequilibrium surface tension	[mN/m]
$\gamma_t$	Surface tension at time $t$	[mN/m]
$\gamma_\tau$	Surface tension at bubble residence time	[mN/m]
$\varepsilon$	2D compression ratio	[m/mN]
$\theta$	Fractional surface coverage	[-]
$\rho$	Resistivity	[M $\Omega$ .m]
$\rho_{foam}$	Foam density	[g/cm <sup>3</sup> ]
$\varsigma$	Concentration of ion	[mol/l]
$\tau$	Residence time	[s]
$\varphi$	Fraction of unbounded surface-active ions	[-]
$v$	Volume of air injected	[m <sup>3</sup> ]
$\phi_{foam}$	Velocity of foam	[cm/s]
$\omega_0$	Molar area of the surfactant at $\Pi = 0$	[m <sup>2</sup> /mol]
$\omega$	Molar area of the surfactant	[m <sup>2</sup> /mol]
$\omega_1$	Molar area of the surfactant in state 1	[m <sup>2</sup> /mol]
$\omega_2$	Molar area of the surfactant in state 2	[m <sup>2</sup> /mol]
$\omega_{10}$	Molar area of the surfactant in state 1 at $\Pi = 0$	[m <sup>2</sup> /mol]
$\Gamma$	Surface excess concentration	[mol/m <sup>2</sup> ]
$\Gamma_1$	Surface excess concentration in state 1	[mol/m <sup>2</sup> ]
$\Gamma_2$	Surface excess concentration in state 2	[mol/m <sup>2</sup> ]
$\Gamma_{eq}$	Equilibrium surface excess concentration	[mol/m <sup>2</sup> ]
$\Gamma_{Lm}$	Langmuir theoretical maximum surface excess concentration	[mol/m <sup>2</sup> ]
$\Gamma_\tau$	Dynamic surface excess concentration	[mol/m <sup>2</sup> ]
$\Pi$	Surface pressure	[mN/m]
$\Sigma$	Bikerman unit of foamability	[s]

## Abbreviations

Abbreviation	Description
Brij 30	Polyoxyethylene-4 lauryl sulfate
CI	Confidence interval
c.m.c.	Critical micelle concentration
CTAB	Cetyltrimethylammonium bromide
DST	Dynamic surface tension

EO	Oxyethylene group
FC	Frumkin compressibility
FIC	Frumkin ionic compressibility
fps	Frames per second
GC	Gas chromatography
MW	Molecular weight
nUF'	Normalized unloading gradient
ppm	Parts per million
RC	Reorientation compressibility
rmse	Root mean square error
SDS	Sodium dodecyl sulfate
ST	Surface tension
TB820	Trifoam block 820
UFt	Mass flow rate of unloading foam



---

# Bibliography

---

- [1] D Weaire and S Hutzler. *The Physics of Foams*. Oxford University Press, 2001.
- [2] J.F. Lea, H.V. Nickens, and M.R. Wells. *Gas Well Deliquification*. Gulf Professional Publishing, 2008.
- [3] R.J. Farn et al. *Chemistry and technology of surfactants*. Wiley Online Library, 2006.
- [4] E. Illy and L. Navarini. Neglected food bubbles: The espresso coffee foam. *Food biophysics*, pages 1–14, 2011.
- [5] V.B. Fainerman, D Möbius, and R Miller. *Surfactants: Chemistry, Interfacial Properties, Applications*, volume 13 of *Studies in interface science*. Elsevier, 2001.
- [6] R. J. Pugh. Foaming, foam films, antifoaming and defoaming. *Advances in Colloid and Interface Science*, 64:67 – 142, 1996.
- [7] J.W. Gibbs. *Scientific Papers of J. Willard Gibbs: Thermodynamics*, volume 1. Longmans, Green and co., 1906.
- [8] M. J. Rosen and X. Y. Hua. Dynamic surface tension of aqueous surfactant solutions. 1. basic parameters. *Journal of Colloid and Interface Science*, 124(2): 652–659, 1988.
- [9] M. J. Rosen and Y. H. Xi. Dynamic surface tension of aqueous surfactant solutions. 2. parameters at 1-s and at mesoequilibrium. *Journal of Colloid and Interface Science*, 139(2):397–407, 1990.
- [10] M. J. Rosen and Y. H. Xi. Dynamic surface tension of aqueous surfactant solutions. 3. some effects of molecular-structure and environment. *Journal of Colloid and Interface Science*, 141(1):180–190, 1991.
- [11] M.J. Rosen, X.Y. Hua, and Z.H. Zhu. Dynamic surface tension of aqueous surfactant solutions: Iv relationship to foaming. *Surfactants in solution*, 11: 315, 1991.
- [12] M. J. Rosen and T. Gao. Dynamic surface tension of aqueous surfactant solutions. 5. mixtures of different charge type surfactants. *Journal of Colloid and Interface Science*, 173(1):42–48, 1995.

- [13] M. J. Rosen and T. Gao. Dynamic surface tension of aqueous surfactant solutions. 6. compounds containing 2 hydrophilic head groups and 2 or 3 hydrophobic groups and their mixture with other surfactants. *Journal of the American Oil Chemists Society*, 71(7):771–776, 1994.
- [14] M. J. Rosen and T. Gao. Dynamic surface tension of aqueous surfactant solutions. 7. physical significance of dynamic parameters and the induction period. *Journal of Colloid and Interface Science*, 172(1):242–248, 1995.
- [15] M. J. Rosen and L. D. Song. Dynamic surface tension of aqueous surfactant solutions. 8. effect of spacer on dynamic properties of gemini surfactant solutions. *Journal of Colloid and Interface Science*, 179(1):261–268, 1996.
- [16] ASTM. Standard test method for foaming properties of surface-active agents. In *D1173 Ú 07*. ASTM, Pennsylvania, US, 2007.
- [17] D. T. Nguyen. Fundamental surfactant properties of foamers for increasing gas production. *Petroleum Science and Technology*, 27(7):733–745, 2009.
- [18] T Tamura, Y Kaneko, and M Ohyama. Dynamic surface tension and foaming properties of aqueous polyoxyethylene n-dodecyl ether solutions. *Journal of Colloid and Interface Science*, 173(2):493–499, 1995.
- [19] R Varadaraj, J. Bock, P. Valint Jr., S Zushma, and N Brons. Relationship between fundamental interfacial properties and foaming in linear and branched sulfate, ethoxysulfate, and ethoxylate surfactants. *Journal of Colloid and Interface Science*, 140(1):31 – 34, 1990.
- [20] Xiao-Chun Wang, Lei Zhang, Qing-Tao Gong, Lu Zhang, Lan Luo, Zhen-Quan Li, Sui Zhao, and Jia-Yong Yu. Study on foaming properties and dynamic surface tension of sodium branched-alkyl benzene sulfonates. *Journal of Dispersion Science and Technology*, 30(1):137–143, 2009.
- [21] Xiao-Chun Wang, Lei Zhang, Qing-Tao Gong, Lin Wang, Lu Zhang, Lan Luo, Zhen-Quan Li, Sui Zhao, and Jia-Yong Yu. A study of dynamic interfacial properties as related to foaming properties of sodium 2,5-dialkyl benzene sulfonates. *Journal of Dispersion Science and Technology*, 30(3):346–352, 2009.
- [22] A Prins and H. K. van Kalsbeek. Foaming behaviour and dynamic surface properties of liquids. *Current Opinion in Colloid & Interface Science*, 3(6):639–642, 1998.
- [23] D Beneventi, B Carre, and A Gandini. Role of surfactant structure on surface and foaming properties. *Colloids and Surfaces A: Physicochemical and Engineering Aspects*, 189:65–73, 2001.
- [24] Jiang Yang, Vladimir Jovancicevic, and Sunder Ramachandran. Foam for gas well deliquification. *Colloids and Surfaces A: Physicochemical and Engineering Aspects*, 309(1-3):177–181, 2007.

- [25] Th. Engels, W. von Rybinski, and P. Schmiedel. Structure and dynamics of surfactant-based foams. In *Structure, Dynamics and Properties of Disperse Colloidal Systems*, volume 111 of *Progress in Colloid and Polymer Science*, pages 117–126. Springer, 1998.
- [26] C.H. Chang and E.I. Franses. Adsorption dynamics of surfactants at the air/water interface: a critical review of mathematical models, data, and mechanisms. *Colloids and Surfaces A: Physicochemical and Engineering Aspects*, 100: 1–45, 1995.
- [27] D. Myers. *Surfactant science and technology*. Wiley Online Library, 1988.
- [28] T.F. Tadros. *Applied surfactants: principles and applications*. Wiley-VCH, 2005.
- [29] K. Lunkenheimer, G. Czichocki, R. Hirte, and W. Barzyk. Novel results on the adsorption of ionic surfactants at the air/water interface—sodium-n-alkyl sulphates. *Colloids and Surfaces A: Physicochemical and Engineering Aspects*, 101(2-3):187–197, 1995.
- [30] J. T. Davies and E. K. Rideal. *Interfacial Phenomena*. Academic press, 1963.
- [31] V. B. Fainerman, V. I. Kovalchuk, E. V. Aksenenko, M. Michel, M. E. Leser, and R. Miller. Models of two-dimensional solution assuming the internal compressibility of adsorbed molecules: A comparative analysis. *The Journal of Physical Chemistry B*, 108(36):13700–13705, 2004.
- [32] C. Stubenrauch, V. B. Fainerman, E. V. Aksenenko, and R. Miller. Adsorption behavior and dilational rheology of the cationic alkyl trimethylammonium bromides at the water/air interface. *The Journal of Physical Chemistry B*, 109(4): 1505–1509, 2005.
- [33] V. B. Fainerman and E. H. Lucassen-Reynders. Adsorption of single and mixed ionic surfactants at fluid interfaces. *Advances in colloid and interface science*, 96 (1-3):295–323, 2002.
- [34] VB Fainerman, SV Lylyk, EV Aksenenko, AV Makievski, JT Petkov, J. Yorke, and R. Miller. Adsorption layer characteristics of triton surfactants:: 1. surface tension and adsorption isotherms. *Colloids and Surfaces A: Physicochemical and Engineering Aspects*, 334(1-3):1–7, 2009.
- [35] V. B. Fainerman, S. A. Zholob, E. H. Lucassen-Reynders, and R. Miller. Comparison of various models describing the adsorption of surfactant molecules capable of interfacial reorientation. *Journal of Colloid and Interface Science*, 261(1):180 – 183, 2003.
- [36] V. B. Fainerman, R. Miller, and V. I. Kovalchuk. Influence of the compressibility of adsorbed layers on the surface dilational elasticity. *Langmuir*, 18(20):7748–7752, 2002.

- [37] E. V. Aksenenko. 7. software tools to interpret the thermodynamics and kinetics of surfactant adsorption. In V. B. Fainerman, D Möbius, and R. Miller, editors, *Surfactants Chemistry, Interfacial Properties, Applications*, volume 13 of *Studies in Interface Science*, pages 619 – 648. Elsevier, 2001.
- [38] Eugene V Aksenenko. Adsorption software, July 2012. URL <http://www.thomascat.info/Scientific/AdSo/AdSo.htm>.
- [39] J. Eastoe and JS Dalton. Dynamic surface tension and adsorption mechanisms of surfactants at the air-water interface. *Advances in colloid and interface science*, 85(2-3):103–144, 2000.
- [40] A.F.H. Ward and L. Tordai. Time-dependence of boundary tensions of solutions i. the role of diffusion in time-effects. *The Journal of Chemical Physics*, 14(7): 453–461, 1946.
- [41] M.J. Rosen. *Surfactants and interfacial phenomena*. Wiley Online Library, 1989.
- [42] D. Langevin. Aqueous foams: A field of investigation at the frontier between chemistry and physics. *ChemPhysChem*, 9(4):510–522, 2008.
- [43] H. Wei, M Yang, and S Lin. An examination on the validity of the assumptions commonly made in dynamic surface tension measurement using a pendant bubble. *Colloids and Surfaces A: Physicochemical and Engineering Aspects*, 317(1–3):284 – 288, 2008.
- [44] K.J. Beers. *Numerical methods for chemical engineering: applications in Matlab*. Cambridge University Press, 2007.
- [45] A.M. Kraynik. Foam flows. *Annual review of fluid mechanics*, 20(1):325–357, 1988.
- [46] K. Malysa, M. Krasowska, and M. Krzan. Influence of surface active substances on bubble motion and collision with various interfaces. *Advances in colloid and interface science*, 114:205–225, 2005.
- [47] V. G. Levich and V. S. Krylov. Surface tension driven phenomena. *Annual Review of Fluid Mechanics*, 1(1):293–316, 1969.
- [48] D. Langevin and A. A. Sonin. Thinning of soap films. *Advances in colloid and interface science*, 51:1–27, 1994.
- [49] D. Exerowa and P. M. Kruglyakov. Chapter 7. foam stability and the stabilising ability of surfactants. In *Foam and Foam Films, Theory, Experiment, Application*, volume 5 of *Studies in Interface Science*, pages 502 – 570. Elsevier, 1998.
- [50] S. R. Derkach, J. Krägel, and R. Miller. Methods of measuring rheological properties of interfacial layers (experimental methods of 2d rheology). *Kolloidnyi Zhurnal*, 71(1):1–17, 2009.

- [51] S. J. Neethling, H. T. Lee, and J. J. Cilliers. A foam drainage equation generalized for all liquid contents. *Journal of Physics: Condensed Matter*, 14:331, 2002.
- [52] A. Patist, J.R. Kanicky, P.K. Shukla, and D.O. Shah. Importance of micellar kinetics in relation to technological processes. *Journal of colloid and interface science*, 245(1):1–15, 2002.
- [53] K. Lunkenheimer and K. Malysa. Simple and generally applicable method of determination and evaluation of foam properties. *Journal of surfactants and detergents*, 6(1):69–74, 2003.
- [54] C. W. Foulk and J. N. Miller. Experimental evidence in support of the balanced-layer theory of liquid film formation1. *Industrial & Engineering Chemistry*, 23(11):1283–1288, 1931.
- [55] J.J. Bikerman. *Surface chemistry: theory and applications*. Academic Press New York, 1958.
- [56] JJ Bikerman. The unit of foaminess. *Trans. Faraday Soc.*, 34:634–638, 1938.
- [57] K. Lunkenheimer and K. Malysa. A simple automated method of quantitative characterization of foam behaviour. *Polymer international*, 52(4):536–541, 2003.
- [58] K. Lunkenheimer, K. Malysa, G. Wienskol, and M. Baranska. Method and procedure for swift characterization of foamability and foam stability, January 2008.
- [59] KRÜSS. Dynamic foam analyser, July 2012. URL <http://www.kruss.de/en/products/foam.html>.
- [60] V. B. Fainerman, A. V. Makievski, and R. Miller. Accurate analysis of the bubble formation process in maximum bubble pressure tensiometry. *Review of Scientific Instruments*, 75(1):213–221, 2004.
- [61] V. B Fainerman and R. Miller. Maximum bubble pressure tensiometry – an analysis of experimental constraints. *Advances in Colloid and Interface Science*, 108–109(0):287 – 301, 2004.
- [62] V. B. Fainerman, V. N. Kazakov, S. V. Lylyk, A. V. Makievski, and R. Miller. Dynamic surface tension measurements of surfactant solutions using the maximum bubble pressure method – limits of applicability. *Colloids and Surfaces A: Physicochemical and Engineering Aspects*, 250(1):97–102, 2004.
- [63] V. B. Fainerman and R. Miller. Dynamic surface tension measurements in the sub-millisecond range. *Journal of Colloid and Interface Science*, 175(1):118–121, 1995.

- [64] J. Boos, W. Drenckhan, and C. Stubenrauch. On how surfactant depletion during foam generation influences foam properties. *Langmuir*, 28(25):9303–9310, 2012.
- [65] K. J. Mysels. Surface tension of solutions of pure sodium dodecyl sulfate. *Langmuir*, 2(4):423–428, 1986.
- [66] V. B. Fainerman, S. V. Lylyk, E. V. Aksenenko, J. T. Petkov, J. Yorke, and R. Miller. Surface tension isotherms, adsorption dynamics and dilational viscoelasticity of sodium dodecyl sulphate solutions. *Colloids and Surfaces A: Physicochemical and Engineering Aspects*, 354:8 – 15, 2010.
- [67] Ming-Wei Yang, Yi-Lin Hung, Hsiu-Fen Huang, and Shi-Yow Lin. A study of  $C_{12}E_4$  adsorption kinetics-considering pendant bubble shape. *Colloids and Surfaces A: Physicochemical and Engineering Aspects*, 317(1 - 3):462 – 472, 2008.
- [68] M. S. Kalekar and S. S. Bhagwat. Dynamic behavior of surfactants in solution. *Journal of Dispersion Science and Technology*, 27(7):1027–1034, 2006.
- [69] V Khosla. Visual investigation of annular flow and the effect of wall wettability. Msc. thesis, Delft University of Technology, 2012.
- [70] R. Höhler and S. Cohen-Addad. Rheology of liquid foam. *Journal of Physics: Condensed Matter*, 17(41):R1041 – R1069, 2005.
- [71] B. Jachimska, P. Warszynski, and K. Malysa. Influence of adsorption kinetics and bubble motion on stability of the foam films formed at n-octanol, n-hexanol and n-butanol solution surface. *Colloids and Surfaces A: Physicochemical and Engineering Aspects*, 192(1-3):177–193, 2001.
- [72] P. Stevenson and C. Stevanov. Effect of rheology and interfacial rigidity on liquid recovery from rising froth. *Industrial & engineering chemistry research*, 43(19):6187–6194, 2004.
- [73] W. D. Harkins and H. F. Jordan. A method for the determination of surface and interfacial tension from the maximum pull on a ring. *Journal of the American Chemical Society*, 52(5):1751–1772, 1930.
- [74] H. Zuidema and G. Waters. Ring method for determination of intrfacial tension. *Industrial & Engineering Chemistry Analytical Edition*, 13(5):312–313, 1941.
- [75] B. E. Poling, J. M. Prausnitz, and O. C. John Paul. *The properties of gases and liquids*, volume 5. McGraw-Hill New York, 2001.

---

# A. Measurement principles

---

## A.1 The du Noüy ring method correction factors

When the ring lifts the air-liquid interface, the force it measures include contribution from a small mass of liquid below the ring. The amount of mass lifted depends on the dimensions of the ring, density difference around the interface, and the surface tension of the interface. Harkins and Jordan<sup>[73]</sup> proposed correction factors by a careful measurement of the mass lifted for various values of ring dimensions, density difference and measured surface tension. The empirical correction factors were fitted to an equation given below by Zuidema and Waters<sup>[74]</sup>. As the data by Harkins and Jordan<sup>[73]</sup> is available in a limited range, the Zuidema and Waters<sup>[74]</sup> equation can be extrapolated to obtain the respective correction factors.

$$\begin{aligned} \left(\dot{F} - a\right)^2 &= \frac{4b}{\pi^2} \cdot \frac{1}{R^2} \times \frac{P}{\rho_{\text{lower}} - \rho_{\text{upper}}} + C & \text{(A.1a)} \\ C &= 0.04534 - 1.679 \frac{r}{R} \\ a &= 0.7252 \quad b = 0.0009075 \end{aligned}$$

where  $\dot{F}$  is the correction factor;  $P$  (mN/m) is the maximum force measured by the ring;  $\rho_{\text{lower}}$  (g/cm<sup>3</sup>) is the density of the lower phase;  $\rho_{\text{upper}}$  (g/cm<sup>3</sup>) is the density of the upper phase;  $R$  (cm) is the radius of the ring;  $r$  (cm) is the radius of the wire in the ring. The correct value of surface tension is then given by the product  $\dot{F} \times P$ .

### A.1.1 Procedure

For accuracy of measurements, it is critical that the ring's motion is perpendicular to the interface and that the ring is perfectly round. As the ring thickness is  $\mathcal{O}(10^{-4})$  m; in practice it is impossible to prevent distortion. Daily, prior to starting measurements a calibration test using ultra pure deionized water having resistivity,  $\rho \geq 10$  M $\Omega$ .m was made to test magnitude of error due to ring distortion. At 20°C and 1 atm, pure water has  $\gamma_{\text{eq}} = 72.8$  mN/m<sup>[75]</sup>. From experience, the ring was assumed to be deformed if  $\gamma_{\text{eq}} < 71.0$  mN/m. The results from calibration tests are maintained in a log book.

Measurement of surface tension is highly sensitive to impurities. Thus utmost care must be taken to clean the vessel which holds the sample and the ring. Rinsing the ring with water and solvents (preferably analytical grade) is essential. Additionally the ring must be heated to red hot using a benson burner. Heating the ring ensures that any organic surface-active impurities are burned off. Using the Benson burner will minimize the deformation due to uneven heating (thermal stresses).

Contact of ring with bare skin should be avoided as the oil from skin can affect subsequent measurements.

While measuring surface tension of solutions exhibiting dynamic surface tension; the ring must be pulled slowly. Ring's motion can put the surface in a non-equilibrium state. Pulling rate of 5 – 10 mm/min by hand was used during measurements.

## A.2 BPA-1S capillary cleaning procedure

While cleaning the capillary air should always be flowing through the capillary, that is, keep it under overpressure to prevent any liquid from entering. The capillary must first be cleaned with ethanol or acetone (preferable analytical grade), then several times with ultra pure deionized water. Each cleaning run should last for 8 – 10 minutes. Alternatively the capillary may also be cleaned in an ultrasonic bath. Make sure that the capillary is not stored near organic substances as they are highly surface active.

As a general note, experiments for the same surfactant solutions should be performed in series with increasing concentration. This ensures that even if the cleaning for next experiment is imperfect, the impurities will be at a lower concentration.

## A.3 Cleaning procedure for the foam column

The cleaning procedure for surfactants which dissolve in water is described in this section. Only water soluble surfactants were used in this thesis, so the cleaning procedure might need some modifications for non-water soluble surfactants.

1. Without removing the connected hose and with N<sub>2</sub> flow turned on, add ample amount of distilled water from the top such that the hose is flushed and the column is filled.
2. Disconnect the hose and block its connection to the column. Flush using distilled water by adding it at the top of the column and allowing it to flow out it from the bottom drain valve on the column (with N<sub>2</sub> flowing always). Siphon out the liquid below the drain valve. Repeat.
3. As surfactant is flushed out, noticeable changes occur in the bubble shapes and velocity. The number of flushes before this happens depends on solubility of the surfactant. It could be from a minimum of three flushing cycles to as much as six flushing cycles.
4. Fill the entire column with ultra pure deionized water and let N<sub>2</sub> sparge for 5 – 10 minutes.
5. Remove the water from the top drain valve first and then from the bottom valve. Use a clean hose to siphon out any remaining liquid.
6. Air dry the column for 15 – 20 minutes.

7. All the removable parts must be cleaned separately by hand. Make sure the cleaning area where this is done is also devoid of organic waste. At all times keep these parts on fresh clean tissues.



---

## B. On the shape of foam bubbles and corresponding foam density

---

The typical range of foam density,  $\rho_{\text{foam}}$  ( $\text{g}/\text{cm}^3$ ), observed is in the range of 0.01 to 0.07. For a mono-disperse spherical foam bubbles the theoretical (fractional) limit is 0.24 of the continuous phase (liquid) <sup>[27]</sup>. This number is considerably larger than the observed foam density. This is surprising as the bubbles seem to be spherical from the recorded movies (see Fig. 1.2 as an example).

For understanding this deviation, let us assume that (somehow) a foam having  $\rho_{\text{foam}} = 0.24 \text{ g}/\text{cm}^3$  is produced. We can then use Equation 3.2 to estimate U Ft (mass flow rate of the unloading foam,  $\text{g}/\text{s}$ ),

$$\begin{aligned}\rho_{\text{foam}} &= \frac{v \times n\text{UF}'}{\phi_{\text{foam}} \times \pi r_c^2} \\ 0.24 &= \frac{150}{\pi \times 1.055^2} \times \frac{n\text{UF}'}{\phi_{\text{foam}}} \\ 0.24 &\simeq 43 \times \frac{n\text{UF}'}{\phi_{\text{foam}}}\end{aligned}$$

Assuming  $\phi_{\text{foam}} = 0.85 \text{ cm}/\text{s}$ , we have

$$\begin{aligned}\text{UFt} &= n\text{UF}' \times 150 \\ &= 0.00474 \times 150 \\ &= 0.71\end{aligned}$$

Thus,  $\text{UFt} = 0.71 \text{ g}/\text{s}$ , for foam consisting of spherical mono-disperse bubbles. In the case of 4 mM/l SDS,  $\text{UFt} = 0.17 \text{ g}/\text{s}$ . This deviation is likely due to, (i) the fact that poly-disperse bubbles are present in the foam (see Fig. 4.8b), and (ii) probably due to non-spherical foam bubbles. The resolution of hi-speed movies is not high enough to confirm the presence of non-spherical bubbles.